Numerical Modelling of Lean Duplex Stainless Steel Hollow and Concrete-filled Columns of Square, L-, T- and +-shape Sections under Pure Axial Compression

A thesis submitted for the degree of

Doctor of Philosophy

by

M. Longshithung Patton

Department of Civil Engineering

Indian Institute on Technology Guwahati

Guwahati – 781 039, India

DECLARATION

I hereby certify that the work embodied in this thesis entitled '***Numerical Modelling of Lean Duplex Stainless Steel Hollow and Concrete-filled Columns of Square, L-, T- and +-shape Sections under Pure Axial Compression***' in partial fulfilment of the requirements for the award of the Degree of Doctor of Philosophy and submitted in the Department of Civil Engineering, Indian Institute of Technology Guwahati, India, is an authentic record of my own work carried out during a period from **July, 2009 to October, 2013** under the supervision of Dr. Konjengbam Darunkumar Singh, Associate Professor, Department of Civil Engineering, Indian Institute of Technology Guwahati, India.

The matter presented in the thesis has not been submitted by me for the award of any other degree of this or any other institute.

Date: (**Mr. M. Longshithung Patton**)

Place: Reg. No: 09610405

CERTIFICATE

This is to certify that the thesis entitled '***Numerical Modelling of Lean Duplex Stainless Steel Hollow and Concrete-filled Columns of Square, L-, T-, and +-shape Sections under Pure Axial Compression***' being submitted by **Mr. M. Longshithung Patton** to the Indian Institute of Technology Guwahati, India, for the award of degree of ***Doctor of Philosophy*** is a record of bonafide research work carried out by him under my supervision.

The thesis work, in my opinion is worthy of considering for the award of degree of ***Doctor of Philosophy*** in accordance with the regulation of the Institute.

(Dr. Konjengbam Darunkumar Singh)
Associate Professor
Department of Civil Engineering
Indian Institute of Technology Guwahati

Date:

Place:

to the Lord Almighty

to my dearest Parents

Mhonbemo and Myingthungbeni

ABSTRACT

Since the last two decades, there has been an accelerating interest in the use of stainless steel in the construction industry (Mann, 1993, Gardner 2005) owing to the benefits of stainless steels in terms of its good structural performance, aesthetic features and ease of construction of structural members. Generally, the austenitic stainless steel grades which contain ~ 8% - 11% nickel feature most prominently within the constructional industry. However, with increasing nickel prices there is an escalation in the demand for Lean Duplex Stainless Steel (LDSS) with low nickel content of ~ 1.5%, such as grade EN 1.4162 (Gardner, 2005b; Baddoo, 2008; EN 10088-4, 2009). LDSS, such as, grade EN 1.4162, has twice the mechanical strength of conventional austenitic and ferritic stainless steel and has a potential for use as main structural members (Gardner, 2005b). Even though there are several favourable characteristics involved in the use of LDSS material, often it may not be economical due to its relatively high material costs. Hence, a promising and innovative way to reduce the cost is through composite construction, where concrete is filled inside the stainless steel hollow sections (also known as Concrete-Filled Stainless Steel Tubular (CFSST) structures), which combines the advantages of both stainless steel and concrete, and thus providing not only an increase in the load-carrying capacity but also rapid construction (i.e. formwork is not required) (e.g. Uy and Patil, 2006; Zhao *et al*., 2010; Young and Ellobody, 2006; Lam and Gardner, 2008; Uy *et al*., 2011). In addition to the benefits gained in terms of economy and strength with the use of LDSS material and a composite construction, further benefits may be gained by combining it with the use of special-shaped sections, such as, L-, T-, and +-shape sections (Non-Rectangular Sections or NRSs). In engineering structures, NRSs are mainly used in reinforced concrete columns because of their convenient construction at beam-column joints, larger moment of inertia of the cross-sections that

leads to much higher capacity for resisting lateral load along with the advantage of providing a flushed wall face, resulting in an enlarged usable and regular indoor floor space area. To the best of author's knowledge, till date, there are no literatures available regarding studies on the structural behavior of LDSS hollow and concrete-filled stub and slender tubular columns with NRSs. Hence, the primary objective of the study undertaken in this research was to explore the structural behavior of LDSS hollow and concrete-filled tubular stub and slender columns with NRSs by comparing with a representative square section having same LDSS material cross-sectional area (i.e. equal LDSS material consumption adopted) under pure axial compressive loading through finite element (FE) analyses using general-purpose FE software package Abaqus (2009).

In the first component of the present study, the effect of cross-sectional shapes and thickness of the LDSS tube on the strength and deformation capacities as well as the failure modes of the LDSS hollow tubular stub and slender columns are reported towards understanding the behavior of NRSs over the representative square section. For LDSS hollow tubular stub columns, it was found that, for LDSS tube thickness < 30 mm, NRSs showed higher strength capacities by about 36 % to 3 %, 72 % to 3 %, and 134 % to 9 % for L-, T- and +-shape section, respectively, over the representative square section, with the percentage difference in strength decreasing with increasing thicknesses of the LDSS tube. But for LDSS tube thickness ≥ 30 mm, the ratio of the strengths for the NRSs and the representative square section tends to 1.0. The axial deformation at ultimate load of the NRSs hollow tubular stub columns are higher compared to the representative square section, with +-shape section estimating a much higher deformation capacity, suggesting that there is a provision for achieving a better ductility in the use of NRSs. And for LDSS hollow tubular slender columns, a range of column lengths *viz*., 3.0 m – 10.0 m, thereby providing a range of non-dimensional member slenderness ($\bar{\lambda}$) from 0.05 to 3.0, was considered to account for the variations in buckling strength with changes in the column lengths, cross-sectional shapes and LDSS tube thickness *viz.* 5.25 mm (Class 3 section) and 2.0 mm (Class 4 section). For Class 3 sections, for $\bar{\lambda} \leq 0.5$, all the sections exhibit similar structural capacities. For $0.5 < \bar{\lambda} \leq 2.0$, there is a nearly linear variation in

strengths (increasing trend for +HC, similar trend for THC and decreasing trend for LHC), with stabilization beyond $\bar{\lambda}$ > 2.0. For $\bar{\lambda}$ > 2.0, P_u for +HC showed ~ 30% higher; THC showed similar strength; and LHC showed ~20% lower than the corresponding value for SHC, indicating that +HC has an improved ultimate strength for all the ranges of $\bar{\lambda}$. For Class 4 sections, in contrast to Class 3 sections, cross-sectional shape becomes increasingly significant with decreasing $\bar{\lambda}$, however, the cross-sectional shape becomes insignificant for very high $\bar{\lambda}$ as also the case for Class 3 sections. The average strength enhancement for the Class 4 NRSs as compared to the representative square section, for all $\bar{\lambda}$ considered, are ~ 10 %, 50 %, and 90 % higher for LHC, THC, and +HC, respectively. The deformation capacities of the LDSS hollow tubular slender columns are similar irrespective of the cross-sectional shapes and class classification. Based on the FE studies, the applicability of the currently available design standards for stainless steel, such as the European specification, EN 1993-1-4 (2006), and the American specification, ASCE 8-02 (2002), for the design of LDSS hollow tubular stub and slender columns were assessed. Both the current design specifications are generally capable of predicting the LDSS hollow tubular column strengths. However, the European specification tends to be more conservative compared to the American specification.

In the next part of the investigation, the benefits in the use of NRSs LDSS hollow tubular columns over those of the representative square section is extended to concrete-filled lean duplex slender stainless steel tubular (CFDSST) columns with an objective to explore and compare the structural behaviours such as the load and deformation capacities as well as to study the effect of the LDSS tube thickness and concrete compressive strength on the CFDSST columns. Similar to the approach followed in the analyses of LDSS hollow tubular columns, the concept of equal LDSS material cross-sectional area was followed (LDSS material being expensive compared to concrete), thereby, resulting in ~ 36 % reduction of concrete core area in the NRSs CFDSST columns as compared to the representative square CFDSST columns. The study suggested that NRSs CFDSST stub columns are more effective for specimens with a normal concrete strength (≤ 40 MPa). Also, NRSs CFDSST stub columns filled with high strength concrete can also be used

with the advantages of providing lighter sections (i.e. 36 % reduction in the concrete core volume) with only 18 %, 15 % and 12 % reduction of strength compared to the representative square section for L-, T-, and +-shape sections, respectively, for 100 MPa concrete strength. The axial deformation at ultimate load in CFDSST stub columns decreases with increasing concrete strengths, but increases as the cross-sectional shape changes from square → L- → T- → +-shape. In fixed-ended CFDSST slender columns, for $\bar{\lambda} \sim < 0.5$, +-shape showed a 7 % higher strength and L- and +-shape showed similar strengths compared to the representative square section. For $0.5 \leq \bar{\lambda} \geq 1.5$, a linear increasing trend in strength is seen with increasing $\bar{\lambda}$. However, for $\bar{\lambda} > 0.5$, T- and +-shape showed a 10 % and 25 % more strength and L-shape showing a 10 % lower strength compared to the representative square section. Thus, in fixed-ended CFDSST slender columns, change of cross-sectional shape from square section to NRSs is significant, especially for T-shape and +-shape sections, and can promote the application of thin-wall LDSS tube. The influence of the cross-sectional shapes on the axial deformation capacity becomes less significant with increasing $\bar{\lambda}$, but becomes increasingly significant with decreasing $\bar{\lambda}$. Also, NRSs shows a higher axial deformation capacity for all $\bar{\lambda}$ considered compared to the representative square section, with +-shape section showing the highest axial deformation capacity. In comparison with the European specification, EN 1994-1-1 (2004), and the American specification, ANSI/AISC 360-05 (2005), for the design of fixed-ended CFDSST columns, FE strengths over predicts the design strengths, and also European specification tends to be more conservative compared to the American specification. For CFDSST slender columns, the design standards show over conservative results for square and L-shape sections and conservative for T-shape and +-shape sections. Also, the European specification gives a conservative estimation of strengths compared to the American specification for square and L-shape sections and vice versa in case of T-shape and +-shape sections.

ACKNOWLEDGEMENT

The following acknowledgements are an account of the indebtedness I feel towards those who have been a guiding light and source of inspiration towards the completion of this thesis.

I express my deepest sense of gratitude and reverence to my supervisor ***Dr. Konjengbam Darunkumar Singh*** for his constant valuable guidance, enthusiastic involvement and kind help throughout my research work. He has been a constant source of motivation and has treated me as a good friend. I will forever remain indebted to him for his untiring effort and help extended to me that went beyond academics. The extraordinary experience of working with him would be remembered in my life.

I am thankful to Dr. Arbind K. Singh, Dr. Arunasis Chakraborty and Dr. K.S.R. Krishna Murthy, my doctoral committee members, who has contributed with valuable remarks and ideas from time to time to give a good shape to this thesis.

I would like to thank the Department of Civil Engineering for providing the required facilities for my research work. Cooperation extended by the Head of the Department and office staffs deserves special thanks from my side. I would like to express my sincere thanks to all faculty members who helped me directly or indirectly during my research work.

I would like to express my sincere gratitude for the privilege of having associated with good friends like Sonu, Sachi, Jackie, Ashish, Moa, Shahnilo, Rosang, Kiran and Narendra.

I will cherish the friendship of Deori, Romen and Bishwa for the enriching experiences, especially having vibrant, cheerful and entertaining company, making life more enjoyable in IIT-Guwahati.

The episode of acknowledgement would remain incomplete without the care and support of my parents, my brothers and sisters who are an inseparable part of my life. I owe my gratitude to all of them.

I would express my deepest gratitude to all my well wishers.

Last but not the least, I express my thanks to Almighty God for his constant guidance and blessing and giving the strength to complete this work.

M Longshithung Patton

CONTENTS

LIST OF FIGURES

LIST OF TABLES

NOTATIONS

A	Cross-sectional area
A_c	Cross-sectional area of the in-filled concrete cor
A_e	Effective cross-sectional area
A_s	Cross-sectional area of the LDSS tube
A_g	Gross cross-sectional area
B	Overall width of the plate
B_e	Effective width of the plate
c	Width of the flat plate
CFDSST	Concrete-filled Lean Duplex Slender Stainless Steel Tubular
CFSST	Concrete-filled Stainless Steel Tubular
D	Overall depth of the plate
E_0	Young's modulus (or initial tangent modulus)
$E_{0.2}$	Tangent modulus (stiffness) at 0.2% proof stress
E_{cc}	Initial modulus of elasticity of the confined concrete
FE	Finite Element
f_c	Unconfined cylindrical compressive strength of concrete = 0.8 f_{ck}
f_{cc}	Confined cylindrical compressive strength of concrete
f_{ck}	Characteristic cubic compressive strength of concrete
P_u	Ultimate load

$P_{u,FE}$	Ultimate load obtained from finite element analysis
$P_{ASCE\ 8\text{-}02}$	Design strength predicted by ASCE 8-02 (2002)
$P_{EN\ 1994\text{-}1\text{-}1}$	Design strength predicted by EN 1994-1-1 (2004)
$P_{EN\ 1993\text{-}1\text{-}4}$	Design strength predicted by EN 1993-1-4 (2006)
$P_{ANSI/AISC\ 360\text{-}05}$	Design strength predicted by ANSI/AISC 360-05 (2005)
i	Second moment of inertia
i_c	Second moment of inertia of concrete
i_s	Second moment of inertia of LDSS
k	Buckling coefficient
K	Ratio of flow stress in triaxial tension to that in compression
L	Length
LDSS	Lean Duplex Stainless Steel
L_e	Effective length
LHC	L-shaped hollow tubular column
n	Ramberg-Osgood exponent between zero strain and $\varepsilon_{t0.2}$
NRSs	Non-rectangular sections such as L-, T-, and +-shape sections
$n'_{0.2,1.0}$	Compound Ramberg-Osgood exponent based on $\sigma_{0.2}$ and $\sigma_{1.0}$
P	Load
P_{nom}	Normalised load = P_u/Af_y
P_u	Ultimate load
r	Radius of gyration
r_i	Internal corner radius
SHC	Square hollow tubular column
t	Thickness of the LDSS tube

THC	T-shaped hollow tubular column
+HC	+-shaped hollow tubular column

α	Imperfection factor
β	Angle of friction
β_0	Reliability Index
δ	Axial displacement
δ_u	Displacement at ultimate load
ε_c	Axial strain
ε_0	Elastic strain at the material 0.2% proof stress = $\sigma_{0.2}/E_0$
ε_c	Unconfined concrete strain
ε_{cc}	Confined concrete strain
ε_{nom}^{pl}	True plastic strain
ε_{nom}	Engineering strain
ε_u	Strain at $P_u = \delta_u / L$
$\varepsilon_{t0.2}$	Total strain at 0.2% proof stress
λ	Slenderness ratio
$\bar{\lambda}$	Non-dimensional member slenderness
λ_0	Limiting member slenderness
ν	Poisson's ratio
ρ	Reduction factor for local buckling
$\sigma_{0.2}$	0.2% proof stress
$\sigma_{1.0}$	1.0% proof stress
σ_{true}	True stress

σ_u	Ultimate stress
σ_y	Yield stress
χ	Buckling reduction factor
ω_0	Imperfection amplitude
μ	Coefficient of friction
μ_s	Poisson's ratio of the LDSS
μ_c	Poisson's ratio of concrete

CHAPTER 1

INTRODUCTION

1.1 BACKGROUND

Since the commercial birth of stainless steel in the early twentieth century, it is seen as the answer to the technical objective of achieving a non-corrosive steel, which not only offers better practical performances but also good aesthetic characteristics of a durable metallic surface compared to the parent carbon steel. Although it cannot replace carbon steel and other widely used construction materials, it has started playing an important role where durability, safety or aesthetic requirements cannot be cost effectively met by other materials.

The industrialization of stainless steel is generally attributed to an English metallurgist, Harry Brearley, in 1913, who referred to the material as 'rustless steel' and it was a cutlery manager, Ernest Stuart, who popularised the term 'stainless'. Stainless steel is an alloy of iron, chromium, nickel and to varying degrees of molybdenum, which does not readily corrode, rust or stain with water as ordinary steel does and is also called corrosion-resistant steel when the alloy type and grade are not detailed. The characteristic corrosion resistance of stainless steels is dependent on the chromium content and is enhanced by additions of molybdenum and nitrogen. Stainless steel contains a minimum of 10.5% to 11 % chromium content by mass. Chromium is the most important alloying element in stainless steels because it provides their basic corrosion resistance by creating

a very thin, invisible surface film in oxidizing environments. This film is an oxide that protects the steel from attack in an aggressive environment. Nickel is added, primarily, to ensure the correct microstructure and mechanical properties of the steel, very good corrosion resistance, constant magnetic permeability, very slight thermal expansion, and extraordinary good properties at high temperatures, excellent weldability, and a very good creep resistance (Buijs, 2008). Molybdenum substantially increases the resistance to both general and localized corrosion. It increases the mechanical strength and hardness and promotes a ferritic structure. Thus, the higher corrosion resistance of the material makes it one of the most durable families of construction materials, gaining clear advantages in terms of economy, reduction in environmental impact and lower maintenance costs.

Owing to the benefits of stainless steel, such as aesthetic appearance, high corrosion resistance, ease of maintenance, smooth and uniform surface, high fire resistance, high ductility and impact resistance, reuse and recycling capability, as well as ease of construction of stainless steel structural members, there has been an accelerating interest in the use of stainless steel in construction industry as structural members (Mann, 1993; Gardner, 2005). A lot of construction projects around the world are now using stainless steel as main structural material. Designers, engineers and architects alike have used stainless steels in most large modern structures, such as stadiums, skyscrapers, residential buildings, bridges and airports, with further use certain to feature a dominant material in the construction industry. Stainless steels are available in the form of plate, sheet, tube, bar, cold-formed structural sections and hot-rolled structural sections, with the most commonly used products for structural applications being cold-formed (square, rectangular and circular) hollow tubular sections, and nowadays elliptical shaped hollow tubular sections are also available (see Figure 1.1). Examples of the use of stainless steel material as structural members in the form of hollow tubular columns in construction fields are shown in Figure 1.2.

However, the use of stainless steel still remains limited in the construction industry due to its high material cost compared to other materials such as concrete. Hence, a composite (stainless steel-concrete) construction remains the ultimate choice for structural engineers, where there is an advantage in utilizing the beneficial material properties of both elements effectively (i.e. high compressive strength of the concrete and good tensile strength of the steel). It was in the late nineteenth century where the composite construction as we know it today was first used in both buildings and bridges in the United States. The use of composite steel-concrete beam, which is the earliest form of composite construction, having many advantages such as economic steel weight, reduced displacements, high ultimate strength and seismic proof (Porco *et al*., 1994), marked the beginning of the development of fully composite systems in steel and concrete. Composite construction can be used in a range of fields, from civil and industrial construction through to the mining industry. In structural engineering, a composite construction has been mainly applied to bridges and multistorey buildings, with the more traditional forms of composite beams and composite columns. Concrete-encased steel sections (see Figure 1.3a) were used as columns in early tall buildings constructions in order to overcome the problem of fire and instability of the steel section (Ellobody and Young, 2011) along with the advantages of the steel section and concrete acting compositely to resist axial force and bending moment. Also, the use of concrete-filled tubular sections (see Figure 1.3b), where concrete is filled inside the stainless steel hollow tubular sections, as structural columns are recently getting popular due to its high strength, high ductility, and large absorption capacity (e.g. Hu *et al*., 2003) along with many inherent aforementioned additional beneficial factors involved in the use of stainless steels. The following sub-sections discusses briefly the beneficial factor involved in the use of lean duplex stainless steel (LDSS) material as a structural member and concrete-filled tubular columns in construction industries.

1.1.1 Lean duplex stainless steel

Over the last 20 years, significant developments have occurred in materials processing, thereby, the number of stainless steel grades have increased rapidly. Based on the composition of alloys and properties, stainless steel are commonly classified as ferritic, martensitic, austenitic and duplex (ferritic-austenitic) stainless steels to suit the structural requirements and environmental conditions. There are several factors, such as cost, strength-to-weight ratios, or location, which had to be taken into account while selecting the stainless steel grades. Cost is also an important factor as the use of stainless steel raises the initial price of the work between 5 % and 15 % (Nurberger, 1996). Generally, austenitic grades which contain ~ 8% - 11% nickel feature most prominently within the constructional industry. However, with increasing nickel prices, which also represents a significant portion of the cost to austenitic stainless steels, there is an escalation in the demand for LDSS, a subset of duplexes steels, with low nickel content ~ 1.5%, such as grade EN 1.4162 (Gardner, 2005b; Baddoo, 2008; EN 10088-4, 2009). This grade (EN 1.4162) of LDSS is generally less expensive and possesses higher strength than the commonly used austenitics (Theofanous and Gardner, 2009), thus enabling a reduction in section sizes leading to higher strength to weight ratios, and still retaining good corrosion resistance and high temperature properties (Gardner *et al*., 2010), weldability (Nilsson *et al*., 2008) and fracture toughness (Sieurin *et al*., 2007). Examples of the recent use of LDSS material as structural member in the form of hollow tubular columns in construction fields are shown in Figure 1.4. More details about the LDSS chemical composition, mechanical and physical properties and fabrication methods are available in Outokumpu (2013).

1.1.2 Concrete-filled tubular column

With the advent of stainless steel, recently, there have been an increasing number of significant uses of stainless steel in the construction industries because of many favourable factors associated in the use of stainless steels (as discussed in previous

sections). However, high material cost limits their use in conventional constructions thus giving rise to a new form of composite construction, such as, concrete-filled tubular columns. These type of construction techniques combines the advantages of both steel and concrete, and thus provide not only an increase in the load-carrying capacity but also rapid construction (Uy *et al*., 2006; Zhao *et al*., 2010). Also, concrete-filled tubular columns in particular does not need any formwork or reinforcement and the amount of stainless steel used can be greatly reduced by concrete filling as reported by several researchers (e.g. Young and Ellobody, 2006; Lam and Gardner, 2008; Dabaon *et al*., 2009; Uy *et al*., 2011). Thus, the use of concrete-filled tubular columns in a building project can significantly reduce the overall cost of a structure (Johansson, 2002). Some of the largest and highest engineering adopted stainless steel concrete-filled tubular columns on tall buildings are given in Figure 1.5.

1.2 OBJECTIVES OF THE INVESTIGATION

The following are the objectives of the investigation:

1) Considering the beneficial factors involved in the use of LDSS material, this thesis adopts LDSS material, to investigate the structural behaviour of LDSS hollow tubular stub and slender columns under pure axial compressive loading in order to give a slight push to further advance in the field of research and to encourage in the use of such material.

2) To investigate the behaviour of LDSS concrete-filled tubular stub and slender columns under pure axial compressive loading.

1.3 OUTLINE OF THE REPORT

This Chapter provides a brief introduction of stainless steel material and its use as an important structural member in the construction industry as well as the driving issues

associated with the use of new grade of stainless steel such as LDSS material. The benefits in the use of concrete-filled tubular columns are also highlited.

Chapter 2 contains a detailed literature review of relevant work carried out by various researchers on stainless steel hollow and concrete-filled tubular columns. As most of the studies were related to conventional shapes such as square, rectangular and circular, the need to extend the studies relating to special shapes such as L-, T-, and +-shape sections are discussed. Limited studies regarding the use of LDSS material as hollow and concrete-filled tubular columns are brought out in this chapter. Based on the literature review it has been concluded that there is still a need for more studies relating to LDSS hollow as well as concrete-filled tubular columns.

In **Chapter 3**, numerical analyses on LDSS hollow tubular stub columns are presented. Finite element (FE) modeling was carried out on hollow tubular stub columns with L-, T, and +-shape sections (Non-Rectangular Sections or NRSs) and representative square section to investigate the behavior of such sections under pure axial compression. The results are shown in the form of load and deformation capacities as well as the failure modes. The applicability of current existing codes, such as European and American specifications, in the design of LDSS hollow tubular stub columns are also discussed.

Chapter 4 presents an extended study of the LDSS hollow tubular stub columns to fixed-ended LDSS hollow tubular slender columns under pure axial compression. The effect of cross-sectional shapes and column length on the load and deformation capacities as well as the failure modes was presented. Discussion on the applicability of current existing codes, such as European and American specifications, in the design of fixed-ended LDSS hollow tubular slender columns was presented.

FE analyses on LDSS concrete-filled tubular stub columns with NRSs and representative square section under pure axial compression are presented in **Chapter 5**. Parametric studies were conducted to investigate the effect of cross-section, LDSS tube thickness and concrete strength on the load and deformation capacities. Comparison of FE results with the codal specifications, such as European and American specifications, was done to

assess the applicability of the codes in the design of LDSS concrete-filled tubular stub columns.

Chapter 6 presents an extended study of the LDSS concrete-filled tubular stub columns to fixed-ended LDSS concrete-filled tubular slender columns. The buckling behavior of concrete-filled LDSS tubular slender columns at different column lengths along with the effects of cross-sectional shape was investigated. FE results are then compared with the codal specifications, such as European and American specifications, to assess the applicability of the codes in the design of fixed-ended concrete-filled LDSS tubular slender columns.

Summary and conclusions of the important findings from the current work are provided in **Chapter 7**.

Few suggestions for further work are highlighted in **Chapter 8**.

Appendices are added in the end of this thesis. **Appendices A, B, D and F** give the detailed design sample calculation of a square LDSS hollow and concrete-filled tubular stub as well as slender columns using the European and American specifications. The detailed modeling of the concrete core in concrete-filled tubular stub columns through Drucker-Prager yield criterion plasticity model have been explained in **Appendix C**. **Appendix E** presents the detailed modeling of the concrete core in concrete-filled tubular slender columns through Concrete Damage Plasticity model.

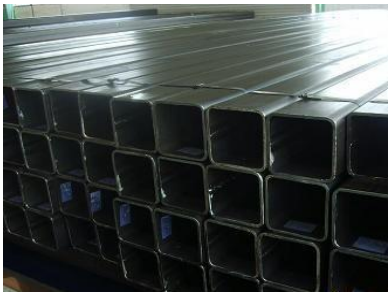

(a) Square

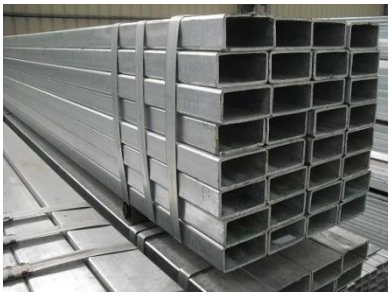

(b) Rectangular

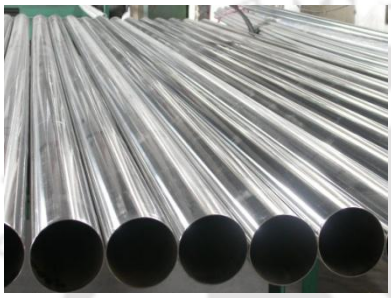

(c) Circular

(d) Oval

Figure 1.1: Hollow tubular stainless steel sections of (a) Square, (b) Rectangular, (c) Circular and (d) Oval (Courtesy: SMC).

(a) Transit terminal in Wisconsin
(Courtesy: SSEF)

(b) Stratford DLR station in London
(Courtesy: SSEF)

(c) Inland Steel Building in Chicago
(Courtesy: Galinsky)

(d) Gatwick Airport in London
(Courtesy: Geograph)

Figure 1.2: Examples of the use of stainless steel hollow tubular columns.

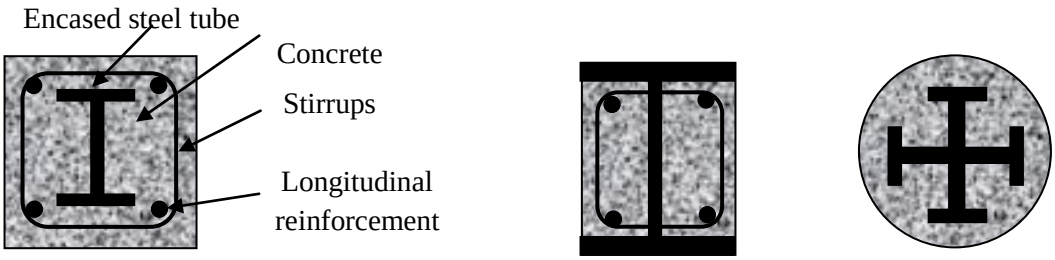

(a) Schematic concrete encased steel sections

(b) Schematic concrete-filled tubular stainless steel sections

Figure 1.3: Examples of composite stainless steel-concrete column sections.

(a) Celtic Gateway footbridge in UK
(Courtesy: Wikimedia)

(b) Siena footbridge in Italy
(Courtesy: Theofanous and Gardner, 2009)

Figure 1.4: Examples of the use of lean duplex stainless steel material.

(a) SEG Plaza in China
(Courtesy: Wikipedia)

(b) Tecno-Station in Japan
(Courtesy: NSSMC)

Figure 1.5: Examples of the use of concrete-filled stainless steel tubular columns.

CHAPTER 2

LITERATURE REVIEW

2.1 INTRODUCTION

In the past, the use of stainless steel has only been limited to minor applications in structural engineering. As the construction industry continues to evolve and with more in-depth research into their structural behavior, stainless steels are used in the construction industry as main structural members due to several advantageous factors involved in the use of such materials as discussed in Chapter 1. Yet the high price of stainless steel greatly limits the application to major construction projects. Hence, a new and innovative approach is to adopt a stainless steel-concrete composite construction, which not only offers several advantages to the structural behavior over stainless steel structural members as discussed in Chapter 1, but also delivers the economies of a concrete construction with the speed of construction and the constructability of stainless steel structural members, resulting in significant economies in the overall structure of a building project (Johansson, 2002).

This chapter presents a critical review of previous work on structural stainless steel hollow and concrete-filled tubular columns under pure axial compressive loading that is pertinent to this report. Development of the stainless steel stress-strain curve through various material models such as Ramberg-Osgood model (Ramberg and Osgood, 1943), Rasmussen model (Rasmussen, 2003), and Gardner and Ashraf model (Gardner and Ashraf, 2006) as well as the development of the stress-strain relationship for the confined

concrete core in concrete-filled tubular columns proposed by Saenez (1964) are presented. A general summary of the types of processes that are used for production of hollow tubular sections are also mentioned in this chapter. On the basis of the literature review, gaps in the current understanding of structural behavior, particularly to LDSS hollow and concrete-filled tubular columns, have been identified.

2.2 STRUCTURAL HOLLOW TUBULAR COLUMNS

Exploiting its corrosion resistance and aesthetic appeal, stainless steel is often employed for exposed structural elements (e.g. Baddoo *et al*., 1997). Stainless steel tubular construction, such as the hollow tubular columns, are also becoming increasingly popular for structural applications as they shows excellent properties with regard to loading in compression, torsion and bending in all directions combined with an attractive characteristics as detailed in Chapter 1. Until recently, the primary tubular cross-section shapes available to structural engineers and architects have been square, rectangular and circular (e.g. Theofanous *et al*., 2009a&b). Hollow tubular columns with square and circular sections are often most effective as compression members (e.g. Virdi, 1981; Young and Hartono, 2002; Lui and Young, 2003; Gardner and Nethercot, 2004c; Gardner and Nethercot, 2004a&b; Zhou and Young, 2005; Ashraf *et al*., 2008; Dabaon *et al*., 2009), rectangular hollow tubular columns, with greater stiffness about one principal axis than the other, are generally more suitable in bending (e.g. Virdi, 1981; Talja and Salmi, 1995; Gardner and Nethercot, 2004c; Ellobody and Young, 2005; Zhou and Young, 2005; Dabaon *et al*., 2009). Nowadays, elliptical sections are also getting popular in many structural applications due to its aesthetic external profile as well as offering inherent torsional stiffness and suitability for resisting flexure similar to that of a rectangular section (e.g. Kempner and Chen, 1974; Chen and Kempner, 1976; Grigorenko and Rozhok, 2002; Gardner, 2005a; Theofanous *et al*., 2009a&b; Nowzartash and Mohareb, 2009; Nowzartash and Mohareb, 2011).

Several researchers have studied on stainless steel (mainly austenitic) hollow tubular stub columns with commonly available cross-sectional shapes such as square (Lui and Young, 2003; Gardner and Nethercot, 2004c; Dabaon *et al*., 2009), rectangular (Talja and Salmi, 1995; Gardner and Nethercot, 2004c; Zhou and Young, 2005; Dabaon *et al*., 2009), circular (Gardner and Nethercot, 2004a&b; Ashraf *et al*., 2008), and elliptical (Gardner and Ministro, 2004; Gardner, 2005a; Gardner and Chan, 2007; Chan and Gardner, 2008; Law and Gardner, 2013). Also, several literatures were reported on the flexural buckling response of stainless steel hollow tubular slender columns with square (Rasmussen, 2000; Gardner, 2002; Lui and Young, 2003; Ellobody, 2007; Dabaon *et al*., 2009), rectangular (Gardner, 2002; Ellobody, 2007; Dabaon *et al*., 2009), circular (Rasmussen, 2000; Young and Hartono, 2002), and elliptical (Zhao *et al.*, 2007; Theofanous *et al.*, 2009) sections. The investigations were focused to assess the effect of cross-sectional aspect ratio, stainless steel tube thicknesses and member slenderness on the strength and structural behavior of such columns. Some examples of experimental investigation on stainless steel hollow tubular columns are shown in Figure 2.1.

2.3 STRUCTURAL CONCRETE-FILLED TUBULAR COLUMNS

In recent years the use of concrete-filled tubular columns has gained its popularity throughout the world, particularly in Australia and the Far East due to the structural (i.e. high strength and high energy dissipation ability) and economical advantages offered by concrete-filled tubular columns over hollow tubular construction (Lam and Gardner, 2008). In addition to the enhancement in structural properties, a considerable amount of construction time can be reduced as formwork can be avoided. Because of its superior structural behavior, concrete-filled tubes have been generally used as columns or piers in buildings or infrastructures. It can be said that a concrete-filled tubular column delivers the economies of a reinforced-concrete column, resulting in significant economies in the overall structure of a building project (Hassanein, 2010). Since the mid-twentieth century, various research on concrete-filled tubular steel columns have been reported (e.g. Furlong, 1967; Knowles and Park, 1969; Furlong, 1974; Ge and Usami, 1992; Ge and

Usami, 1994; Boyd *et al*., 1995; Bradford, 1996; Hajjar and Gourley, 1996; Shams and Saadeghvaziri, 1997; Morino 1998; Schneider, 1998; Uy, 1998; Zhang and Shahrooz, 1999; Liang and Uy, 2000; Bradford *et al*., 2002).

There are several investigations related to concrete-filled stainless steel tubular (CFSST) stub columns under pure axial compression with sections, such as, square (e.g. Han and Yao, 2004; Ellobody and Young, 2006a&b; Uy *et al*., 2011; Yang and Han, 2012), rectangular (e.g. Young and Ellobody, 2006a&b; Uy *et al*., 2011), circular (e.g. Giakoumelis and Lam, 2004; Han and Yao, 2004; Uy *et al*., 2011; Yang and Han, 2012), and elliptical (e.g. Zhao *et al*., 2007; Yang *et al*., 2008; Zhao and Packer, 2009; Jamaluddin *et al*., 2013) sections, reporting the effect of cross-section capacities, concrete compressive strength and stainless steel tube thickness on the structural behavior. Also, several studies has been performed on CFSST slender columns pertaining to sections such as square (Vrcelj and Uy, 2002; Uy *et al*., 2011), rectangular (Gho and Lui, 2004; Uy *et al*., 2011), circular (Kato, 1996; Uy *et al*., 2011; An *et al*., 2012), and elliptical (Jamaluddin *et al*., 2013), to quantify the influence of member geometry and constituent material properties on the structural behavior. Some examples of recent experimental investigation on stainless steel concrete-filled tubular columns are shown in Figure 2.2.

2.4 STRUCTURAL LDSS MATERIAL

Although good amount of literatures are available on the studies relating to stainless steel tubular columns, there are still limited studies done on LDSS tubular columns. Due to the benefits in the use of LDSS material as structural members (and its early application in construction fields as discussed in Section 1.1.1), its use has seen significant growth and development over the past two decades. The following sections presents the study reported on LDSS hollow tubular and concrete-filled tubular columns, followed by a report on the currently available design standards for stainless steels, and the assessment by various researchers on their applicability for the design of structural LDSS.

2.4.1 Previous research on LDSS

Till date, not much literature is available on studies relating to LDSS hollow and concrete-filled tubular columns. Theofanous and Gardner (2009) performed experimental studies on LDSS square and rectangular hollow tubular columns under axial compression and supplemented by FE studies, and parametric studies were performed to generate results over a wider range of cross-sectional and member slenderness. The results were presented in terms of ultimate loads and comparison with the currently available design standards for stainless steel was achieved. A comparison of structural performance of LDSS and that of the other more commonly used austenitic grades was made. It was found that; overall, LDSS is shown to offer superior structural performance compared to the austenitic grades and at a lower cost. A test program on cold-formed LDSS square and rectangular hollow tubular columns at different lengths compressed between pinned ends was conducted by Huang and Young (2013). The results are resented in terms of ultimate loads and the failure modes, and also compared with the available design standards. Umbarkar *et al*., 2013 presented a FE study to see the effect of various geometrical parameters of circular single perforation on the critical/ultimate buckling load of a LDSS circular stub column loaded axially. Also, recent investigation on structural LDSS sections includes the flexural behavior of LDSS girders with slender stiffened webs (Hassanein and Silvertre, 2013); shear failure mechanisms characteristics of LDSS plate girders with slender webs (Hassanein, 2011; Saliba and Gardner, 2013b); and cross-section stability of LDSS welded I-sections (Saliba and Gardner, 2013a), suggests an increasing interest in the use of LDSS as a structural material and has a great potential for replacing other stainless steel grades as it betters in terms of structural performance along with lower cost, making it an attractive choice in the future for structural applications.

Hassanein (2010) was the first to report studies regarding FE modeling for LDSS concrete-filled tubular stub columns under uniform axial compression loading. The study was predominantly concerned with two parameters: cross-sectional shape and concrete compressive strength. Based on the study, new design strength was proposed to represent

the behaviour of LDSS concrete-filled tubular stub columns. Hassanein *et al*. (2013) presented the study on the fundamental behavior of circular LDSS concrete-filled tubular stub column under axial compression. Parametric studies were undertaken to investigate the effects of concrete compressive strength and diameter-to-steel tube thickness (*D*/*t*) ratio on the behavior of LDSS concrete-filled tubular stub columns. The results showed that the ultimate axial strength of the column increases with increasing concrete compressive strength but decreases with an increase in the *D*/*t* ratio.

2.4.2 Design guidance on structural stainless steel

Design of stainless steel structures is supported by various design standards, such as, American, European, Japanese, Canadian, Australian and New Zealand specifications. This section reviews currently available design standards for stainless steel structures, with particular emphasis on the American and European specifications as the other design standards are based on these two design standards.

Hammer and Peterson (1955) performed the first research program on structural stainless steel. The first specific design rules for structural stainless steel was produced in America by the AISI (1968) based of the research program carried out by Johnston and Winter (1966). Following an extensive research project at Cornell University, in 1974 the specification was revised and published as the AISI (1974). In 1990, the first ASCE standard ANSI/ASCE-8-90 was introduced to provide the Load and Resistance Factor Design (LRFD) method and the Allowable 132 Stress Design (ASD) method criteria for the design of structural stainless steel. This ASCE standard has been revised in 2002 as SEI/ASCE 8-02 (2002) based on a larger amount of available test data. In 2006, the specification ANSI/AISC 360-05 (2005) provided an integrated treatment of ASD and LRFD, and thus combines and replaces earlier specifications that treated the two design methods separately.

In 1988, a joint industry project was undertaken by The UK Steel Construction Institute to develop the Euro Inox ‘Design Manual for Structural Stainless Steel’ for European

stainless steel structures; but not published until 1994 (Euro Inox, 1994). In 1996, the European Standards organization (CEN) issued the 'pre-standard' Eurocode ENV 1993-1-4 (1996): Design of steel structures, and contains supplementary rules for stainless steels. This standard (ENV 1993-1-4, 1996) is closely aligned with the guidance in the Euro Inox (1994), with some changes arising from the need to align to the provisions for carbon steel in ENV 1993-1-1 (1996) as much as possible. The standard ENV 1993-1-4 (1996) has now been published as a full European standard EN 1993-1-4 (2006). Also, EN 1993-1-1 (2004) which applies to a design of composite structures and members for building and civil engineering works, using the limit state design philosophy, was approved by CEN in 2004.

In 1995, the Japanese stainless steel structural design standard was issued (SSBJA, 1995). Based largely of the Canadian design standard for carbon steel, the South African structural stainless steel code was published in 1997 (SABS, 1997). Most recently, in 2001, the Australian and New Zealand design code for cold-formed stainless steel structures (Aust/AZS, 2001) was published. Development of the code was described by Rasmussen (2000b).

Currently, there is only one grade of lean duplex included (1.4362) in EN 1993-1-4 (2006), and the amendment of EN 1993-1-4 (2006) is underway to include different grades of lean duplexes to provide engineers with a useful sub-set of stainless steels to specify in structural applications (Gardner, 2013).

Based on the experimental investigation conducted for LDSS hollow tubular columns (Theofanous and Gardner, 2009; Huang and Young, 2012), the current buckling curve for stainless steel hollow sections given by European specification (EN 1993-1-4, 2006) is deemed suitable. Also, Huang and Young (2012) suggested that the currently available American specification (ASCE 8-02, 2002) is capable of predicting the column test strengths of LDSS material. Hassanein (2010) performed numerical studies on concrete-filled LDSS tubular stub columns; it was found that the design rules specified in the American specification (ASCE 8-02, 2002) are highly conservative for square and

rectangular sections while they are conservative in the case of European specification (EN 1994-1-1, 2004).

2.5 STRUCTURAL TUBULAR COLUMNS WITH NRSs

In engineering structures, special-shaped reinforced concrete columns with L-, T-, and +-shape sections (Non-Rectangular Sections or NRSs) (see Figure 2.4) are extensively used because of their convenient construction at beam-column joints, larger moment of inertia of cross-section that leads to much higher capacity for resisting lateral load, and ability to provide a flushed wall face, resulting in an enlarged and more regular usable indoor floor space area (Xu and Wu, 2009). So, reinforced concrete columns with NRSs were used in residential high-rise buildings and are welcomed by architects.

Some of the studies reported on the behavior of reinforced concrete columns with NRSs, such as, L- and T-shape (e.g. Joaquin, 1979; Cheng and Thomas, 1989; Mallikarjuna and Mahadevappa, 1992; Dundar and Sahin, 1993; Yau *et al*., 1993; Zhang and Ye, 2003; Gao *et al*., 2005; Wang *et al*., 2007; Xu and Wu, 2009) and +-shape (e.g. Xu and Wu, 2009), suggests a research interest and importance in the use of such specially shaped columns and the need for more study to understand their structural behaviours.

Extensive investigations have also been carried out to study the mechanical performance of concrete-filled steel tubular columns with NRSs, such as L-shape (e.g. Ohashi, 1992; Lin *et al*., 2009; Zuo *et al*., 2012; Zhang and Yang, 2012) and T-shape section (e.g. Du *et al*., 2008; Wang *et al*., 2009; Yang *et al*., 2010) in order to assess the effect of steel tube thicknesses, concrete strengths and stiffeners on the load and deformations capacities as well as the failure modes of such columns.

2.6 MATERIAL MODELLING

Accurate representation and good understanding on the basic material behaviour, such as, the stainless steel and the concrete core in concrete-filled tubular columns, are fundamental to any research project as it contributes to the prediction of the structural behavior of the members during loading. The following sub-sections explain briefly the various material models available in describing the material behavior of stainless steel as well as for the confined concrete core through a widely adopted three stage model proposed by Saenz (1964).

2.6.1 Stainless steel

The stress-strain behavior of stainless steel differs from that of carbon steel in a number of respects. The most important difference is in the shape of the stress-strain curve, with carbon steel exhibiting a linear elastic behavior up to the yield stress (σ_y) and a plateau before strain hardening, unlike stainless steel which has a more rounded response with no well-defined yield stress and the material exhibiting significant strain hardening (Bearley, 1989) (see Figure 2.5). As the transition between elastic and plastic behavior is not well defined, convention defines the yield point as the 0.2 % proof stress ($\sigma_{0.2}$) obtained at the point of the 0.2% plastic strain and the limit of proportionality of the stainless steel is generally defined as the stress at 0.01 % plastic strain ($\sigma_{0.01}$). For improved efficiency, several types of models describing existing functions that have been applied to the modelling of the stainless steel non-linear behavior are discussed on their suitability for describing accurate material stress-strain response for all the stainless steel families.

2.6.1.1 Ramberg-Osgood model

The Ramberg-Osgood model (1943) (defined in Equation 2.1) is a popular material model which provides a smooth stress-strain curve for all values of strain for nonlinear

materials with fewer physical parameters e.g., Initial Young's modulus of Elasticity of stainless steel (E_s), and material constants K and n. Considering the proof stress as the stress value associated with 0.2% plastic strain the Ramberg–Osgood expression is generally given by Equation 2.1.

$$\varepsilon = \frac{\sigma}{E_s} + K\left(\frac{\sigma}{\sigma_{0.2}}\right)^n \tag{2.1}$$

where K and n are the material nonlinearity indices of the stress-strain behaviour. The degree of non-linearity varies with different grades of stainless steel. Using K = 0.002, Equation 2.1 has been reported to give reasonably good predictions of stainless steel material stress–strain behaviour up to the $\sigma_{0.2,}$ but observed to overestimate the corresponding stress beyond $\sigma_{0.2}$ (see Figure 2.6).

2.6.1.2 Rasmussen model

Rasmussen (2003) adopted Mirambell and Real's (2000) modified Ramberg-Osgood model by using an expression beyond $\sigma_{0.2}$ for the complete stress-strain curve for stainless steel alloys (see Equation 2.2).

$$\varepsilon = \frac{(\sigma - \sigma_{0.2})}{E_{0.2}} + \varepsilon_u \times \left(\frac{\sigma - \sigma_{0.2}}{\sigma_u - \sigma_{0.2}}\right)^m + \varepsilon_{t0.2} \tag{2.2}$$

where, σ_u, $\varepsilon_{u,}$ m and $E_{0.2}$ are the ultimate tensile strength, ultimate strain, additional strain hardening exponent and the tangent stiffness at $\sigma_{0.2,}$ respectively, (see Figure 2.6). $E_{0.2}$ is given in Equation 2.3.

$$E_{0.2} = \frac{\sigma_{0.2} E_s}{\sigma_{0.2} + 0.002 n E_s} \tag{2.3}$$

The additional strain hardening exponent m proposed by Rasmussen (2003) is given Equation 2.4.

$$m = 1 + 3.5\frac{\sigma_{0.2}}{\sigma_u} \tag{2.4}$$

The ultimate tensile stress (σ_u) and ultimate strain (ε_u) are determined by using Equation 2.5 and 2.6 in terms of $\sigma_{0.2}$, E_0 and n.

$$\frac{\sigma_{0.2}}{\sigma_u} = \frac{0.2 + 185\left(\frac{\sigma_{0.2}}{E_s}\right)}{1 - 0.0375(n-5)} \tag{2.5}$$

$$\varepsilon_u = 1 - \frac{\sigma_{0.2}}{\sigma_u} \tag{2.6}$$

EN 1993-1-4 (Annexure C) (2006) adopted the model proposed by Rasmussen (2003) as a guideline for material modelling of stainless steel.

2.6.1.3 Gardner and Ashraf model

In the absence of necking phenomena in compression, Gardner and Nethercot (2002) noted that the two stage model given in Equation 2.2 was limited to the description of tensile stress–strain behaviour because of its dependency on the ultimate stress σ_u and the corresponding ε_u. Hence, Gardner (2005) proposed that 1% proof stress, $\sigma_{1.0}$ and corresponding strain, $\varepsilon_{t1.0}$ be adopted in place of the ultimate stress. The resulting model as recently proposed by Gardner and Ashraf (2006) is given by Equation 2.7, which applies for stresses greater than $\sigma_{0.2}$.

$$\varepsilon = \left(\frac{\sigma - \sigma_{0.2}}{E_{0.2}}\right) + \left(\varepsilon_{t1.0} - \varepsilon_{t0.2} - \frac{\sigma_{1.0} - \sigma_{0.2}}{E_{0.2}}\right) \times \left(\frac{\sigma - \sigma_{0.2}}{\sigma_{1.0} - \sigma_{0.2}}\right)^{n'_{0.2,1.0}} + \varepsilon_{t0.2} \tag{2.7}$$

where $\varepsilon_{0.2}$ and $\varepsilon_{t1.0}$ are the total strains at $\sigma_{0.2}$ and $\sigma_{1.0}$, respectively and $n'_{0.2,0.1}$ is a strain hardening exponent. Equation 2.7 has been found to give good agreement with measured stress–strain curves in both tension and compression. Ashraf (2006) analysed all available coupon tests performed on stainless steel and proposed specific values for $n, n'_{0.2,0.1}$, and $\frac{\sigma_{1.0}}{\sigma_{0.2}}$ for commonly used stainless steel grades so that Equation 2.7 can be used with the knowledge of only two common parameters, *viz.* — $\sigma_{0.2}$ and E_0. Table 2.1 lists the values

proposed for the coefficients involved. Ashraf *et al*. (2006) compared the numerical models with experimentally obtained load–deformation response and failure modes, and found that Gardner and Ashraf (2006) model given by Equation 2.7 gives the best prediction.

2.6.2 Confined concrete core

In reinforced concrete columns, the increase in strength and ductility of the concrete confined by lateral reinforcements is well documented now (Mander *et al*., 1988; Sheikh and Uzmeri, 1988; Cusson and Paultre, 1994). On application of compressive loading, concrete undergoes volumetric changes with a lateral increase in dimensions due to Poisson's effect. The lateral expansion of the concrete is resisted when transverse reinforcements are provided in the form of the spirals, hoops or ties by developing tensile forces, consequently exerting a compressive reaction force on the concrete core. Thus, the concrete core experiences a state of multi-axial compression enhancing both the deformation capacity and strength of the concrete. The concrete core in such state is said to be confined.

The response of CFSST members is determined in part by the material response of the confined concrete core of which it is composed. Thus, analysis and prediction of structural response of CFSST members to static or dynamic loadings requires accurate prediction of the confined concrete core response to such loadings. In CFSST columns, the stainless steel tube provides passive confinement to the concrete core. In the case of passive confinement, the confining pressure is not constant as is the case for active confinement, and it also depends on the lateral deformation of the concrete core under axial load and the stress-strain relationship of the confining steel. However, it has been found that the concrete behavior is similar irrespective of whether the confining pressure is active or passive (Attard and Setung, 1996). Also, several researchers have studied on the triaxial state of stresses in concrete-filed steel tubular columns (Gardner and Jacobson, 1967; Tomii *et al.,* 1977; Orito *et al.,* 1987; Schneider, 1998). Concentrically

loaded CFSST stub columns are significantly affected by the difference between the values of Poisson's ratio of the steel tube (v_s) and the concrete core (v_c). At the initial stage of loading, Poisson's ratio of concrete is lower than that of steel; therefore, the steel tube expands faster in the radial direction than the concrete core, i.e. the steel does not restrain the concrete core. As the load increases and the compressed concrete starts to plasticize, the lateral deformations of the concrete catch up with those of the steel and, for further increase in load, the steel tube restrains the concrete core and the hoop stresses in the steel become tensile. At this stage and later, the concrete core is stressed triaxially and the steel tube biaxially. The following discusses the development of constitutive material model for the concrete core based on the current focus of research pertaining to the concrete confined by composition of plated elements rather than circular elements.

In CFSST columns, the confinement provided by the steel tube on the concrete depends on the steel depth-to-thickness (*D/t*) ratio. A lower value of *D/t* ratio provides high considerable confinement for the concrete, thereby improving the strength of CFSST columns. However, with inadequate confinement (i.e. a higher *D/t* ratio), there is a premature failure of the CFSST columns due to local buckling of steel tubes. Mander *et al.* (1988) defined the limiting *D/t* ratio between confined and unconfined concrete to be equal to 29.2. Figure 2.7 presents the equivalent uniaxial stress-strain curve for confined concrete, as well as the unconfined stress-strain concrete curve.

The value of unconfined concrete strain (ε_c) is usually taken as 0.003 as suggested by ACI specification (1999). Poisson's ratio (μ_c) in the elastic part of concrete under uniaxial compression stress ranges from 0.15 to 0.22, with a representative value of 0.19 to 0.2 according to ASCE (1982). In the current study, μ_c is taken as 0.2. The confined cylindrical concrete compressive strength (f_{cc}) and the corresponding confined strain (ε_{cc}) can be calculated from Equations 2.8 and 2.9, respectively, proposed by Mander *et al.* (1988).

$$f_{cc} = f_c + k_1 \sigma_{lat} \tag{2.8}$$

$$\varepsilon_{cc} = \varepsilon_c \left(1 + k_2 \frac{\sigma_{lat}}{f_c} \right) \tag{2.9}$$

where, σ_{lat} is the lateral confining pressure imposed on the concrete by the steel tube and dependent on σ_y, D/t ratio, cross-sectional shape, and stiffening means. The approximate values of σ_{lat} can be interpolated from the measured values given by Hu *et al*. (2003). The value of σ_{lat} has significant effect for steel tubes with small D/t ratio. However, with steel tube D/t ratio greater than or equal to 29.2, the value of σ_{lat} is taken as zero (i.e not significant) (Mander *et al*., 1988). The factors k_1 and k_2 are taken as 4.1 and 20.5, respectively, as given by Richart *et al*. (1928).

The first part of the curve is the elastic part upto the proportional limit, which is taken as ($0.5f_{cc}$). The initial modulus of elasticity of the confined concrete (E_{cc}) (in MPa) is highly correlated to its compressive strength and can be calculated with reasonable accuracy from the empirical equation ACI (1999) as given in Equation 2.10:

$$E_{cc} = 4700\sqrt{f_{cc}} \tag{2.10}$$

The second part of the curve is the nonlinear portion, starting from the proportional limit stress ($0.5f_{cc}$) to the confined concrete strength (f_{cc}). The stress-strain relationship proposed by Saenz (1964) has been widely adopted as the uniaxial stress-strain curve for concrete and it has the following form:

$$f = \frac{E_{cc}\varepsilon}{1+(R+R_E-2)\left(\frac{\varepsilon}{\varepsilon_{CC}}\right)-(2R-1)\left(\frac{\varepsilon}{\varepsilon_{CC}}\right)^2+R\left(\frac{\varepsilon}{\varepsilon_{CC}}\right)^3} \tag{2.11}$$

Where:

$$R_{cc} = \frac{E_{cc}\varepsilon_{cc}}{f_{cc}} \tag{2.12}$$

$$R = \frac{R_E(R_\sigma - 1)}{(R_\varepsilon - 1)^2} - \frac{1}{R_\varepsilon} \tag{2.13}$$

The constants R_σ and R_ε are taken equal to 4.0 as recommended by Hu and Schnobrich (1989).

The third part of the confined concrete stress–strain curve with $\varepsilon > \varepsilon_{cc}$, which is used to describe the softening behavior of the concrete, is the linear descending line from the f_{cc} to a value lower than or equal to rk_3f_{cc} with the corresponding strain of 11 ε_{cc}. The

material degradation parameter (k_3) depends on the steel D/t ratio and σ_y, and can be approximately calculated from the empirical equations given by Hu *et al*. (1989). The reduction factor (r) was introduced by Ellobody *et al*. (2006) based on the experimental investigation conducted by Giakoumelis and Lam (2004), to account for the effect of different concrete strengths. The value of r is taken as 1.0 for concrete with cube strength (f_{ck}) equal to 30 MPa. While, the value of r is taken as 0.5 for concrete with f_{ck} greater than or equal to 100 MPa, as given by Tomii (1991) and Mursi and Uy (2003), and linear interpolation is used to determine the value of r for concrete cube strength between 30 and 100MPa.

2.7 INITIAL GEOMETRIC IMPERFECTIONS

The importance of initial geometric imperfections in thin-walled structures has been recognized by researchers for more than three decades, which was limited to ordinary carbon steel sections. More recently, the development of design codes for stainless steel requires identification of initial geometric imperfection characteristics for stainless steel members.

Apart from many beneficial factors involved in the use of stainless steel hollow tubular sections in structural applications, they are often susceptible to initial geometric imperfections (local or global or both). These imperfections are an inseparable property of real structures and may arise during manufacturing, carrying and fabrication, etc, in the form of bowing, warping, and twisting as well as local deviations and greatly influences the structural behavior. Hence, the knowledge of the magnitude of member imperfections is required because it affects the member capacity and especially those carrying axial compressive loads (ENV 1993-1-1, 1992). There are several studies which consider different types of initial geometric imperfections and ways of their introduction into a numerical model. One way of taking initial geometric imperfections into account, which dominates in design codes, is to induce them by applying an appropriate pattern of additional loading. However, it works well only for the global type of imperfections, e.g.

in the case of multistory frames with columns exhibiting deviations from the vertical direction. In the case of local geometric imperfections, it seems reasonable to introduce perturbed geometry by measured values of imperfections. However, this procedure can be tedious when the FE method is used. Moreover, it is not a general procedure since it can be applied only to those members for which the imperfections have been measured. Thus, the following sub-sections reviews a general approach of tackling these imperfections pertaining to thin-walled hollow tubular columns.

2.7.1 Local geometric imperfections

In real life, stainless steel hollow tubular columns composed of plates are often affected by local geometric imperfections, which are characterized by dents and regular undulations in the plates. Initial plate imperfection magnidute (ω_0) given by Equation 2.14 is often considered as a fixed multiple of plate thickness.

$$\omega_0 = K_p t \tag{2.14}$$

where K_p is a constant.

Dawson and Walker (1972) considered a value of 0.2 for K_p which conservatively fit to test data on cold-formed steel cross-sections. However, its general applicability is questionable since it does not consider the other important parameters such as material strength, fabrication process and boundary conditions. They also proposed the following expressions for simply supported steel plates under compression and bending as:

$$w_0 = \tau\left(\frac{\sigma_y}{\sigma_{cr}}\right)t \tag{2.15}$$

$$w_0 = \gamma\left(\frac{\sigma_y}{\sigma_{cr}}\right)t \tag{2.16}$$

$$\sigma_{cr} = E_s\varepsilon = E_s\lambda\left(\frac{\Delta l}{L}\right) \tag{2.17}$$

where σ_{cr} is the elastic critical buckling stress determined from the buckling analysis, τ and γ are constants, λ is the eigen value obtained from the results of FE analysis, Δl is the

initial displacement at the movable end input in the boundary conditions, and L is the length of the column. These two equations are much more rational in the sense that they include both material property and boundary conditions in addition to the plate thickness of the plate. For convenience in both hand and numerical analyses, the shape of a local initial geometric imperfection is often assumed to be the same as that of the lowest buckling mode, or eigenmodes (Dawson & Walker, 1972).

Sun and Butterworth (1998) incorporated initial geometric imperfections on the developed non-linear FE model in the form of half sine waves along the length and with four different values of K_p, such as 0.167, 0.333, 0.5, and 0.667, and found that, K_p = 0.167, gave the best agreement with the test results.

Chou *et al*. (2000) conducted FE modeling of cold-formed lipped channel and hat section carbon steel stub columns and used various values of K_p, such as, 0.1, 0.5 and also Dawson and Walkers's (1972) proposal. Ultimate load predictions obtained using Dawson and Walkers's (1972) proposal with $\tau = 0.3$ gave consistent results.

Gardner (2002) investigated the suitability of Dawson and Walkers's (1972) proposed formulations, Equations 2.15 and 2.16, for roll-formed stainless steel hollow tubular members under compression, and based of the studies Equation 2.18 was proposed (i.e the local geometric imperfection magnitude for plates), based on the measured imperfections,

$$w_0 = 0.023\left(\frac{\sigma_{0.2}}{\sigma_{cr}}\right)t \qquad (2.18)$$

Gardner (2002) found that the proposed equation gave good predictions, which predicts imperfection amplitudes on the basis of both geometric and material properties of cross-sections.

Theofanous and Gardner (2009) conducted FE studies on LDSS hollow tubular columns with square and rectangular sections under axial compression with K_p = 0.1 and 0.01 and and also the imperfection amplitude proposed by Gardner (2002) (Equation 2.18). It was

found that the ultimate load and end shortening at ultimate load are generally well-predicted for the measured imperfection amplitude proposed by Gardner (2002) and K_p = 0.01, whereas with the value of K_p = 0.1, there is a clear underestimation of the load carrying capacity and end shortening at ultimate load of the stub columns.

However, in contrast to the use of local geometric imperfections in any FE studies for hollow tubular columns, generally the effect of local geometric imperfections on CFST columns were neglected because the strength reduction is not significant compared to thin-walled hollow tubes owing to the delaying effect of steel tube local buckling by the core concrete (e.g. Tao *et al*., 2009, Hassanein, 2010).

2.7.2 Global geometric imperfections

In fact, all stainless steel hollow tubular columns in framed structures in reality are geometrically imperfect in some degree and if a frame is geometrically imperfect, lateral deflection commences as soon as a loading is applied, which create bending deformation on the columns. In framed structures, global geometric imperfections are initial out-of-straightness of a member, which is described as a lateral deflection of a member relative to a straight line between its end points. As a result of initial out-of-straightness, even a column with perfectly aligned axial load undergoes compression and bending. In design of any stainless steel hollow tubular columns, initial out-of-straightness is to be considered as it is one of the main effect factors on the ultimate strength (Galambos, 1998). The following discusses some general approach of representing the initial out-of-straightness in hollow and concrete-filled slender tubular columns.

Galambos (1998) reported that due to the manufacturing process employed, stainless steel hollow tubular columns were generally much straighter than steel columns. Stainless steel hollow tubular columns could have the maximum initial out-of-straightness from *L*/3000 to L/8000 (where *L* in the specimen length) with an average of around *L*/ 6500. Lui and Young (2003) performed experimental studies on fixed-ended stainless steel square hollow tubular column compression members, where, the value of the initial out-of-

straightness of the columns measured at the mid-heights were ranged from *L*/950 to *L*/4970. Han (2007) took the maximum value of initial out-of-straightness of *L*/1000 according to the Chinese code (GB50017-2003, 2003). Hong and Varma (2009) performed sensitivity analysis on the imperfection magnitude and considered *L*/7500 as the value of maximum initial out-of-straightness for modeling and analysis. Theofanous and Gardner (2009) conducted an experimental test on pin-ended LDSS hollow tubular columns by considering an initial out-of-straightness in all the test specimens as *L*/1500. This value is the statistical mean of geometric imperfections in steel structural members as suggested by Bjorhovde (1972). Sensitivity analysis through FE study was also performed, in which the values of initial out-of-straightness considered were *L*/500, *L*/1000, *L*/1500 and *L*/2000. It was found that the most accurate and consistent prediction of test response is obtained for an imperfection magnitude of *L*/1500. Huang and Young (2013) measured the initial out-of-straightness on the test specimens of pin-ended cold-formed LDSS hollow tubular slender columns. The average overall initial out-of-straightness at mid-height ranged from *L*/2085, *L*/2167, *L*/2157, *L*/2435, *L*/1992 and *L*/2155.

In general, global geometric imperfections for real columns vary randomly depending on different supplied stainless steel tubes. To the best of author's knowledge, there are no specific rules regarding selection of an appropriate value of initial out-of-straightness for hollow tubular slender columns. Based on the literature survey, the magnitude of initial out-of-straightness chosen in the studies usually ranges from *L*/1000 to *L*/10000. Further research is needed to recommend a codified initial out-of-straightness, and to present a suitable design method for stainless steel hollow tubular slender columns.

2.8 THE PRODUCTION OF STAINLESS STEEL TUBULAR SECTIONS

Stainless steel is typically produced in an electric arc furnace (EAF) from a mixture of alloying elements and scrap carbon steel and/or stainless steel. Partial products such as blooms, billets and slabs which are produced from the continuous caster are the starting material for the manufacture of a number of final products, such as, tubular and hot rolled sections (see Figure 2.8). Hot rolled sections (I-, C-, or L-sections) are formed through reheated blooms and billets, whilst tubular sections are formed by reheating the slabs.

For stainless steel hollow tubular sections, the production route has an important influence on the stainless steel final material properties as it is sensitive to plastic deformation and thermal effects, thereby, influencing the residual stress and geometric imperfections found in the sections. Structural stainless steel tubular sections are typically produced in two principal ways, such as, the seamless method or by welding (see Figure 2.9). The majority of seamless tube is made by piercing the solid ingot or bar and then elongating it in a rotary forge (called the Pilger process). Welded hollow sections for structural applications are produced by electric or submerged arc welding.
For the very thick sections, seamless sections may be used. Square or rectangular hollow sections are sometimes made by using channel sections, which are welded together or by shaping a single strip to the required shape and closing it by a single weld, preferably in the middle of a face. Similar approach as discussed may be followed in making NRSs with ease. More detailed information about the manufacturing processes and the limitations in sizes can be obtained from CIDECT (1984) and Dutta and Wurker (1988).

2.9 SUMMARY OF THE LITERATURE REVIEW

This chapter presents an overview of previous research on stainless steel and LDSS tubular (both hollow and concrete-filled) columns. The development of stress-strain curve for stainless steel material and the confined concrete core in concrete-filled tubular

column based on the material models available has been presented. Based on the literature review, the following concluding remarks can be made:

1) The structural behavior of stainless steel hollow tubular columns with commonly available shapes, such as, square, rectangular, circular and elliptical, have been extensively investigated and are getting very popular in structural application due to its excellent properties with regard to loading in compression, torsion and bending in all directions combined with its aesthetic external profile in the use of such structural stainless steel sections.
2) The use of concrete-filled tubular columns has gained its popularity throughout the world, and such composite construction delivers the economies of a reinforced-concrete column, resulting in significant economies in the overall structure of a building project.
3) Several literatures have been reported to understand the structural behavior of CFSST columns with square, rectangular, circular and elliptical sections, and to quantify the influence of member geometry and constituent material properties on the structural behavior.
4) The benefits in the use of LDSS material in terms of its superior structural performance along with lower cost compared with other stainless steel grades have been addressed and indicate a great potential in the future for replacing other stainless steel grades for structural applications.
5) There are many design standards available in the design of stainless steel structures. Currently the amendment of EN 1993-1-4 (2006) is underway to include different grades of lean duplexes to provide engineers with a useful sub-set of stainless steels to specify in structural applications.
6) The importance and advantages in the use of special-shaped reinforced-concrete columns with NRSs has been addressed. More studies are required to better understand the benefits in the use of such special-shaped sections as hollow or concrete-filled tubular columns.

7) Elaborate discussions on the various material models available in describing the material behavior of stainless steel families as well as confined concrete core model development are detailed. Stainless steel material model development proposed by Gardner and Ashraf (2006) was found to give the best prediction. For the confined concrete core material model development, the widely used stress-strain relationship proposed by Saenz (1964) was adopted.
8) Many researchers have recognized the importance of initial geometric imperfections, such as the local and global geometric imperfections, in thin-walled structures. The local geometric imperfection equation proposed by Gardner (2002) gave good predictions. The magnitude of initial out-of-straightness chosen in the studies usually ranges from L/1000 to L/10000. Further research is needed to recommend a codified initial out-of-straightness, and to present a suitable design method for stainless steel hollow tubular slender columns.

In the context of this thesis, the following areas have been identified justifying the present investigation.

Many have studied and analysed the structural behaviours of stainless steel hollow and concrete-filled tubular columns pertaining to commonly available shapes such as square, rectangular, circular and elliptical sections. The benefits in the use of LDSS material in terms of its superior structural performance along with lower cost and the importance and advantages in the use NRSs to columns has been brought out. However, relatively little attention being paid on the structural behaviour of tubular columns (both hollow and concrete-filled) having equal material consumption, as stainless steel material being expensive, along with the beneficial factors involved in the use of special shaped sections, such as the NRSs. Such a study would be particularly relevant to predictive assessment of mechanical strength and behavior of structures under axial compression and would serve as a valuable addition to the scarce body of literature on this issue in the literature.

Table 2.1: Compound Ramberg–Osgood parameters obtained from coupon test results.

Type	Grade	Forming process	Tension or compression	n	$n'_{0.2,1.0}$	$\frac{\sigma_{1.0}}{\sigma_{0.2}}$
Austenitic	1.4301	Press-braked	Tension	5.8	2.7	1.20
			Compression	5.3	2.5	1.20
		Roll-formed	Tension	5.4	3.4	1.14
			Compression	4.3	2.7	1.25
Ferritic	-	-	-	4.4	3.1	1.17
	-	-	-	6.4	3.2	1.16
	-	-	-	7.3	3.3	1.14
Duplex	-	-	-	5.0	3.4	1.15

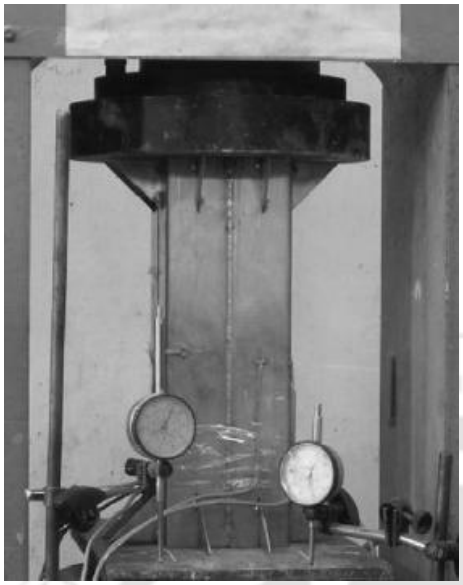

(a) Square stub column
(Dabaon *et al*., 2009)

(b) Rectangular slender column
(Ellobody and Young, 2005).

Figure 2.1: Examples of experimental test on stainless steel hollow tubular columns.

(a) Square stub column
(Young and Ellobody, 2006)

(b) Square slender column
(Uy *et al*., 2011)

Figure 2.2: Examples of experimental test on stainless steel concrete-filled tubular columns.

(a) Square stub column
(Theofanous and Gardner, 2009)

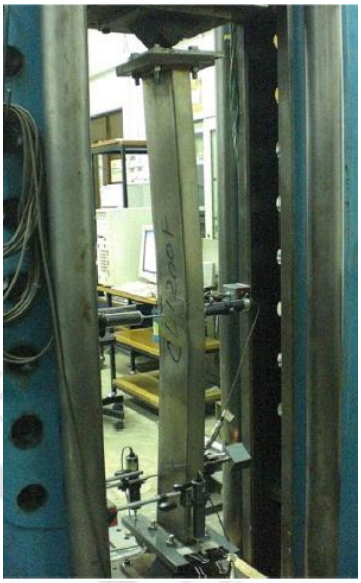

(b) Rectangular slender column
(Huang and Young, 2013).

Figure 2.3: Examples of experimental test on LDSS hollow tubular columns.

(a) L-shape

(a) T-shape

(a) +-shape

Figure 2.4: Tested specimens of specially shaped reinforced concrete columns (Xu and Wu, 2009).

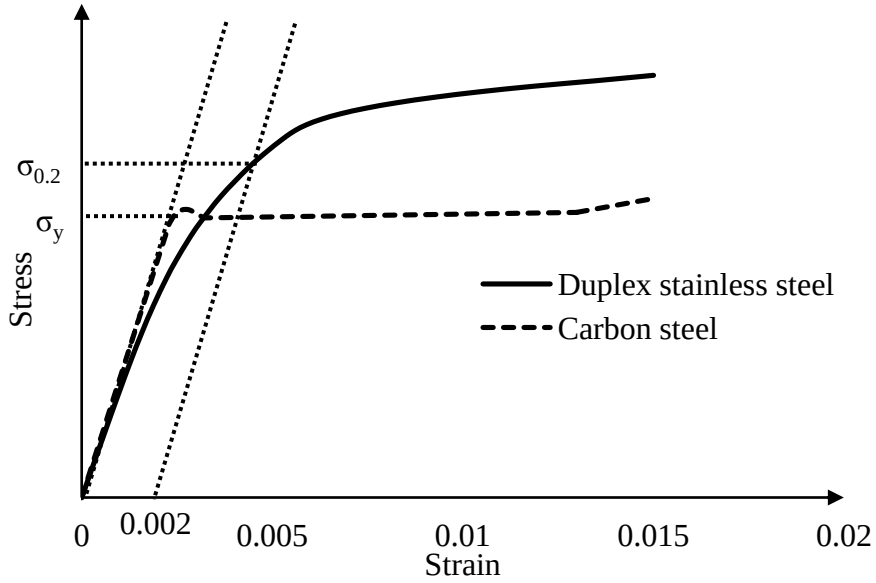

Figure 2.5: Schematic diagram of stainless steel and carbon material stress-strain behavior (Courtesy: BSSA).

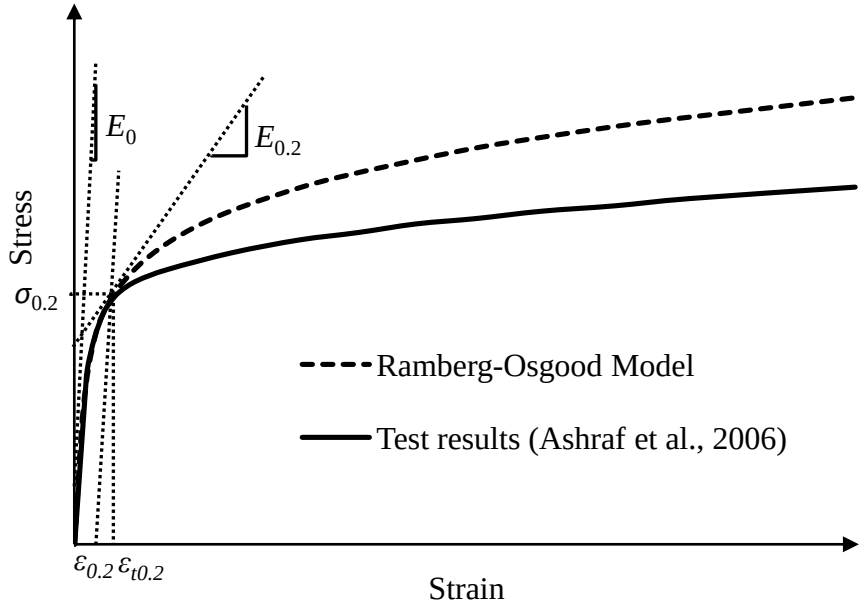

Figure 2.6: Illustration of the stress-strain curve of the Ramberg-Osgood model with test results (Ashraf *et. al.*, 2006) for an austentic Grade 1.4301 tensile coupon with $\sigma_{0.2}$ = 296 Mpa and n = 5.8.

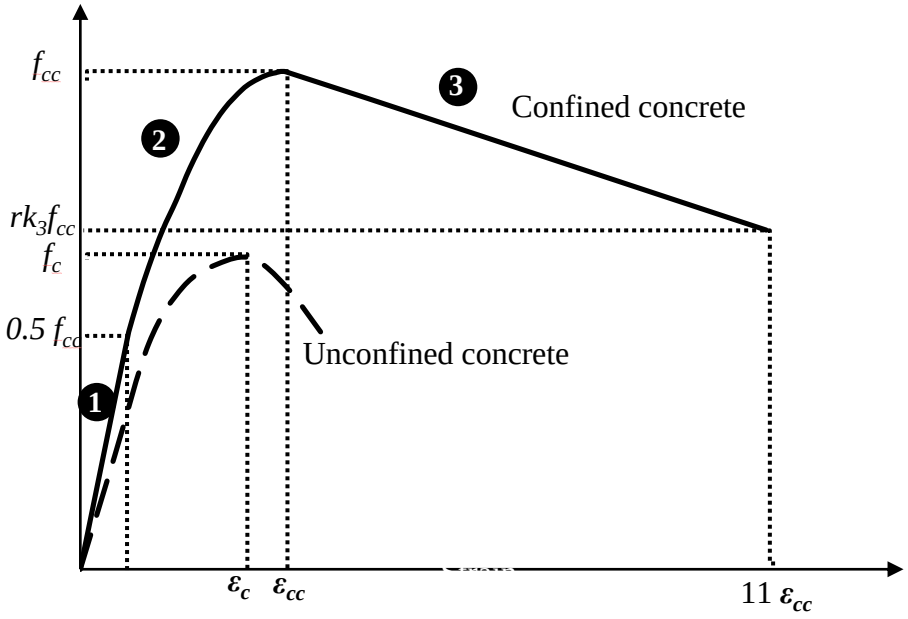

Figure 2.7: Equivalent uniaxial stress-strain curve for confined and un-confined concrete (after Sanez, 1967).

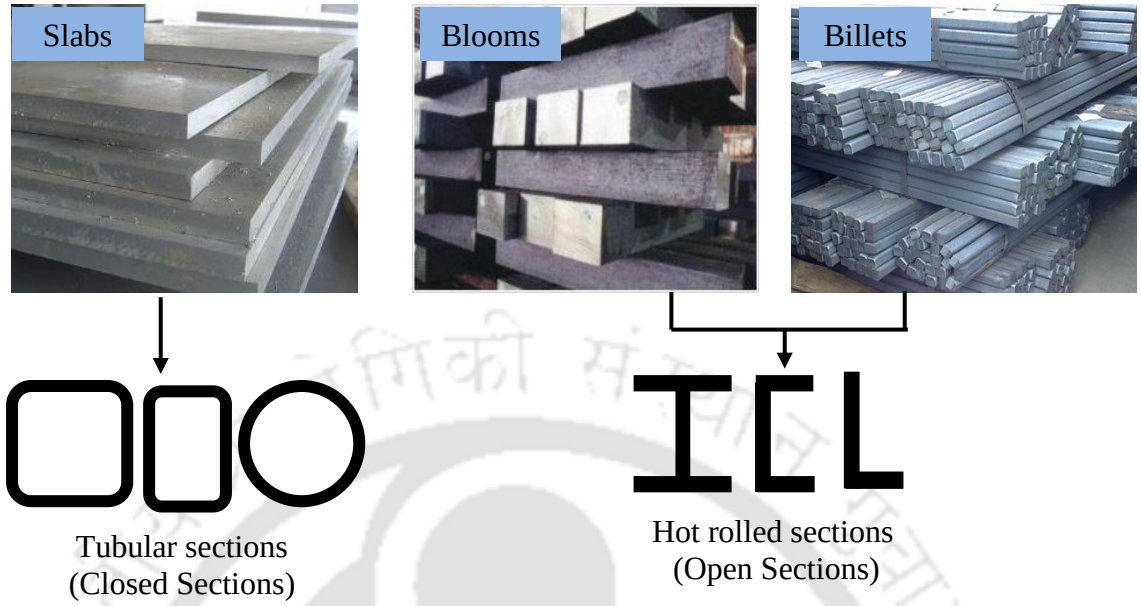

Figure 2.8: Identification of partial products (slabs, blooms and billets) and finished products (tubular and hot rolled sections).

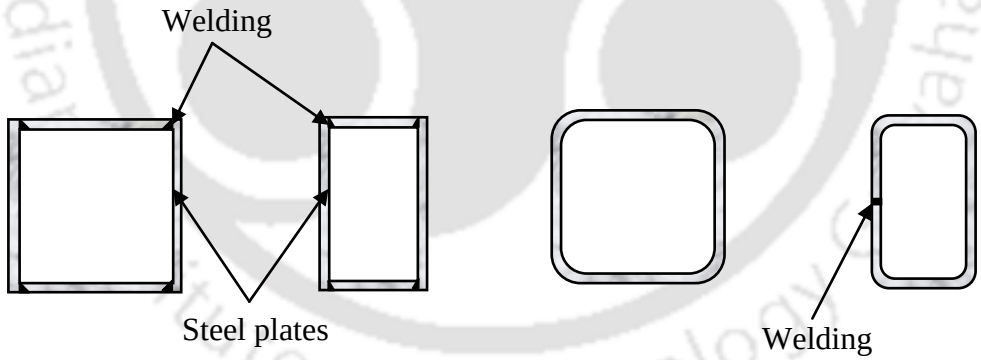

(a) Welded plate sections (b) Hot-rolled and cold-rolled sections

Figure 2.9: Examples of hollow tubular sections formed from different processes.

CHAPTER 3

NUMERICAL MODELLING OF LEAN DUPLEX STAINLESS STEEL HOLLOW STUB COLUMNS

3.1 INTRODUCTION

Numerical techniques have now become an efficient tool for analyzing the behavior of structures provided that suitable care is taken to ensure that the finite element (FE) model is appropriate and the input parameters are accurately specified. Owing to the expense and impracticality of generating comprehensive data on the behaviour of stainless steel structures through experimentation, a FE study was undertaken using the general-purpose FE software package Abaqus (2009) throughout the study. In the present work, the FE models were verified with the experimental test done by other researchers based on similar areas of work, to generate further results through variation of appropriate parameters in the FE models.

This chapter focuses on the axial compressive resistance of hollow tubular stub columns with NRSs and a representative square section having equal LDSS material cross-sectional area as that of the NRSs (i.e. equal material consumption). The main objective of the study is to see the effect of cross-sectional shape and thickness of the LDSS tube on the structural behavior, such as, the load and deformation capacities of hollow tubular stub columns. The FE results were compared with the currently available design standards for stainless steel, such as the European specification (EN 1993-1-4, 2006) and the American specification (ASCE 8-02, 2002), to assess their applicability in the design

of LDSS hollow tubular columns. Reliability analysis of the design standards was also carried out based on the FE studies.

3.2 FE MODELLING

Compared to carbon steel which has a well defined yield point, LDSS exhibits a rounded stress-strain curve with no sharp yield point as discussed in Section 2.6.1. Accurate representation of the basic material behavior forms the most important aspects of any FE simulation. The following sub-sections presents various details for achieving an accurate FE model representation of LDSS hollow tubular stub columns as also followed by several researchers.

3.2.1 Boundary conditions and analysis technique

The present modeling approach follows those published in the literature (e.g. Gardner and Nethercot, 2004; Ellobody and Young, 2006; Theofanous and Gardner, 2009; Dai and Lam, 2010; Hassanein, 2010). Figure 3.1 shows a typical geometry of a square LDSS hollow tubular stub column. The bottom part is fixed while the top loaded part is allowed to have free vertical translation (i.e. along the loading axis line). The boundary condition is accomplished using two rigid plates that were tied to the column ends via surface-to-node tie constraints available in Abaqus (2009). The rigid body reference nodes (RP-1 and RP-2 for bottom and top, respectively) associated with the rigid plates was then used to restrain all degrees of freedom apart from vertical translation at the loaded end, which was constrained via kinematic coupling to follow the same vertical displacement. A central concentrated normal load was applied statically at the RP-2 (see Figure 3.1) using displacement control, thus applying uniform pressure at the top edges of the column through the rigid plate.

In the present study, linear elastic analysis technique using the *BUCKLING command was employed to obtain the relevant eigenmodes, which were subsequently used to represent initial geometric imperfections in subsequent nonlinear analyses. All the stub columns were treated as geometrically nonlinear static problems involving buckling. Abaqus (2009) offers several techniques to analyse this type of problem and among the available options the 'modified RIKS method' was chosen because of its simplicity and widespread use by several researchers in similar applications (e.g. Ashraf *et al*., 2006; Huang and Young, 2012). In the modified RIKS method, the load is applied proportionally in several load increments. In each load increment the equilibrium iteration is performed and the equilibrium path is tracked in the load displacement space. The nonlinear effects arising from geometric and material nonlinearity were included using the 'NLGEOM' option and *PLASTIC command respectively as stated in Abaqus (2009).

3.2.2 FE mesh

Shell elements are generally used to model thin-walled structures. Abaqus (2009) includes general-purpose shell elements as well as elements that are specifically formulated to analyse 'thick' and 'thin' shell problems. The general purpose shell elements provide robust and accurate solutions to most applications although, in certain cases, enhanced performance may be obtained using the thin or thick shell elements (Ashraf *et al*., 2006). General purpose shell elements include transverse shear deformation, whilst thin shell elements may be used in cases where transverse shear flexibility is negligible. Stainless steel structural members are generally modeled using either of the following two shell elements available in Abaqus (2009): general-purpose thin-shell S9R5 (e.g. Mirambell and Real, 2000; Gardner and Nethercot, 2004; Ashraf *et al*., 2006) or S4R, (e.g. Gardner and Nethercot, 2004; Ellobody and Young, 2005; Ashraf *et al*., 2006; Theofanous and Gardner, 2009; Theofanous *et al*., 2009; Hassanein, 2010; Hassanein, 2011). Ashraf *et al*. (2006) suggested that there is no significant difference

between the results obtained using the two commonly employed shell elements. However, in line with similar previous investigations on the behavior of LDSS hollow tubular sections, S4R elements are known to provide accurate solutions to most applications (for both thin and thick shell problems) and agreed well with the test results (Theofanous and Gardner, 2009; Hassanein, 2010; Hassanein, 2011). Hence, S4R elements has been utilised in the current study to discretize the FE models. The aspect ratios of the elements are kept at ~ 1.0 in all the FE models (see Figure 3.1).

One of the most important aspects of FE modeling is to identify a suitable mesh size. Finer meshes are always preferred to obtain better predictions. But there is no general guidance for this fineness. As a result a convergence study is a pre-requisite to find a suitable mesh for FE investigation. Although finer meshes are expected to provide better predictions, they make the whole process more expensive in terms of the computational time. A compromise is therefore needed between the level of accuracy and the solution cost. In the present study, σ_{cr}, which is expressed by Equation 2.15 and calculated first by obtaining the eigen value through elastic linear analysis technique, was used to check mesh convergence by monitoring the σ_{cr} with mesh refinement (see Figure 3.2). A suitable mesh size is chosen at a point where there is little improvement in the σ_{cr} with further mesh refinement. Accordingly, the element size of about 20 – 30 mm was chosen in all the FE models and the aspect ratio of the elements are kept at ~ 1.0.

3.2.3 Appraisal of existing material models

This section describes existing functions that have been applied to the modelling of non-linear behavior, and discusses their suitability for describing LDSS material stress-strain response. The minimum specified material properties of LDSS Grade EN 1.4162 according to EN 10088-4 (2009) are $\sigma_{0.2}$ of 530 MPa and ultimate stress (σ_u) of 700-900 MPa. The Poisson's ratio of the LDSS material was suitably chosen as 0.3 (e.g. Theofanous and Gardner, 2009; Hassanein, 2010; Hassanein, 2011). The compressive flat

material properties given by Theofanous and Gardner (2009) (see Table 3.1) were used in deriving the stress-strain curve of LDSS material through three models *viz.*, Ramberg-Osgood (Ramberg and Osgood, 1943; Hill, 1944), Rasmussen (2003) and Gardener and Asraf (2006) models, as discussed in the previour chapter. The last two models are modified versions of the original Ramberg–Osgood model. These models are tested in the present FE analyses by comparing with an experimental result from Theofanous and Gardener (2009) to select a suitable model appropriate for the present work.

3.2.4 Local geometric imperfections

Hollow tubular stub columns are often subjected to local geometric imperfections rather than global geometric imperfections, hence, local geometric imperfections was applied. In Section 2.8.1, a detailed discussion on local imperfection magnitude based on several literatures for inclusion in the FE models to accurately simulate the tests was shown. It was found that the value of ω_0 proposed by Gardner (2002) as given in Equation 2.16 also gave good agreement with the test results performed on structural LDSS hollow tubular columns. Hence, Gardner`s (2002) model was employed in deriving the ω_0 for further parametric studies of the LDSS hollow tubular columns. The proposed ω_0 by Gardner (2002) was used to perturb the geometry of the columns by scaling the lowest eigenmode in all the NRSs and the representative square section (see Figure 3.3).

3.3 VERIFICATION OF THE FE MODELS

In order to validate and compare the three material models mentioned in Section 2.7.1, the experimental result obtained by Theofanous and Gardner (2009) for LDSS (Grade EN 1.4162) square hollow-section columns (80x80x4-SC2) has been considered as the benchmark. The LDSS material properties and the measured dimensions by Theofanous and Gardner (2009) are given in Tables 3.1 and 3.2, respectively. It may be noted that this column has been formed using cold-form technique, resulting in different properties

between flat and corner portions of the column, and as a result residual stresses are induced due to inelastic material deformations during cold-forming. However, Gardner (2002) presented a study on the effect of residual stresses on hollow tubular columns and found that it causes only a small reduction in the stiffness but have little or negligible influence on the overall behavior or ultimate load carrying capacities. Hence, in the present study, only flat material properties are used in describing the FE models.

Figure 3.4 shows the stress-strain plot of LDSS material using the experimental values obtained by Theofanous and Gardner (2009) through various materials models *viz.*, Ramberg-Osgood, Rasmussen and Gardner and Ashraf models. It can be seen that beyond $\sigma_{0.2}$, Ramberg-Osgood model predicts higher stress values as compared to the Gardner and Ashraf and Rasmussen models. The material models shown in Figure 3.4 are then used as input parameters to Abaqus, by converting into true stresss (σ_{true}) and true plastic strains (ε^{pl}_{true}) using the following Equations 3.1 and 3.2.

$$\sigma_{true} = \sigma_{nom}\,(1+\varepsilon_{nom}) \tag{3.1}$$

$$\varepsilon^{pl}_{true} = \ln(1+\varepsilon_{nom}) - \frac{\sigma_{true}}{E_0} \tag{3.2}$$

where σ_{nom} and ϵ_{nom} are engineering stress and strain, respectively. Imperfection magnitude was seeded in the FE model as discussed in Section 3.2.4.

The deformed shape of a typical LDSS hollow tubular stub column is shown in Figure 3.5. It can be seen from Figure 3.5 that the column fails by local buckling and it occurs near the middle length consistent with other FE models (e.g. Gardner, 2005; Ellobody and Young, 2006) and experimental studies reported in the literature (e.g. Ellobody and Young, 2006; Lu *et al*., 2010; Yang *et al*., 2010; Zuo *et al*., 2010). Figure 3.6 presents the load (P)-axial displacement (δ) curves for the LDSS hollow tubular column (80x80x4-SC2). It is observed that all the three models predicts similar trend up to a load of ~ 800 kN (see Figure 3.6). From Figure 3.6, it can be seen that compared to Ramber-Osgood and Rasmussen models, Gardner and Ashraf model predicts closer ultimate load (P_u) (~ -0.18 %) and axial displacement at peak load (δ_u) (~ -3.85%) with the experimental values

(Thefanous and Gardner, 2009). Hence for all the subsequent FE analyses in the present study, the material model proposed by Gardner and Ashraf (2006) is used.

3.4 HOLLOW TUBULAR STUB COLUMN MODELLING

3.4.1 Introduction

As part of the current study, a series of FE models are investigated to provide data on the load and deformation capacity of LDSS hollow tubular stub columns with NRSs and representative square section under pure axial compression. Parametric studies are conducted to investigate the influence of key variables, such as thickness and cross-sectional shape, and to generate further results.

3.4.2 Development of the FE models

A total of 176 LDSS hollow tubular stub columns FE models were considered for the parametric studies. Figure 3.7 shows the LDSS hollow tubular stub column cross-sections considered in the study. The columns are labeled such that the cross-sectional shape can be identified from the label. For example, the label “SHC” and “+HC” defines the LDSS Hollow tubular stub Columns with a Square and +-shape sections, respectively.

The thickness of the LDSS tube was varied from 5 mm to 40 mm to encompass a wide range of cross-sectional slenderness, such as Class 3 (stocky) and Class 4 (slender) sections, as per EN 1993-1-4 (2006) codal provision, and will be discussed further in Section 3.5.7.1. The stub column lengths were set equal to three times the maximum outer dimension (i.e. 3 x 600 mm = 1800 mm), to avoid the effects of flexural buckling and end conditions similar to the approach followed by several other researchers (e.g. Ellobody and Young, 2006; Theofanous & Gardner, 2009; Hassanein, 2010). To simplify the modeling process corners of the NRSs and representative square section are assumed

to be at right angles (i.e. corner radii as in the validation (detailed in Section 3.3) are not considered), together with the possibility of welding at the corners and due to the lack of experimental material properties available for the corner region (in case of cold work techniques adopted in the manufacturing of hollow tubular members). Further, it is assumed that the material properties are same both at the flat and corner regions (also detailed in Section 3.3).

3.5 RESULTS and DISCUSSION

3.5.1 Introduction

The results of the FE analysis for hollow tubular stub columns was presented in terms of variation in the load and deformation capacities and failure modes with change in the cross-sectional shape and thickness of the LDSS tube as well as the presence of initial geometric imperfections in such columns. The FE results was then compared with the design strengths predicted by the EN1993-1-4 (2006) and ASCE 8-02 (2002) specifications. The applicability and reliability of these codes on LDSS hollow tubular stub columns was also assessed based on the FE studies.

3.5.2 Deformed shapes of NRSs and square section

Figure 3.8 shows typical failure modes at four times δ_u ($4x\delta_u$) for stocky and slender section of hollow tubular stub columns with NRSs and representative square section. It can be seen from Figure 3.8 that slender NRSs and representative square sections (both stocky and slender sections) failed with the same characteristic failure mode, whereby, all the faces of a section buckles locally alternately outward and inward (see Figures 3.8a-d and 3.8e). However, for stocky NRSs, local buckling is effectively prevented as compared to the representative square section. As the sectional shape changes from square → L → T → +-shape (i.e number of sides in a section increases), more effective

the section becomes in controlling local buckling due to increase in the stiffness of the section.

3.5.3 Load-axial deformation profile

Figure 3.9 shows the variation of $P/A_g f_y$ (or P_{nom}) (where A_g is the LDSS tube material gross cross-sectional area) with δ is shown for NRSs and the representative square section for LDSS tube thickness of 5 mm and 20 mm (i.e. to compare slender section (5 mm) and stocky section (20 mm)). The term $A_g f_y$ can be considered as the global yield load. A ratio of $P_{nom} < 1.0$ indicates that the sections are slender and can buckle prior to yield. For $P_{nom} \geq 1.0$ (i.e. stocky sections), yielding precedes buckling, and may be followed by hardening prior to buckling. It can be observed from Figure 3.9 that all the specimens (slender and stocky sections of NRSs and representative square section) possess similar ascending stiffness but the ultimate strength of the column increases as it goes from square, L-, T-, to +-shaped sections.

For slender sections, NRSs shows higher P_u compared to the representative square section in order of square < L < T < +-shape, and may be related to the higher stiffening effects of the corner regions and the potential for stress redistribution once local buckling of the wider plate face occurs. As the numbers of corners (right angled joints) are increased the P_u also increases. It can be primarily noticed that as it goes from square to +-shaped section, the sharper is the load-axial deformation behaviour (for t = 5mm). For stocky sections, the P_u is similar for all the sections due to all the cross-sectional shape considered effectively preventing the local buckling befor yielding, thus reaching the full material capacity. During the decending stage, load-axial displacement profile for slender section specimens of NRSs and representative square section are similar, however, for stocky sections, as the cross-sectional shape changes from square → L → T → +-shape, the descending tendency is slowed down and the ductility of the specimen is improved.

3.5.4 Strength capacity of NRSs and square section

Figure 3.10 shows a plot of P_u versus t to see the effect of cross-sectional shape on the load capacity of hollow tubular stub columns. It can be seen from Figure 3.10 that, for NRSs, there is approximately a linear increase of P_u with increasing LDSS tube thicknesses, whereas, for the representative square section, a milder increase of P_u is seen at lower thickness and linear increase at higher LDSS tube thicknesses. Also, for LDSS tube thickness < 30 mm, NRSs shows a higher strength capacity compared to the representative square section, with +-shaped section having the highest strengths, possibly due to the better delay in the local buckling shown by the NRSs. This may be attributed to the presence of shorter plate faces and more number of corners in the NRSs compared to the representative square section. However at LDSS tube thicknesses ≥ 30 mm, all the sections considered gave similar strengths, which may be due to the sections reaching the ultimate material capacity rather than failing by local buckling before yielding (see Figure 3.9). It can also be observed from Figure 3.10 that, for all the cross-sections considered, there appears to be a linear increase in P_u with increasing thicknesses of the LDSS tube.

Figure 3.11 shows the variation of P_u with cross-sectional shapes for different thicknesses of the LDSS tube. It can be observed from Figure 3.11 that there is a linear increase of P_u at lower thicknesses with change in the cross-section from S → L- → T- → +-shape. For changes in the cross-sectional shape from square to + shape, the increase in P_u are ~ 136%, 109%, 72%, 26%, 9% for 5mm, 10, mm, 15 mm, 20 mm and 25 mm, respectively, showing that the increase in P_u is more effective at thinner sections. At higher thickness (i.e $t \geq 30.0$ mm), all the section analysed gives similar strengths.

Variation of $P_u/P_{u,\mathrm{SHC}}$ (where $P_{u,SHC}$ is the P_u of the representative square section) with cross-sectional shape are shown in Figure 3.12. It can be seen from Figure 3.12 that the gain in P_u with change in the cross-sectional shape from square to L, T and +-shape are in the range 120%-150%, 130%-170%, 140%-230%, respectively, at lower thicknesses of

the steel tube (< 20 mm). Thus, it can be seen that by switching over to + shape sections, significant gain in ultimate strength can be obtained for all the thicknesses considered, with thinner sections giving more pronounced gain. Hence, it is possible to achieve higher P_u with increasing number of corners/sides rather than increasing thickness, providing a potential application for a much lighter structures and hence economizing construction cost.

3.5.5 Deformation capacity of NRSs and square section

Figure 3.13 shows a typical plot of ultimate strain at P_u ($\varepsilon_u = \delta_u/L$) versus t to see the effect of cross-sectional shape on the deformation capacity of hollow tubular stub columns. It can be seen that NRSs have notably better deformation capacity compared to the representative square section, with +-shape section estimating a much higher deformation capacity. The reason may be due to delay in the local buckling provided by the NRSs, thus providing a substantial strain hardening before failure giving a much higher ε_u (see Figure 3.9). Also, the deformation capacity increases with increasing thickness for all the hollow tubular stub columns analysed.

3.5.6 Comparison with design codes

The FE results for the LDSS hollow tubular stub columns are given in this chapter, where comparison is made between all the available FE results and predicted cross-section resistances according to EN 1993-1-4 (2006) and ASCE 8-02 (2002) specifications. A sample cross-sectional resistance calculation of a square hollow tubular stub column with the two design standards is given in Appendix A. The design based on the current existing design specifications are given only for stainless steel material and hence their applicability on LDSS is discussed through comparison with the FE results analyses.

3.5.6.1 Effective area determination

The current study comprises of two classes of cross-sectional slenderness for the hollow tubular stub columns considered *viz.*, Class 3 and Class 4 sections as per EN 1993-1-4(2006). For Class 3 sections, no deduction in the material cross-sectional area is made (i.e. A_g is considered) in the calculation of axial strengths of the column. However, for Class 4 sections, effective area (A_e) of the cross-section is used to account for the reduction in the resistance due to the effects of local buckling. Cross-section slenderness of a given section is calculated by $c/t\varepsilon$, where for Class 3 ($c/t\varepsilon \leq 30.70$) and Class 4 ($c/t\varepsilon > 30.70$). Here, c is the flat element width (see Figure 3.16), t is the element thickness and $\varepsilon = \left(\frac{235}{f_y} \frac{E_0}{210000} \right)^{0.5}$, f_y is the material yield stress.

For sections lying under Class 4, effective area (A_e) is to be calculated using the following Equation 3.3.

$$A_e = A_g - n_s t(c - B_e) \tag{3.3}$$

where n_s is number of sides of the column and B_e is the effective width ($B_e = \rho c$). The expressions used for computing the reduction factor (ρ) for local buckling by EN 1993-1-4 (2006) and ASCE 8-02 (2002) is given in Equation 3.4 & 3.5, respectively.

$$\rho = \frac{0.772}{\bar{\lambda}_p} - \frac{0.125}{\bar{\lambda}_p^{\,2}} \qquad \text{but} \leq 1.0 \tag{3.4}$$

$$\rho = \frac{1}{\lambda} - \frac{0.22}{\lambda^2} \qquad \text{but} \leq 1.0 \tag{3.5}$$

where $\bar{\lambda}_p$ and λ are the element slenderness as defined EN1993-1-4 (2006) and ASCE 8-02 2002), and given by Equation 3.6 & 3.7, respectively.

$$\bar{\lambda}_p = \frac{\left(\frac{c}{t}\right)}{28.4\varepsilon\sqrt{k}} \tag{3.6}$$

$$\lambda = \left(\frac{1.052}{\sqrt{k}}\right)\left(\frac{c}{t}\right)\left(\sqrt{\frac{f}{E_0}}\right) \quad (3.7)$$

Where k is the plate buckling coefficient and can be conservatively taken as 4.0, f is taken equal to F_n for compression members as per Section 3.4 of ASCE 8-02 (2002) specification.

3.5.6.2 Cross-section resistance

For the calculation of the cross-section resistance, the stub columns were considered as concentrically loaded compression members. The cross-section resistance based on EN1993-1-4 (2006) and ASCE 8-02 (2002) specifications is defined by Equation 3.8 & 3.9, respectively.

$P_{EN1993\text{-}1\text{-}4} = f_y A$ (3.8)

$P_{ASCE\ 8\text{-}02} = f_y A$ (3.9)

where A is the area of the section and determined as detailed in Section 3.5.6.1.

3.5.6.3 Comparison of FE strengths with design strengths

The variation of P_u with t is shown in Figure 3.17 for LDSS hollow tubular stub columns. It can be seen from Figure 3.17 that the variation of FE results of P_u with t is nearly linear (R^2 = ~ 0.99) for NRSs, in comparison to the representative square section where the increase in P_u is relatively slower in thinner sections (t < 12.5 mm). The % increase in P_u with 8 times increase in t (from 5 m to 40 mm) is of the order ~ 32 times, 22 times, 19 times and 13 times for SHC, LHC, THC and +HC, respectively.

The cross-sectional resistance according to the EN 1993-1-4 (2006) and ASCE 8-02 (2002) specifications are also plotted for comparison taking account of sectional classification as detailed in Section 3.5.7.1. From Figure 3.17, It can be seen that FE results over-predicts the codal design strengths, as also reported for similar studies of

LDSS hollow tubular stub column with square sections in the literatures (Theofanous and Gardner, 2009; Huang and Young, 2013).

For stocky sections both the specification predicts similar strengths due to the fact that the calculation of the cross-section resistance for both the specifications (Equations 3.8 and 3.9) is based on the gross area, thus giving similar prediction. It is seen that for stocky sections (t ~ > 20 mm), FE strengths over predicts the codal strengths by about 28 % for all the section studied. This may be related to the hollow tubular stub column tests approximately reaching the ultimate strength of the material, whereas the design strengths were calculated based on the $\sigma_{0.2}$ of the LDSS material.

For slender sections, at lower thicknesses of the steel tube (t ~ < 20 mm), FE strengths over predicts the European specification, EN 1993-1-4 (2006), by 28 %, 26 %, 21 % and 23 % for SHC, LHC, THC and +HC, respectively, and American specification, ASCE 8-02 (2002), by 5%, 6%, 9% and 17 % for SHC, LHC, THC and +HC, respectively. The difference in the values of cross-sectional resistance calculated by the two codal specifications for slender sections is related to the way the code takes care of the reduction in the resistance due to local buckling by calculating A_e as mentioned in Section 3.5.7.1. Based on the FE studies it can be inferred that, for slender sections, the American specification provides closer values as compared to the European specification, thus, providing a significant material saving through design by the American specification for slender sections.

3.5.6.4 Reliability analysis of the codes

In order to compare and assess the relative reliability inherent in the current stainless steel design codes to LDSS hollow tubular columns, such as, EN 1993-1-4 (2006) and ASCE 8-02 (2002), which is not covered in the current design specification, reliability analysis was carried out based on the FE studies.

A reliability analysis is detailed in the ASCE 8-02 (2002) specification, and a target reliability index (β_0) of 2.5 for stainless steel structural members as a lower limit is recommended. The design rules are considered to be reliable if the β_0 is greater than 2.5. When two or more designs are compared, the one with the larger β_0 is more reliable and is expressed by Equation 3.10.

$$\beta_0 = \frac{\ln\left(\frac{R_m}{Q_m}\right)}{\sqrt{V_R^2 + V_Q^2}} \tag{3.10}$$

$$\frac{R_m}{Q_m} = \frac{1.521}{\phi}(P_m M_m F_m) \tag{3.11}$$

where R_m, Q_m are the mean resistance, mean load effect, V_R , R_Q are the coefficient of variation of resistance and mean load effect, respectively, defined by Equation 3.12, 3.13, respectively.

$$V_R = \sqrt{(V_P^2 + V_M^2 + V_F^2)} \tag{3.12}$$

$$V_Q = \frac{\sqrt{(D_m V_D)^2 + (L_m V_L)^2}}{D_m + L_m} \tag{3.13}$$

where R_n is the nominal resistance, D_m & L_m are the mean dead and live load, respectively, and ASCE 8-02 (2002) specifies D_m = 1.05D_n and $L_m = L_n$, V_D and V_L are the corresponding coefficient of variation and takes the value of 0.1 and 0.25, respectively. As per Section 3.4.1 of ASCE 8-02 (2002), sections not subjected to torsional or torsional-flexural buckling, the values of mean ratio of yield strength to minimum specified value (M_m) and mean ratio of section modulus to published (nominal) value (F_m) are 1.10 and 1.00, respectively, V_M & V_F are the mean values and coefficients of variation of material and fabrication factors and takes the value of 0.10 and 0.05, respectively. In the reliability analyses, a resistance factor (φ) of 1/1.1 and 0.85 for concentrically loaded compression members as given by the EN 1993-1-4 (2006) and ASCE 8-02 (2002) specifications, respectively, were considered. The load combinations

used are $1.35D_n + 1.5L_n$ and $1.2D_n + 1.6L_n$ for EN 1993-1-4 (2006) and ASCE 8-02 (2002) specifications, respectively, where DL is the dead load and LL is the live load. Mean value (P_m) and coefficient of variation (V_p) of FE-to-codal load ratios are tabulated in Table 3.3 along with β_0 considering both the specifications.

Based on the reliability analyses it can be seen that, both the codes show $\beta_0 \geq 2.5$ when compared with the present FE results. Considering the lower limit of $\beta_0 = 2.5$ suggested by ASCE 8-02 (2002) specification for structural members, it can be inferred that both specifications can be adopted for all the design of LDSS hollow tubular stub columns. However, for LDSS hollow tubular stub columns, design based on the European specification tends to be slightly more reliable compared to the American specification, except for +-shape section, where the American specification tends to be more reliable.

3.8 CONCLUSIONS

Finite element analyses of LDSS hollow tubular stub columns with NRSs and representative square section for various thicknesses are presented using Abaqus (2009), to understand the cross-sectional shape effects on the load and deformation capacity. Based on the study following conclusions are identified:

1) As the section goes from square → L → T → +-shape (i.e number of sides in a section increases), more effective the section becomes in controlling local buckling due to increase in the stiffness of the section.

2) For NRSs, there is approximately a linear increase of P_u with increasing LDSS tube thicknesses, whereas, for the representative square section, a milder increase of P_u is seen at lower thickness and linear increase at higher LDSS tube thicknesses.

3) For LDSS tube thickness < 30 mm, NRSs shows a higher strength capacity compared to the representative square section, with +-shaped section having the highest strengths. However at LDSS tube thicknesses ≥ 30 mm, all the sections considered gave similar strengths.

4) For changes in the cross-sectional shape from square to + shape, the increase in P_u are ~ 136%, 109%, 72%, 26%, 9% for 5mm, 10, mm, 15 mm, 20 mm and 25 mm, respectively, showing that the increase in P_u is more effective at thinner sections.

5) The gain in P_u with change in the cross-sectional shape from square to L, T and +-shape are in the range 120%-150%, 130%-170%, 140%-230%, respectively, at lower thicknesses of the steel tube (< 20 mm). Thus, it can be seen that by switching over to + shape sections, significant gain in ultimate strength can be obtained for all the thicknesses considered, with thinner sections giving more pronounced gain.

6) NRSs have notably better deformation capacity compared to the representative square section, with +-shape section estimating a much higher deformation capacity. Also, the deformation capacity increases with increasing thickness for all the hollow tubular stub columns analysed.

7) Both the current design specifications are generally capable of predicting the LDSS hollow tubular column strengths. For stocky sections, FE strengths over predicts both the codal strengths (European and American specifications) by about 28 % for all the section studied. For slender sections, at lower thicknesses of the steel tube (i.e t ~ < 20 mm), FE strengths over predicts the European specification by 28 %, 26 %, 21 % and 23 % for SHC, LHC, THC and +HC, respectively, and American specification by 5%, 6%, 9% and 17 % for SHC, LHC, THC and +HC, respectively. Based on the FE studies it can be inferred that, for slender sections, the American specification provides closer values as compared to the European specification, thus, providing a significant material saving through design by the American specification.

8) Based on the reliability analyses it can be inferred that both specifications can be adopted for all the design of LDSS hollow tubular stub columns. However, for LDSS hollow tubular stub columns, design based on European specification tends to be slightly more reliable compared to the American specification, except for +-shape section, where the American specification tends to be more reliable.

Table 3.1: Compressive flat material properties (Theofanous and Gardener, 2009)

Cross-section	E (Mpa)	$\sigma_{0.2}$ (Mpa)	$\sigma_{1.0}$ (Mpa)	Compound R-O coefficients	
				n	
80x80x4-SC2	197200	657	770	4.7	3.6

Table 3.2: Measured dimensions of stub columns (Theofanous and Gardener, 2009)

Specimen	L (mm)	B (mm)	H (mm)	t (mm)	r_i (mm)	w_0 (mm)
80x80x4-SC2	332.2	80	80	3.81	3.6	Eq. (3.2)

Table 3.3: Comparison of FE strengths with codal design strengths for Class 3 sections

Thickness (mm)	$P_{FE}/P_{EN\ 1993\text{-}1\text{-}4}$				$P_{FE}/P_{ASCE\ 8\text{-}02}$			
	SHC	LHC	THC	+HC	SHC	LHC	THC	+HC
5.0	1.428	1.431	1.294	1.228	1.131	1.151	1.058	1.030
7.5	1.325	1.326	1.889	1.209	1.060	1.086	1.089	1.120
10	1.226	1.291	1.685	1.227	1.100	1.079	1.109	1.143
12.5	1.210	1.215	1.326	1.260	1.050	1.043	1.062	1.186
15.0	1.213	1.152	1.211	1.229	1.002	1.066	1.104	1.226
17.5	1.260	1.164	1.164	1.242	1.056	1.080	1.098	1.242
20.0	1.330	1.218	1.168	1.246	1.130	1.133	1.129	1.246
25.0	1.308	1.259	1.228	1.257	1.153	1.184	1.191	1.257
30.0	1.249	1.260	1.260	1.271	1.242	1.257	1.258	1.271
35.0	1.271	1.272	1.278	1.283	1.271	1.272	1.278	1.283
40.0	1.290	1.290	1.297	1.296	1.290	1.290	1.297	1.296
Mean, P_m	1.283	1.262	1.232	1.25	1.135	1.149	1.152	1.209
COV, V_p	0.048	0.059	0.047	0.020	0.081	0.074	0.073	0.065
Reliability index, β_0	3.11	3.02	2.96	3.05	2.83	2.89	2.90	3.10

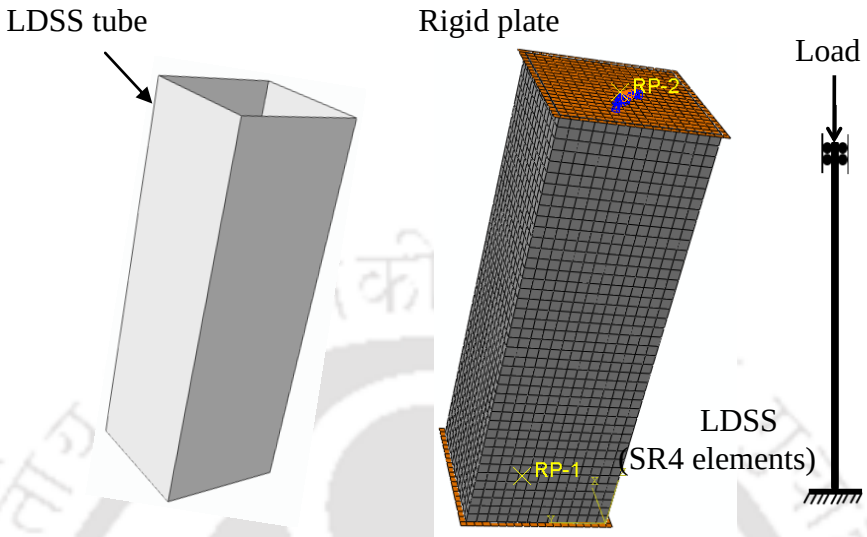

Figure 3.1: Boundary conditions applied to a square LDSS hollow tubular stub column FE models.

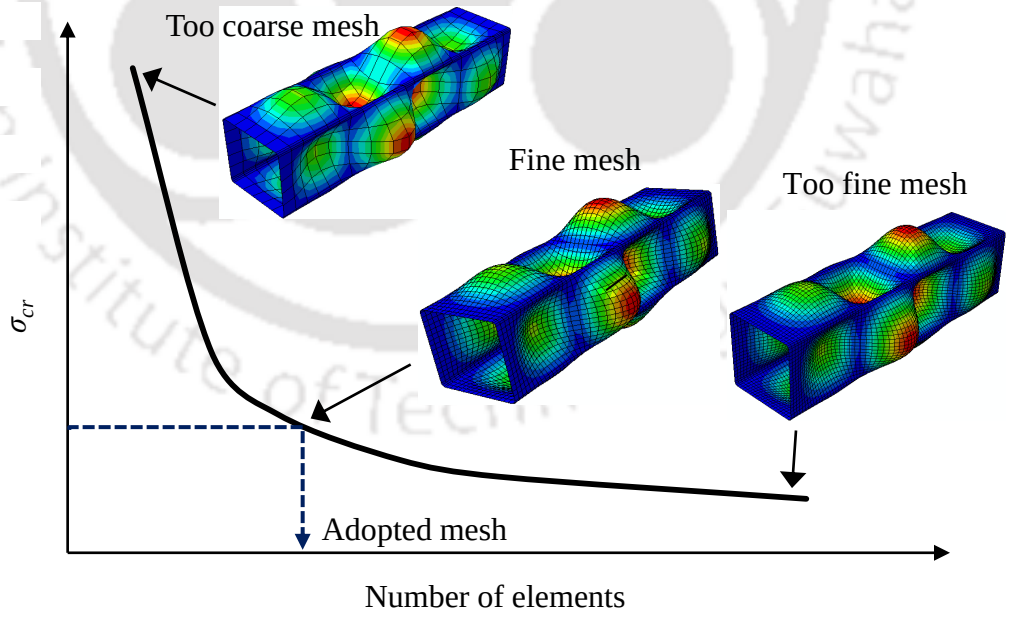

Figure 3.2: Typical mesh convergence study of FE models.

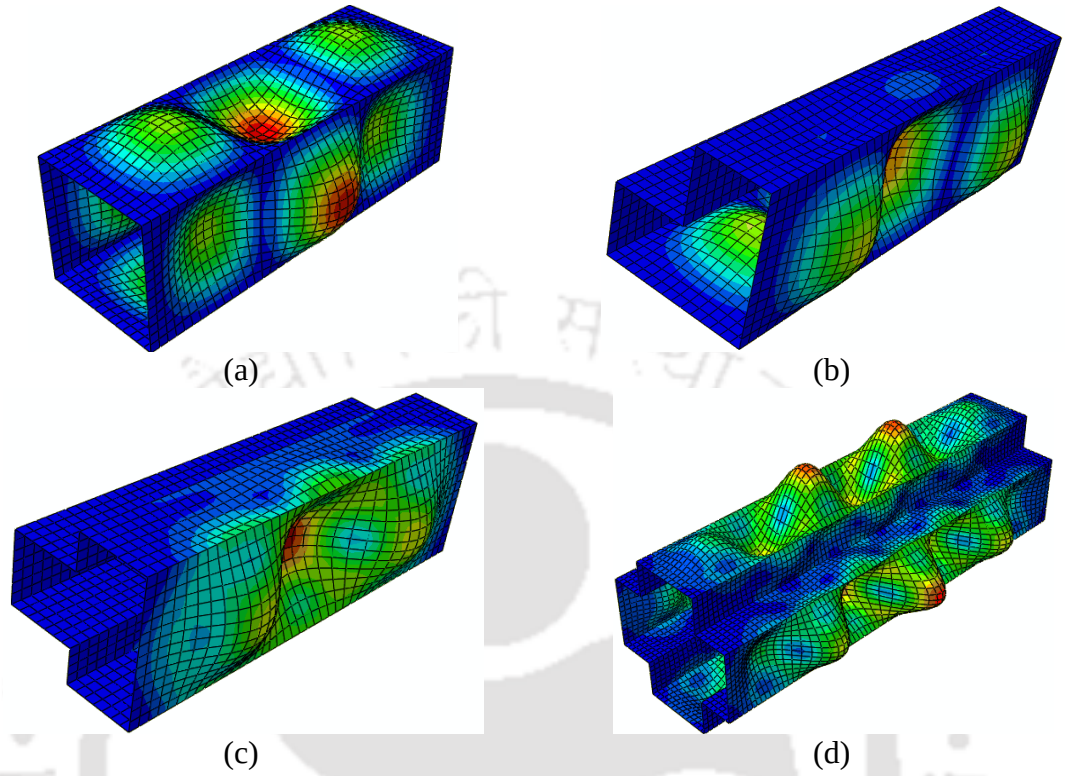

Figure 3.3: First eigen buckling modes for (a) SHC; (b) LHC, (c) THC, & (d) +-HC.

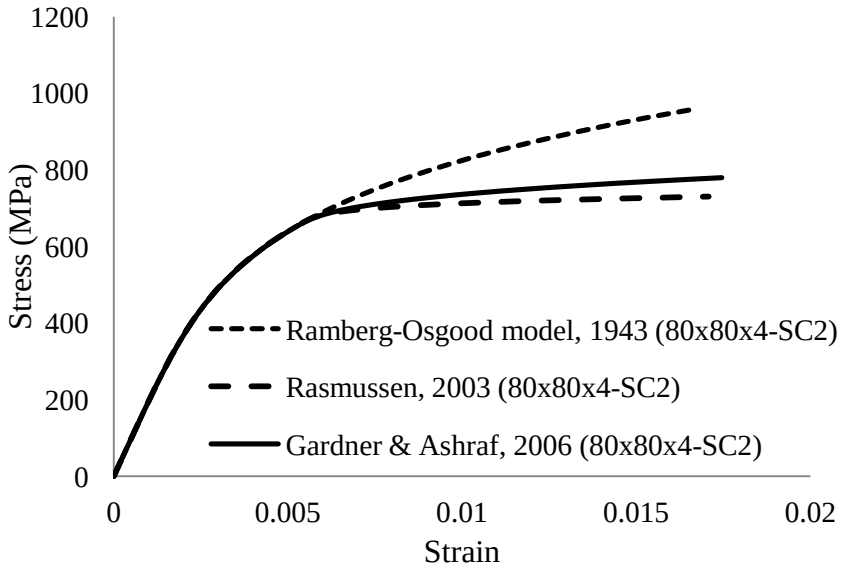

Figure 3.4: Stress-strain curve of LDSS Grade EN 1.4162 using the experimental results provided by Theofanous and Gardner (2009).

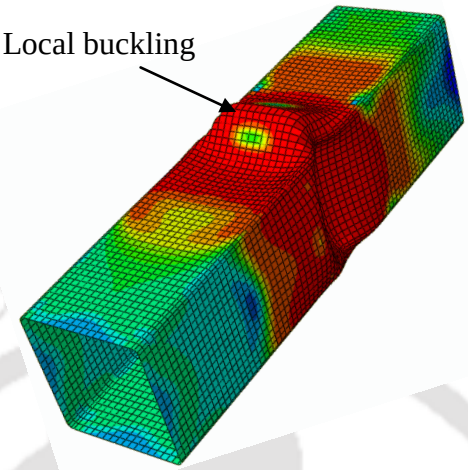

Figure 3.5: Typical FE deformed shape of 80 X 80 X 4-SC2.

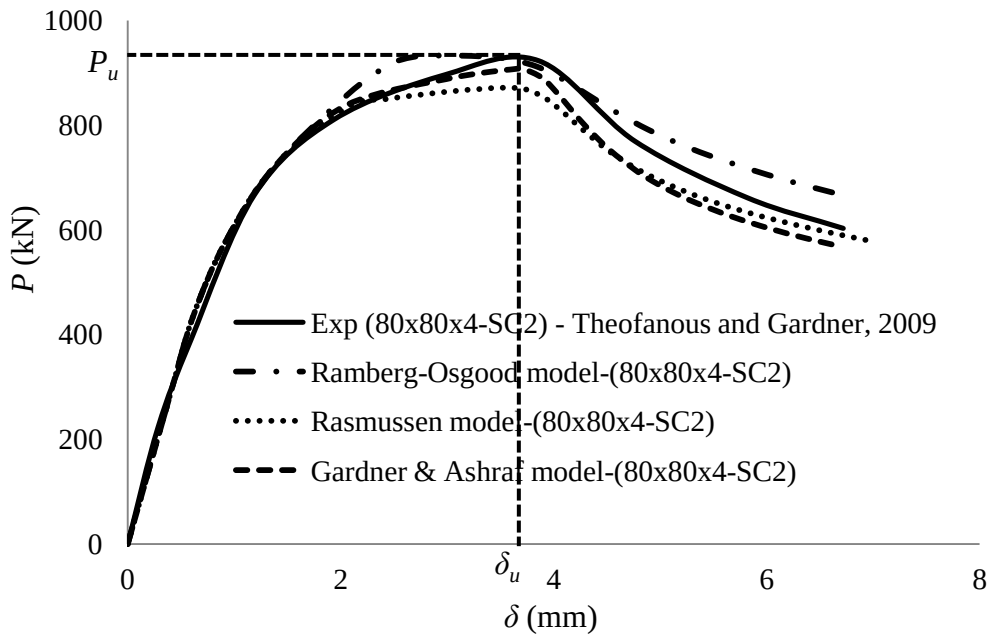

Figure 3.6: Variation of P with δ for 80x80x4-SC2.

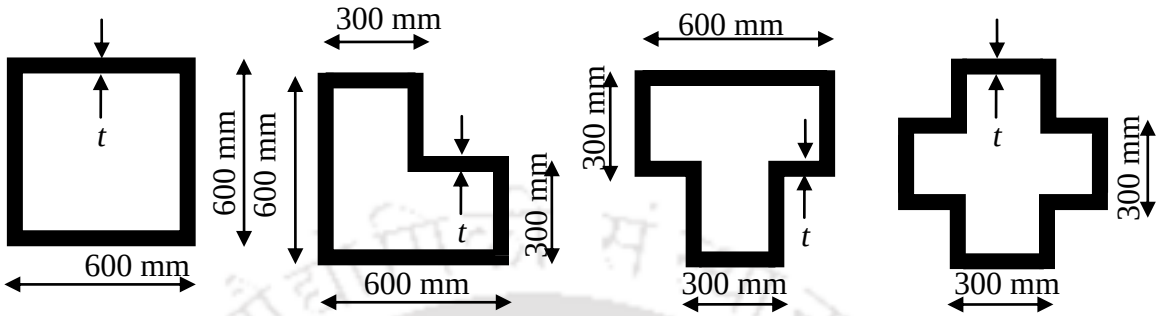

(a) SHC (b) LHC (c) THC (d)+HC

Figure 3.7: Specimen cross-sections of (a) square and (b - d) NRSs.

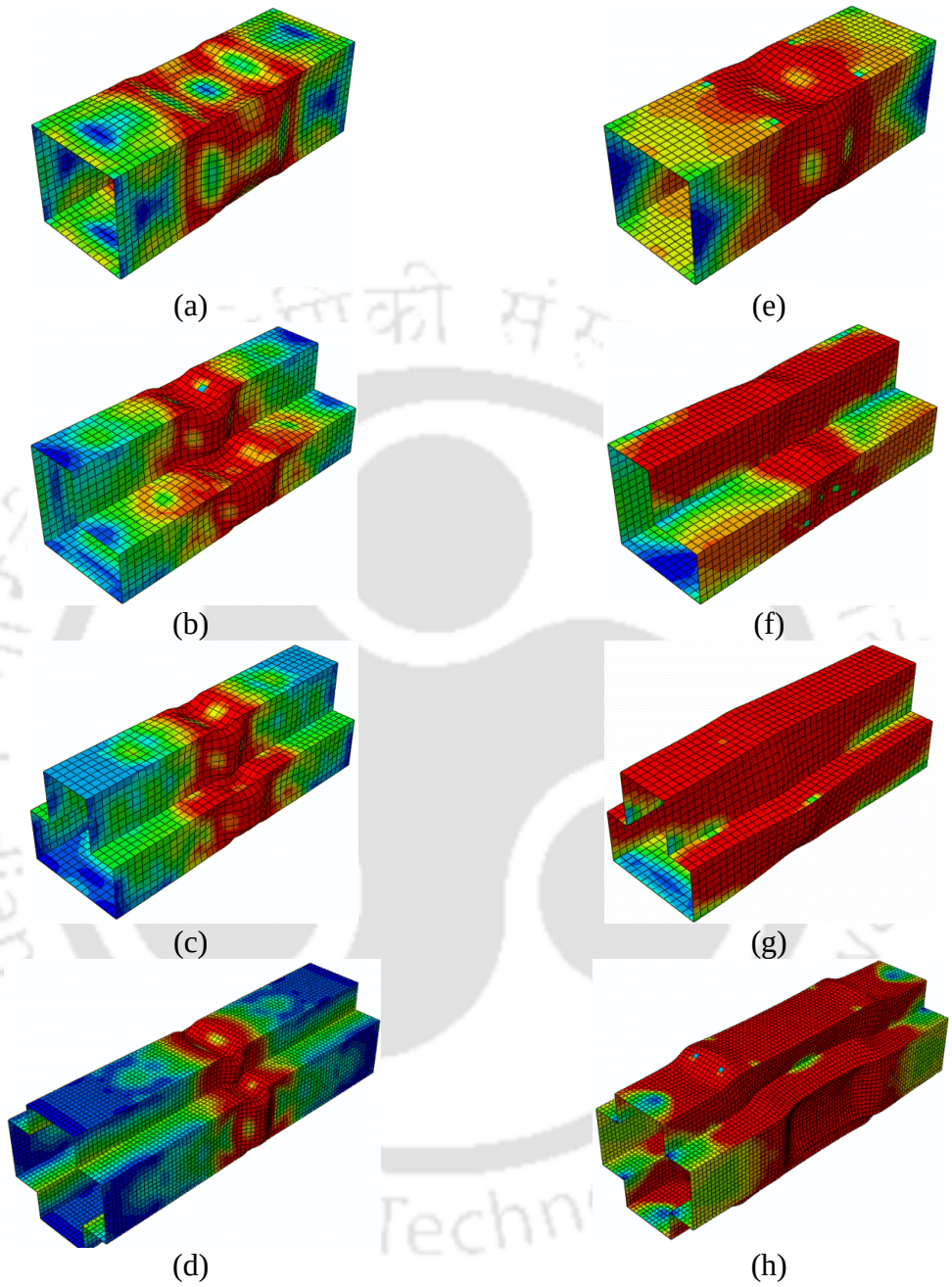

Figure 3.8: Typical failure modes for hollow tubular stub columns with NRSs and square section for (a-d) slender and (e-h) stocky sections at axial deformation corresponding to 4xδ_u.

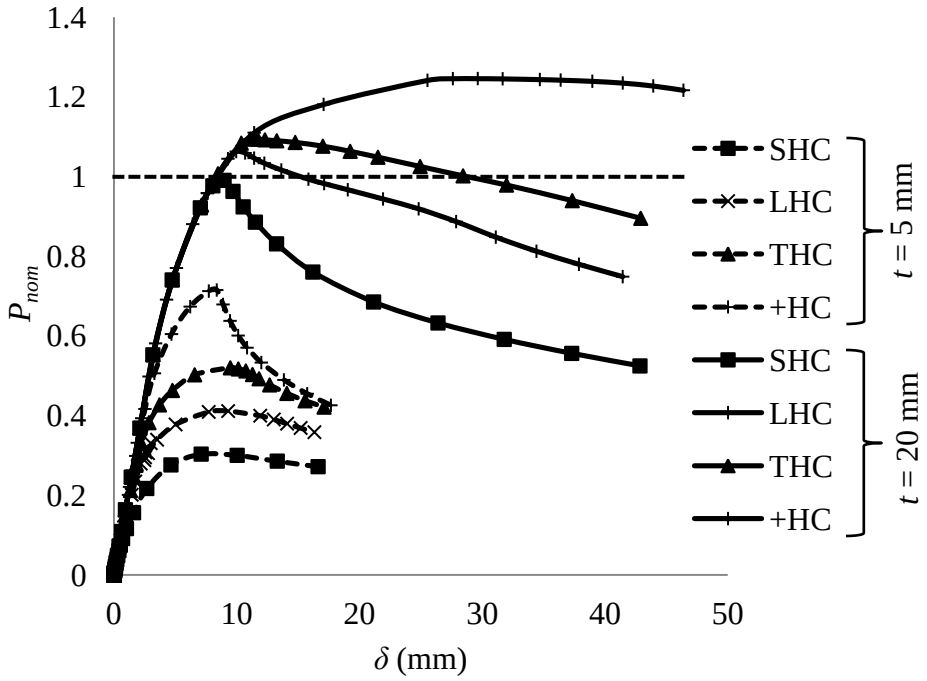

Figure 3.9: Variation of $P/A_g f_y$ with δ for hollow tubular stub columns with NRSs and representative square section.

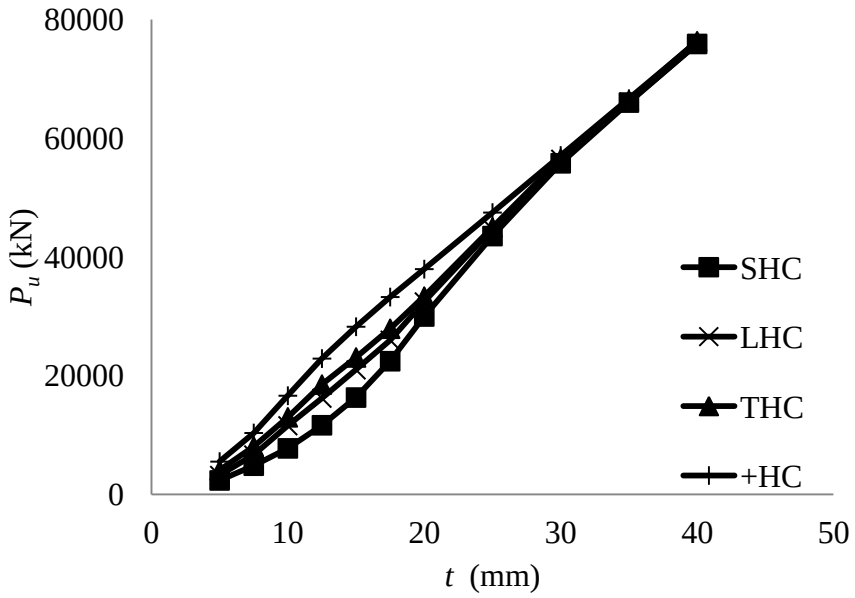

Figure 3.10: Effect of cross-sectional shape on the load capacity of hollow tubular stub columns.

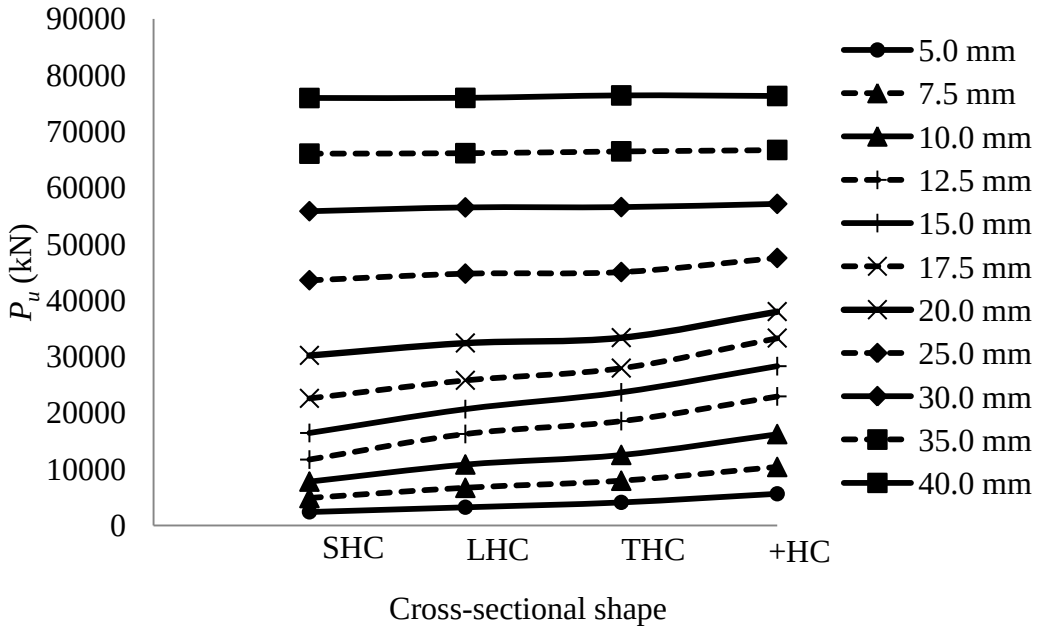

Figure 3.11: Variation of P_u with cross-sectional shapes.

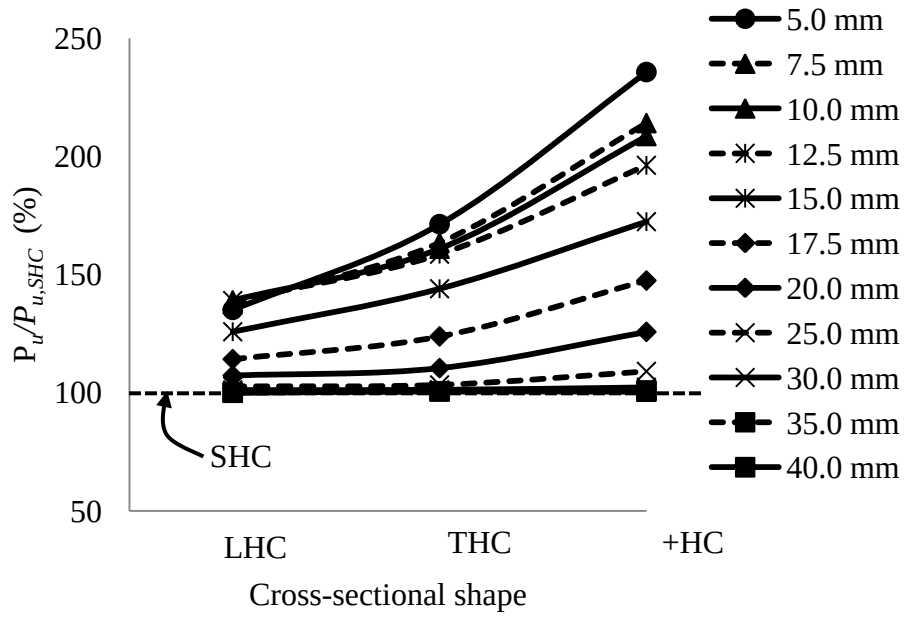

Figure 3.12: Variation of perfentage $P_u/P_{u(sq)}$ with cross-sectional shapes.

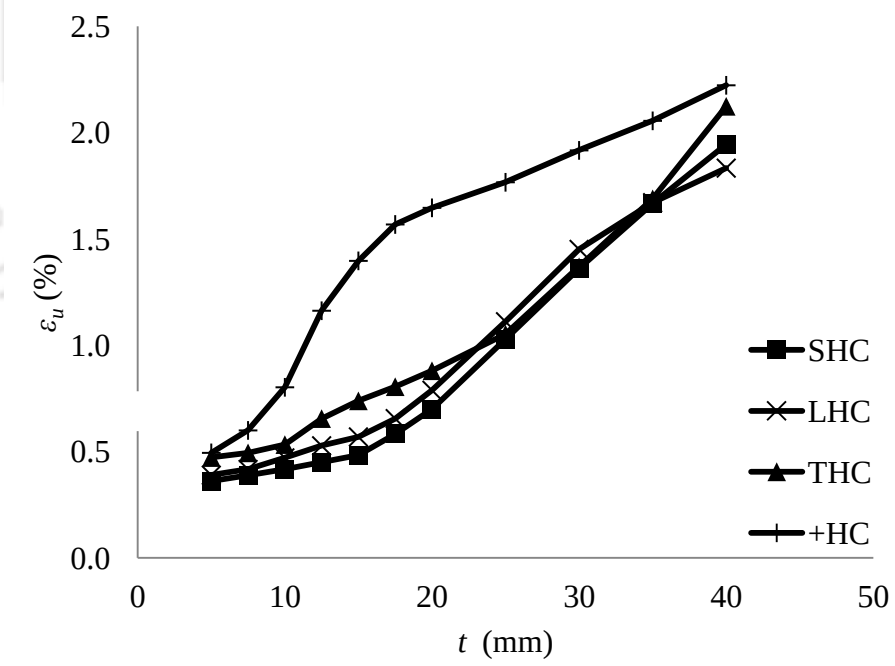

Figure 3.13: Effect of cross-sectional shape on the deformation capacity of hollow tubular stub columns.

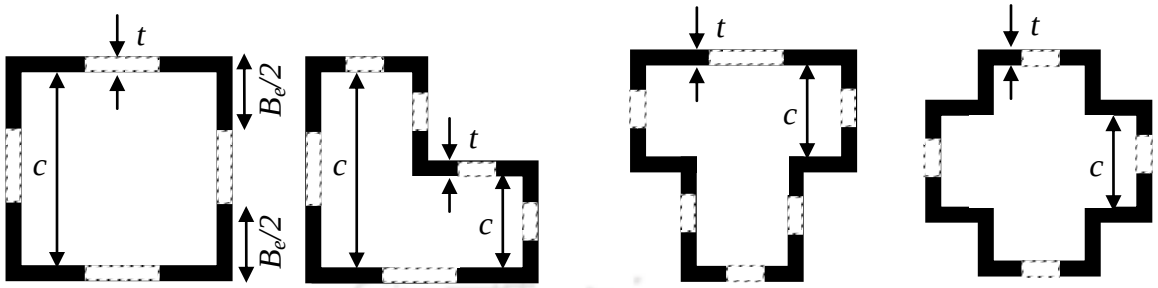

(a) (b) (c) (d)

Figure 3.14: Schematic diagam showing determination of B_e.

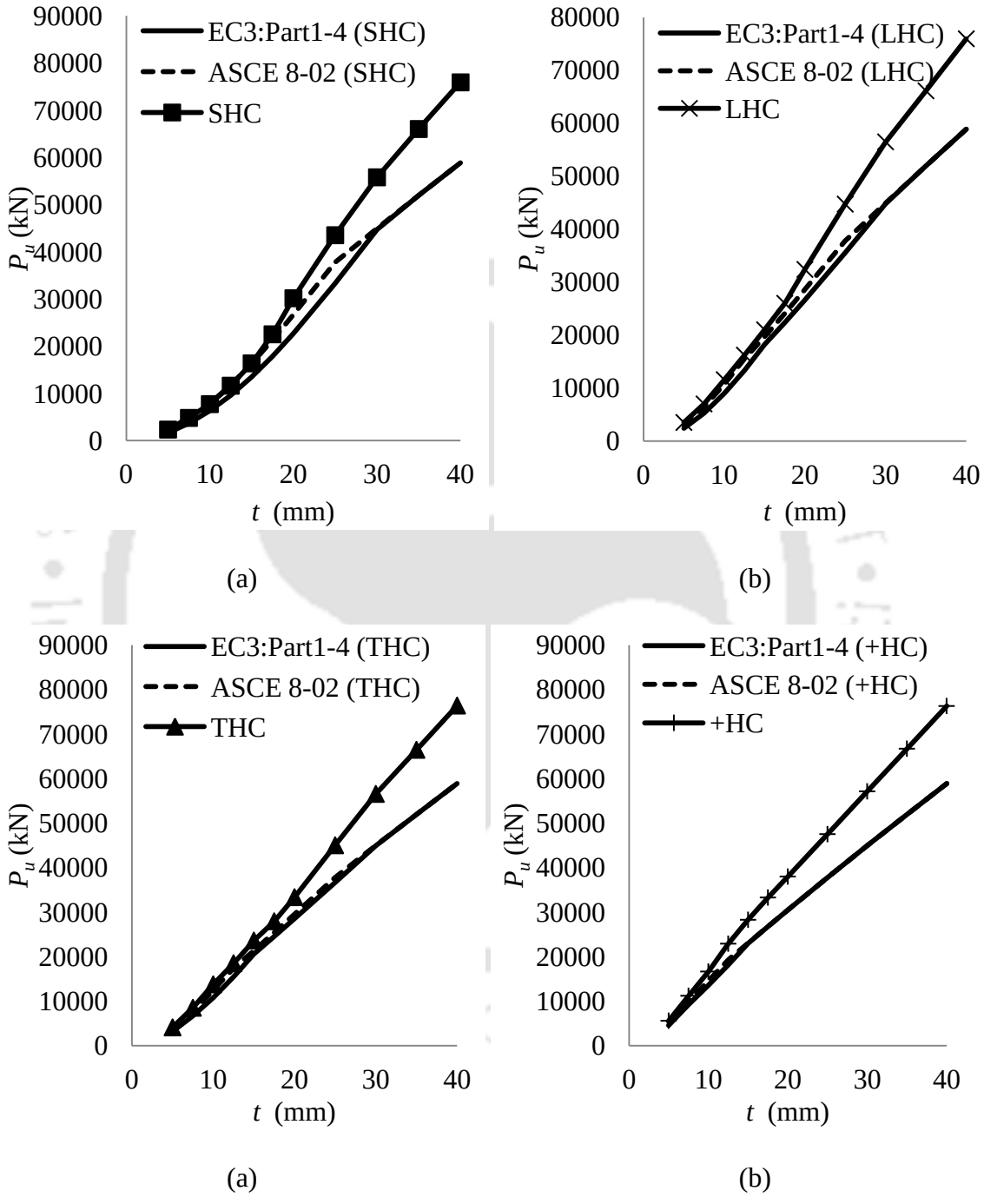

Figure 3.15: Variation of P_u with t for LDSS hollow tubular stub columns.

CHAPTER 4

NUMERICAL MODELLING OF LEAN DUPLEX STAINLESS STEEL HOLLOW SLENDER COLUMNS

4.1 INTRODUCTION

In the previous chapter, FE analyses on the structural behavior of LDSS hollow tubular stub columns of NRSs and representative square section was performed. This chapter presents an extension of the studies to fixed-ended hollow tubular slender columns employing FE approach. Two classes of cross-sections, such as Class 3 & 4 sections, as per EN 1993-1-4 (2006) codal provision were considered for studying the variations in buckling strength of varying cross-sectional shapes (keeping equal material cross-sectional areas or equal material consumption), over a range of column lengths involving both local buckling and global flexural buckling. The applicability of the currently available design standards for stainless steel, such as the European specification (EN 1993-1-4, 2006) and the American specification (ASCE 8-02, 2002) in the design of LDSS hollow tubular stub columns was assessed based on the FE studies. Reliability analysis of the design standards was also carried out based on the FE studies.

4.2 FE MODELLING

LDSS material stress-strain curve developed through Gardner and Ashraf (2006) model (as discussed in Section 3.3) was further used in the FE analyses of fixed-ended LDSS hollow tubular slender columns, which was found to give the best agreement through validation with an expermintal test performed on hollow tubular stub column by Thefanous and Gardner (2009). The following sub-sections presents various details for achieving a reliable FE model representation of LDSS hollow tubular slender columns as also followed by several researchers.

4.2.1 Boundary conditions and analysis technique

The boundary conditions for the fixed-ended LDSS hollow tubular slender columns are similar to that followed for the stub columns (as detailed in Section 3.2.1), whereby the ends are fixed while the top loaded part is allowed to have free vertical translation, and also followed by other researcher for fixed-ended hollow tubular slender columns (e.g. Lui and Young, 2003; Ellobody, 2007; Ellobody and Young, 2005) (see Figure 4.1). Similar analyses technique as that detailed in Section 3.2.1, in which elastic linear analysis technique was employed for obtaining the relevant eigenmodes and the modified RIKS method for further nonlinear analyses of the FE models was followed.

4.2.2 FE mesh

As discussed in Section 3.2.2, S4R elements were employed to discretize the slender column FE models. The aspect ratios of the elements are kept at ~ 1.0 in all the FE models. Similar approach of mesh convergence study by monitoring the σ_{cr} as detailed in Section 3.2.2 was followed in achieving a suitable mesh for further nonlinear analysis of hollow tubular slender columns.

4.2.3 Initial geometric imperfections

Linear elastic analysis technique was initially performed on the fixed-ended hollow tubular slender column FE models to extract both local and global buckling mode shapes. The first (i.e. lowest) local and global buckling mode shapes are then utilised as initial geometric imperfections pattern to perturb the geometry of the slender columns as also followed by several researchers (e.g. Ellobody, 2007; Ellobody and Young, 2005). For slender columns superposition of the two provided the final imperfection pattern. The lowest local and global buckling modes generally appeared in the first few eigen modes. Typical first global and local eigenmodes for the hollow tubular slender columns of NRSs and the representative square section are shown in Figure 4.2.

The magnitude of the local geometric imperfection is taken equal to ω_0 as discussed in Section 3.2.4. As discussed in Section 2.7.2, there is no clear cut evidence on the basis for selection of an appropriate value of initial out-of-straightness pertaining to hollow tubular columns. Thus, in the current study, the initial out-of-straightness for the fixed-ended column was assumed to be same as that of the experimental tests conducted by Theofanous and Gardner (2009) for pinned-ended LDSS hollow tubular columns, which is a fraction of L of the order of $L/1500$. This imperfection magnitude was applied at the mid-height of the column in the plane of the weaker principal axis for all the fixed-ended hollow tubular slender columns studied.

4.3 VERIFICATION OF THE FE MODELS

Development of the FE models for fixed-ended LDSS hollow tubular slender columns was similar to that of the hollow tubular stub columns as discussed in Chapter 3. Models included predicted material properties and initial plate imperfections as described in Section 4.2.3. In order to validate the FE analyses approach in predicting the behaviors of fixed-ended LDSS hollow tubular slender columns, experimental test conducted by

Theofanous and Gardner (2009) on pinned-ended hollow tubular columns with three different lengths was considered as the benchmark. Figure 4.3 shows a variation of P_u with effective length (L_e) for a pinned-ended columns from experimental (Theofanous and Gardner, 2009) as well as FE results. It can be seen that the present modelling approach is able to achieve good agreement with the experimental values, for L_e varying from 300 mm to 2000 mm. As a result, the verification ensures the accuracy of simulating the slender LDSS columns with a high degree of confidence. Figure 4.4 shows a typical experimental (Theofanous and Gardner, 2009) and FE failure mode for a pinned-ended slender column with a square section. It can be seen from Figure 4.4 that the experimental and FE model failure mode is also similar.

4.4 HOLLOW TUBULAR SLENDER COLUMN MODELLING

4.4.1 Introduction

The behaviour of fixed-ended LDSS hollow tubular slender columns can be accurately replicated using the described modelling techniques and assumptions (as detailed in Section 4.2). This demonstrates the ability to predict the load and deformation capacities of the fixed-ended LDSS hollow tubular slender columns. The chapter encompasses a series of FE models to understand the structural behavior of fixed-ended hollow tubular slender columns with NRSs and representative square section subjected to pure axial compression. The effects of column lengths and cross-section thicknesses (i.e encompassing Class 3 (stocky) and Class 4 (slender) sections) on the buckling strength of these columns were analysed.

4.4.2 Development of the FE models

A total of 56 fixed-ended LDSS hollow tubular slender column FE models of NRSs and representative square sections with thicknesses of 5.25 mm and 2.0 mm, over a range of column lengths *viz.*, 3.0 - 10.0 m, which provided a range of non-dimensional member slenderness ($\bar{\lambda}$), defined through by Equation 4.1, in accordance with EN1993-1-4 (2006), from 0.05 to 3.16, were considered for the parametric studies.

$$\bar{\lambda} = \frac{L_e}{r}\frac{1}{\pi}\sqrt{\frac{\sigma_y \beta_A}{E_s}} \tag{4.1}$$

where, L_e, r and β_A are the effective length, radius of gyration of the gross cross-section, and ratio of the effective cross-section area to the gross cross-section area. The two thicknesses of 5.25 mm and 2.0 mm were chosen to represent Class 3 and Class 4 sections, respectively, as per EN 1993-1-4 (2006) codal provision (see Figure 4.5). Similar labelling approach as mentioned in Section 3.4.2 is also followed for the fixed-ended LDSS hollow tubular slender columns.

4.5 RESULTS AND DISCUSSION

4.5.1 Introduction

The results of the FE analyses for the fixed-ended LDSS hollow tubular slender columns was presented in terms of the variations in buckling strength with changes in the column lengths, cross-sectional shapes and thicknesses of the LDSS tubes (i.e involving Class 3 and Class 4 sections). The FE results was then compared with the design strengths predicted by the EN1993-1-4 (2006) and ASCE 8-02 (2002) specifications. The applicability and reliability of these codes on the design of fixed-ended LDSS hollow tubular slender columns was also assessed based on the FE studies.

4.5.2 Deformed shapes of NRSs and square section

Figures 4.6 and 4.7 show Von-Mises stress (superimposed on deformed shape) at P_u for Class 3 and Class 4 NRSs and representative square section for L = 300 mm. For this particular length considered in Figure 4.6, it can be seen that the four sections i.e., square, L-, T-, and +-shape are all uniformly stressed without noticeable signs of local buckling. However for slender sections, i.e. t = 2.0 mm (Class 4 sections), the onset of local buckling modes at ultimate load could be seen for SHC, LHC and THC, whereas it is uniformly stressed for the +HC (see Figure 4.7).

The deformed shapes corresponding to 2xδ_u are shown in Figures 4.8 and 4.9 for Class 3 and Class 4 sections, respectively, where, the appearances of post-ultimate local buckling are seen. As compared to Class 3 sections, the corresponding cross-section types with Class 4 sections showed larger distressed surface areas. This may be related to earlier occurrence of local buckling in slender sections (Class 4) as compared to that of stocky sections i.e. Class 3 sections.

Figure 4.10 shows typical Von-Mises stress variation superimposed on deformed shape corresponding to axial deformation at 1.5xδ_u, for slender columns (L = 3000 mm). The local buckling near the mid-height can be seen for all the sections analyzed. The slender columns fails first by overall flexural buckling followed by local buckling at mid-height of the column, irrespective of the cross-sectional shape considered, and is seen to be typical for both the Class 3 and 4 sections. The direction for the flexural buckling of the hollow tubular slender columns follows the lowest principal buckling axis (see Figure 4.10), whereby, square, T-, and +-shape sections buckles in the y-y direction and L-shape section buckles in the x-y direction. The flexural buckling axes are based on the limitations of the cross-sectional dimensions considered in the current study (see Figure 4.5).

4.5.3 Load-axial deformation profile

Figure 4.11 shows a typical variation of effect of column lengths on P versus δ curve for hollow tubular columns with square section under Class 3 category. Since hollow tubular slender columns with NRSs showed the same nature as those with a square section in terms of the effect of lengths, no curves of NRSs were given. It can be observed from Figure 4.11 that the buckling strength of fixed-ended hollow tubular slender columns (both Class 3 and Class 4 sections) decreases with increasing lengths due to reduction in the stiffness of the columns, with very slender columns failing by elastic instability failure where the P_u is mainly dominated by flexural rigidity.

4.5.4 Buckling strength of NRSs and square section

4.5.4.1 Class 3 sections

Figure 4.12 shows the variation of P_u and $P_u/P_{u,SHC}$ with $\bar{\lambda}$ for Class 3 sections. It can be seen from Figure 4.12a that FE analysis predicted a general trend of asymptotic decrease of P_u with increasing $\bar{\lambda}$. For $\bar{\lambda} \leq 0.5$ and at high $\bar{\lambda}$, all the sections exhibit similar structural capacities. The reason being, at lower $\bar{\lambda}$, regardless of the cross-sectional shapes, all the sections experiences hardening above the global yielding load ($A_g f_y$) without any occurrences of local buckling at ultimate load; and the failure for high slender columns are governed principally by member stiffness rather than the cross-sectional shape.

However, for $0.5 < \bar{\lambda} \geq 2.0$, there is a nearly linear variation in strengths (increasing trend for +HC, similar trend for THC and decreasing trend for LHC), with stabilization beyond $\bar{\lambda} > 2.0$. For $\bar{\lambda} > 2.0$, P_u for +HC showed ~ 30% higher; THC showed similar strength; and LHC showed ~20% lower than the corresponding value for SHC, indicating that +HC has an improved ultimate strength for all the ranges of $\bar{\lambda}$ (see Figure 4.12b). The

reason for LHC showing lower flexural buckling strength may be related to the unsymmetrical buckling of the L-shape section in the direction of x-y axis (as discussed in Section 4.5.2), thereby, resulting in lesser bending stiffness of the column.

4.5.4.2 Class 4 sections

Figure 4.13 shows the variation of P_u and $P_u/P_{u,SHC}$ with $\bar{\lambda}$ for Class 4 sections. It can be seen from Figure 4.13a that in contrast to Class 3 sections, cross-sectional shape becomes increasingly significant with decreasing $\bar{\lambda}$, which is due to the reduction in the local buckling effect as the cross-section changes from S → L → T → +-shape. However, the cross-sectional shape becomes insignificant for very high $\bar{\lambda}$ as also the case for Class 3 sections.

It is seen that the average strength enhancement ($P_u/P_{u(SHC)}$ > 100 %) as compared to the representative square section are ~ 10 %, 50 %, and 90 % higher for LHC, THC, and +HC, respectively (see Figure 4.13b). Hence, for fixed-ended columns with slender cross-sections, NRSs gives better structural performances over those of the representative square section.

4.5.5 Deformation capacity of NRSs and square section

4.5.5.1 Class 3 sections

Figure 4.14 shows the plot of ε_u (%) with $\bar{\lambda}$ for Class 3 sections. It can be observed from Figure 4.14 that at lower $\bar{\lambda}$ < ~ 0.50, the values of ε_u are found to be highest for +HC, whilst SHC, LHC and THC predicted similar values. However, at higher $\geq$ 0.50, ε_u values lies in the range of ~ 0.2 – 0.6 % for all the section analysed.

Figure 4.15 shows the plot of the plot of $\delta u/\delta_{u,SHC}$ (%) with $\bar{\lambda}$ for Class 3 sections. It can be seen from Figure 4.15 that, at lower $\bar{\lambda}$ < ~ 0.50, +HC shows greater deformation at peak load which decreased linearly and becomes similar to that of SHC beyond $\bar{\lambda}$ ~ 0.50. The observed higher deformation in the case of +HC may be related to a hardening process as a result of the interaction between neighboring faces, which occurs at post-global yield load ($A_g f_y$) thereby delaying local buckling through enhanced member stiffness.

4.5.5.2 Class 4 sections

Figure 4.16 shows the plot of variation of ε_u with $\bar{\lambda}$ for Class 4 sections. Similar to Class 3 (see Figure 4.14), +HC predicted higher deformation at peak load, as compared to SHC, LHC and THC, at lower values of $\bar{\lambda}$ (< ~ 1.0). Similar to Class 3 sections, at higher slenderness ($\bar{\lambda}$ > ~ 1.0), ε_u values also lies in the range of ~ 0.2 – 0.5 % for all the section analysed. This may again be related to higher values of δ_u for +HC at $\bar{\lambda}$ < ~ 1.0 associated with corresponding possible stiffness enhancement *via* interaction between neighboring faces, which occurs at post-global yielding load.

Figure 4.17 shows a comparison of $\delta u/\delta_{u,SHC}$ (%) with $\bar{\lambda}$. From Figure 4.17, it can be observed that in comparison to SHC, +HC showed higher deformation compared to SHC at $\bar{\lambda}$ > ~ 1.0, which decreased linearly and approaches the SHC values beyond $\bar{\lambda}$ ~ 2.0. Similar to Class 3 sections (see Figure 4.15), it can be seen that δ_u values for LHC and THC are closer to SHC for all the ranges of $\bar{\lambda}$ considered.

4.5.6 Comparison with design codes

The results from the FE analyses were compared with the unfactored design strengths predicted using the EN1993-1-4 (2006) and ASCE 8-02 (2002) specifications. A sample

design strength calculation of a square hollow tubular stub column with the two design standards is given in Appendix B. As the current design standards are based on stainless steel material, the applicability of these codes in the design of LDSS hollow tubular columns are assessed through the FE studies. A detail comparison between the FE results and the design standard predictions are discussed in the following sub-sections.

4.5.6.1 Effective area determination

As mentioned in the previous sections, two classes of cross-sectional slenderness were considered in the study *viz*., Class 3 and Class 4 sections as per EN 1993-1-4 (2006). For Class 3 sections, no deduction in the material cross-sectional area is made (i.e. A_g is considered) in the calculation of axial strengths of the column. However, for Class 4 sections, A_e of the cross-section is used to account for the reduction in the resistance due to the effects of local buckling and detailed in Section 3.5.7.1.

4.5.6.2 Design strengths

Design strengths for the fixed-ended hollow tubular slender columns were also designed as concentrically loaded compression members and L_e was assumed to be $L/2$ as recommended in the literatures. The design strengths based on the EN1993-1-4 (2006) and ASCE 8-02 (2002) specifications are defined by Equation 4.2 and 4.3, respectively.

$$P_{EN1993\text{-}1\text{-}4} = \chi f_y A \quad (4.2)$$

$$P_{ASCE\ 8\text{-}02} = A f_n \quad (4.3)$$

where;

$$\chi = \frac{1}{\varphi + \left[\varphi^2 - \overline{\lambda^2}\right]^{0.5}} \leq 1.0 \quad (4.4)$$

$$\varphi = 0.5\left(1 + \alpha\left(\overline{\lambda} - \overline{\lambda_0}\right) + \overline{\lambda^2}\right) \quad (4.5)$$

$$f_n = \frac{\pi^2 E_t}{\left(\frac{L_e}{r}\right)^2} \leq f_y \tag{4.6}$$

$$E_t = \frac{f_y E_s}{f_y + 0.002 n E_s \left(\frac{f}{f_y}\right)^{n-1}} \tag{4.7}$$

where, A is determined as detailed in Section 3.5.7.1, χ is the reduction factor to account for flexural buckling, E_t is the tangent modulus in compression corresponding to the buckling stress, α and are the imperfection factor and limiting slenderness taken as 0.49 and 0.40, respectively, which were obtained from Table 5.2 of the EN1993-1-4 (2006) specification, n is the Ramberg-Osgood parameter, and f is the stress (f_n) in the member. ASCE 8-02 (2002) specification replaces the E_s with the tangent modulus (E_t), in order to take account of the non-linearity of the stainless steel.

4.5.6.3 Comparison of FE strengths with design strengths

Figures 4.18 and 4.19 show a plot of P_{nom} with $\bar{\lambda}$ for Class 3 and Class 4 NRSs and representative square section, respectively. For Class 3 and 4 sections, A_g and A_e, respectively, were used in the normalization of P_u. The results from FE analyses were compared with the unfactored design strengths predicted through the European and American specifications.

From Figures 4.18 and 4.19, it is observed that, for both the Class 3 and Class 4 sections, at lower $\bar{\lambda}$ (≤ 0.40 for EN 1993-1-4, 2006 and ≤ 0.51 for ASCE 8-02, 2002), FE predicted higher P_{nom} as compared to the codal design strengths, as also observed in Section 3.5.7.3 for the hollow tubular stub columns. A higher $\bar{\lambda}$, for both the Class 3 and Class 4 sections, European specification gives a conservative estimation of strengths compared to the American specification, which gives slightly conservative value, in the design of LDSS hollow tubular slender columns. However, the design of hollow tubular slender

column with L-shape section through the American specification tends to be critical where it over predicts the FE strengths.

4.5.6.4 Reliability analysis of the codes

In order to compare the design column curves obtained through the EN 1993-1-4 (2006) and ASCE 8-02 (2002) specifications, a reliability analysis was carried out based on the FE studies and are presented in Tables 4.1 and 4.2 for both the Class 3 and 4 sections, respectively. Reliability index determination is detailed in Section 3.5.7.4.

Based on the reliability analyses it can be seen that except for Class 3 LHC, both the codes show $\beta_o \geq 2.5$ when compared with the FE results. Considering the lower limit of $\beta_o = 2.5$ suggested by ASCE 8-02 (2002) specification for structural members, it can be inferred that both the specifications can be adopted for all the design of fixed-ended LDSS hollow tubular slender columns except for Class 3 LHC, wherein a suitable modification may be employed after systematic studies (including experiments). For the design of Class 3 sections, European specification tends to be more reliable compared to the American specification and vice versa in the design of Class 4 sections.

4.6 CONCLUSIONS

FE analyses on fixed-ended LDSS hollow tubular slender columns with NRSs and representative square section subjected to pure axial compressive loading are presented in this chapter. Two thicknesses of steel tube with 5.25 mm and 2.0 mm, which lie in Class 3 (stocky) and Class 4 (slender) sections, respectively, as per EN 1993-1-4 (2006) classification were considered in the study. Variations in buckling strength with changes in the cross-sectional shapes were studied by considering NRSs having equal material cross-sectional areas (or equal material consumption) as that of the representative square section over a range of column lengths. The FE results of the hollow tubular slender

columns were then compared with the design strengths predicted by the EN1993-1-4 (2006) and ASCE 8-02 (2002) specifications. Based on the present study the following conclusions are drawn:

1) Hollow tubular slender column fail first by overall flexural buckling followed by local buckling at mid-height of the column, irrespective of the cross-sectional shape considered, and is seen to be typical for both the Class 3 and 4 sections.

2) The buckling strength of the fixed-ended hollow tubular slender columns (both Class 3 and Class 4 sections) decreases with increasing lengths due to reduction in the stiffness of the columns, with very slender columns failing by elastic instability failure where the P_u is mainly dominated by flexural rigidity.

3) For Class 3 sections:

   a) For $\bar{\lambda} \leq 0.5$ and at high $\bar{\lambda}$, all the sections exhibit similar structural capacities. The reason being, at lower $\bar{\lambda}$, regardless of the cross-sectional shapes, all the sections experiences hardening above the global yielding load without any occurrences of local buckling at ultimate load; and the failure for high slender columns are governed principally by member stiffness rather than the cross-sectional shape.

   b) For $0.5 < \bar{\lambda} \geq 2.0$, there is a nearly linear variation in strengths (increasing trend for +HC, similar trend for THC and decreasing trend for LHC), with stabilization beyond $\bar{\lambda} > 2.0$. For $\bar{\lambda} > 2.0$, P_u for +HC showed ~ 30% higher; THC showed similar strength; and LHC showed ~20% lower than the corresponding value for SHC, indicating that +HC has an improved ultimate strength for all the ranges of $\bar{\lambda}$.

   c) At lower $\bar{\lambda} <$ ~ 0.50, the values of ε_u are found to be highest for +HC, whilst SHC, LHC and THC predicted similar values. However, at higher ≥ 0.50, ε_u values lies in the range of ~ 0.2 – 0.6 % for all the section analysed.

4) For Class 4 sections:

   a) In contrast to Class 3 sections, cross-sectional shape becomes increasingly significant with decreasing $\bar{\lambda}$, however, the cross-sectional shape becomes insignificant for very high $\bar{\lambda}$ as also the case for Class 3 sections.

   b) The average strength enhancement as compared to the representative square section are ~ 10 %, 50 %, and 90 % higher for LHC, THC, and +HC, respectively.

   c) Similar to Class 3, +HC predicted higher deformation at peak load, as compared to SHC, LHC and THC, at lower values of $\bar{\lambda}$ (< ~ 1.0). At higher slenderness ($\bar{\lambda}$ > ~ 1.0), ε_u values also lies in the range of ~ 0.2 – 0.5 % for all the section analysed.

5) A higher $\bar{\lambda}$, for both the Class 3 and Class 4 sections, European specification gives a conservative estimation of strengths compared to the American specification, which gives slightly conservative value, in the design of LDSS hollow tubular slender columns. However, the design of hollow tubular slender column with L-shape section through the American specification tends to be critical where it over predicts the FE strengths.

6) Based on the reliability analyses it is recommended that both the specifications can be adopted for all the design of fixed-ended LDSS hollow tubular slender columns except for Class 3 LHC, wherein a suitable modification may be employed after systematic studies (including experiments). For the design of Class 3 sections, European specification tends to be more reliable compared to the American specification and vice versa in the design of Class 4 sections.

Table 4.1: Comparison of FE strengths with codal design strengths for Class 3 sections.

Lengths in mm	$P_{u,FE}/P_{EN\ 1993\text{-}1\text{-}4}$				$P_{u,FE}/P_{ASCE\ 8\text{-}02}$			
	SHC	LHC	THC	+HC	SHC	LHC	THC	+HC
300	1.26	1.24	1.26	1.27	1.26	1.24	1.26	1.27
1690	1.09	1.01	1.05	1.05	1.09	1.01	1.05	1.05
3000	1.09	1.01	1.11	1.23	1.05	0.95	1.05	1.14
4000	1.11	1.05	1.19	1.38	1.03	0.92	1.04	1.16
5000	1.24	1.07	1.28	1.52	1.08	0.92	1.09	1.23
7000	1.27	1.03	1.33	1.56	1.03	0.84	1.09	1.29
10000	1.24	0.98	1.27	1.51	1.03	0.84	1.09	1.32
Mean, P_m	1.186	1.06	1.21	1.36	1.08	0.96	1.1	1.21
COV, V_p	0.065	0.076	0.079	0.128	0.07	0.133	0.066	0.073
Reliability index, β_0	3.03	2.54	3.06	3.27	3.07	2.35	3.16	3.52

Table 4.2: Comparison of FE strengths with codal design strengths for Class 4 sections.

Lengths in mm	$P_{u,FE}/P_{EN\ 1993\text{-}1\text{-}4}$				$P_{u,FE}/P_{ASCE\ 8\text{-}02}$			
	SHC	LHC	THC	+HC	SHC	LHC	THC	+HC
300	1.20	1.15	1.23	1.26	1.20	1.15	1.23	1.26
1690	1.20	1.04	1.12	1.09	1.20	1.04	1.12	1.09
3000	1.24	0.99	1.12	1.19	1.31	0.94	1.03	1.07
4000	1.23	1.07	1.20	1.29	1.30	1.00	1.05	1.08
5000	1.34	1.13	1.27	1.40	1.32	1.05	1.12	1.12
7000	1.41	1.07	1.24	1.43	1.33	0.90	1.02	1.16
10000	1.76	1.01	1.19	1.39	1.12	0.85	0.99	1.20
Mean, P_m	1.341	1.07	1.19	1.3	1.253	0.991	1.081	1.142
COV, V_p	0.14	0.054	0.045	0.089	0.059	0.096	0.069	0.057
Reliability index, β_0	3.25	2.74	3.23	3.40	3.72	2.63	3.08	3.34

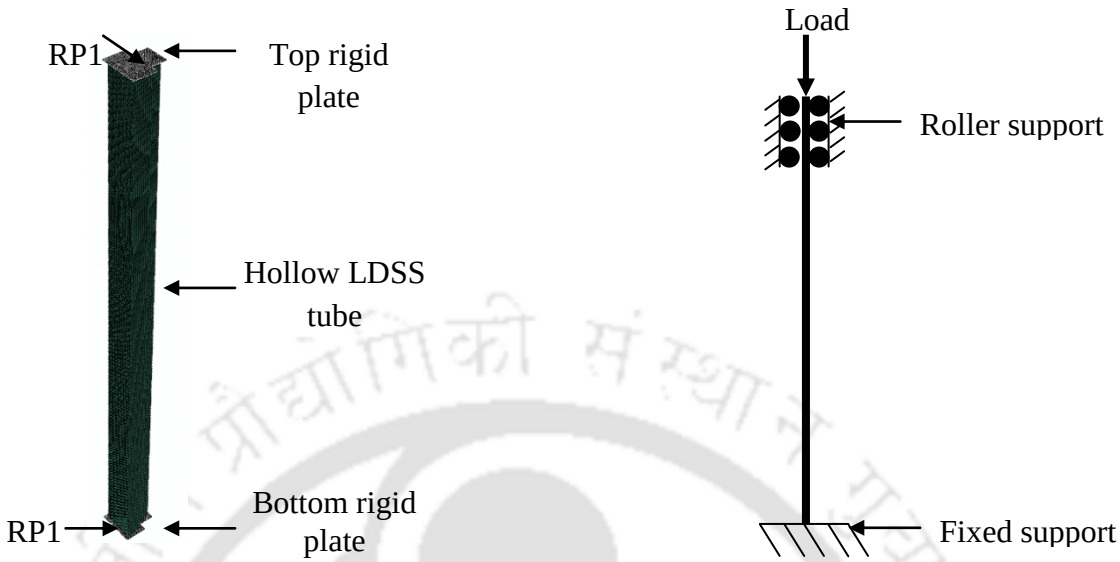

Figure 4.1: Typical boundary conditions applied to fixed-ended slender column FE models.

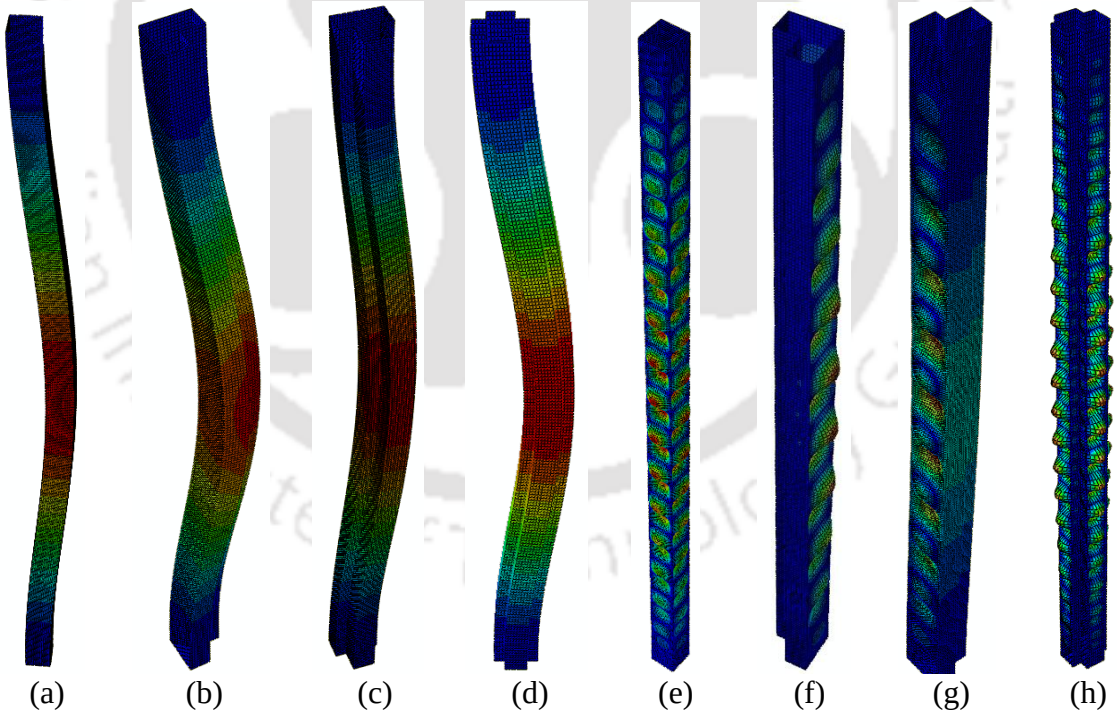

Figure 4.2: Typical lowest eigen modes for fixed-ended hollow tubular slender columns with NRSs and representative square section showing (a-d) global buckling modes and (e - h) local buckling modes.

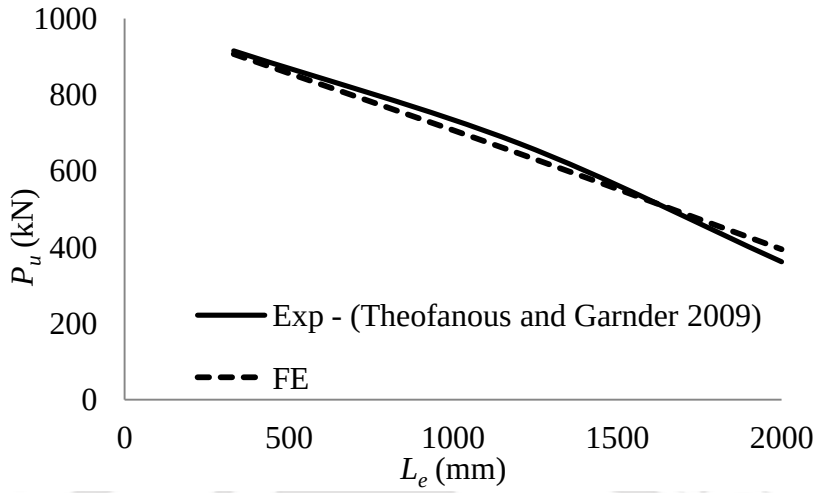

Figure 4.3: Variation of P_u vs L_e for SHC 80 x 80 x 4.

(a) Test deformed shape (Theofanous and Gardner, 2009)

(b) FE deformed shape

Figure 4.4: Typical deformed shapes for hollow tubular slender column with a square section.

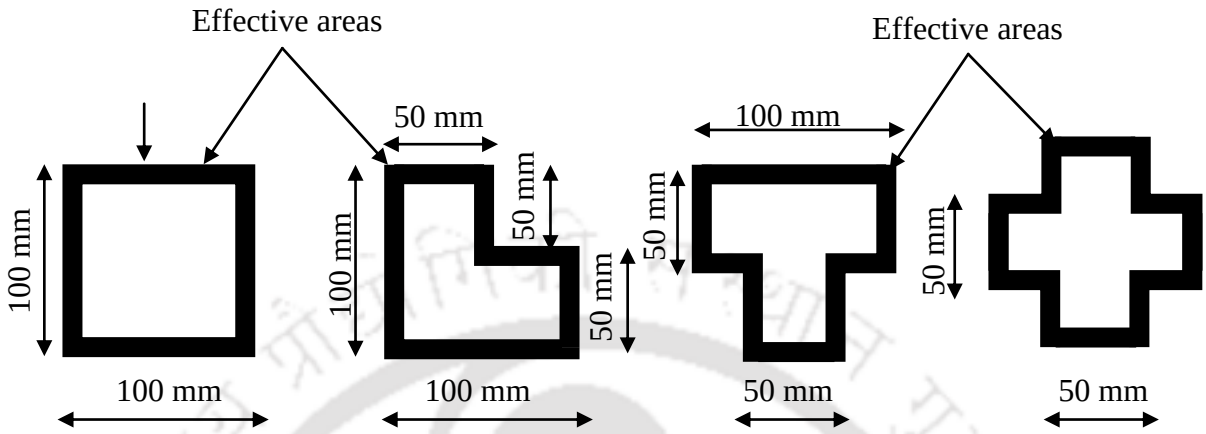

(a) Class 3 sections (stocky sections)

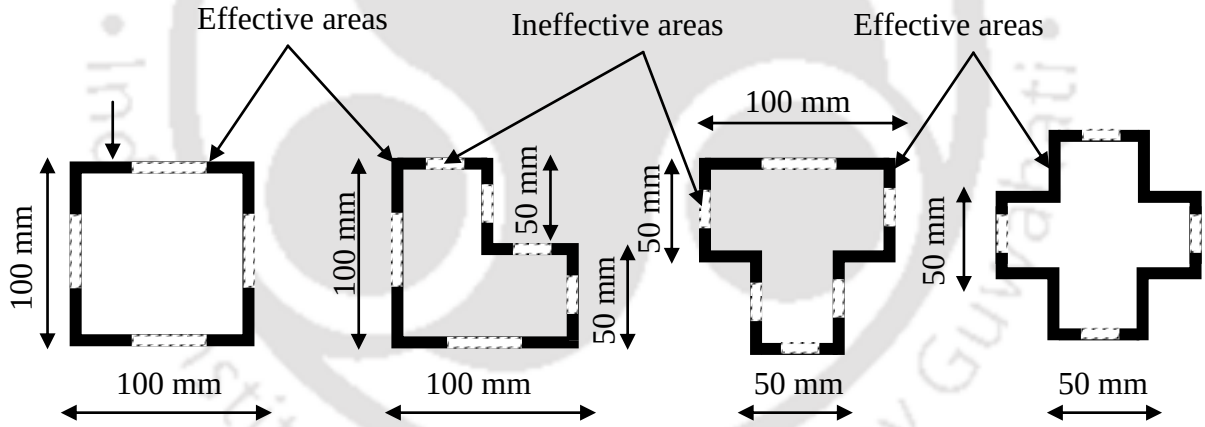

(b) Class 4 sections (slender sections)

Figure 4.5: Class 3 and 4 sections with LDSS tube thicknesses of 5.25mm and 2.0 mm, respectively, as per EN1993-1-4 (2006) for NRSs and representative square section.

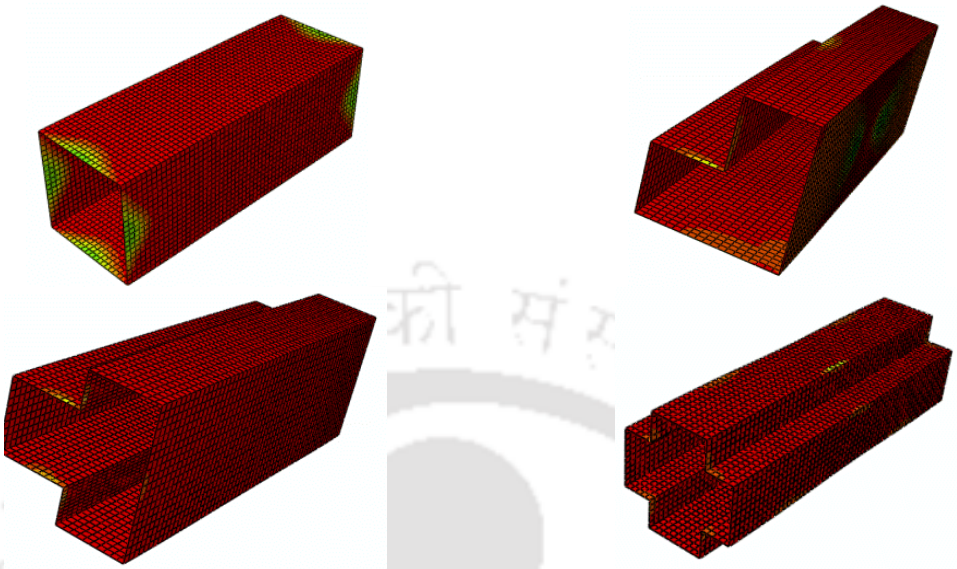

Figure 4.6: Von-Mises stress (superimposed on deformed shape) at P_u for Class 3 NRSs and representative square section (L = 300 mm).

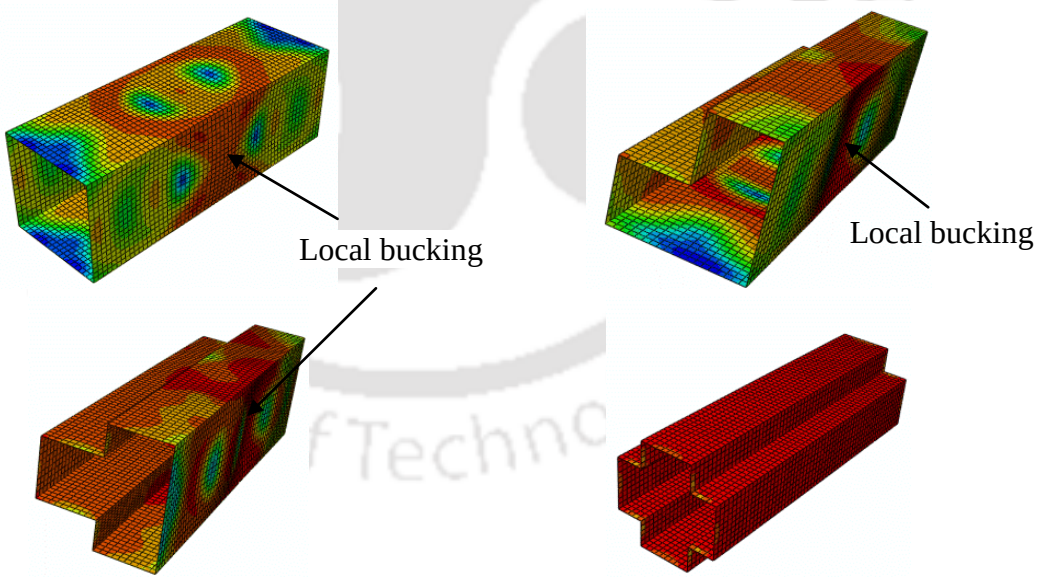

Figure 4.7: Von-Mises stress (superimposed on deformed shape) at P_u for Class 4 NRSs and representative square section (L = 300 mm).

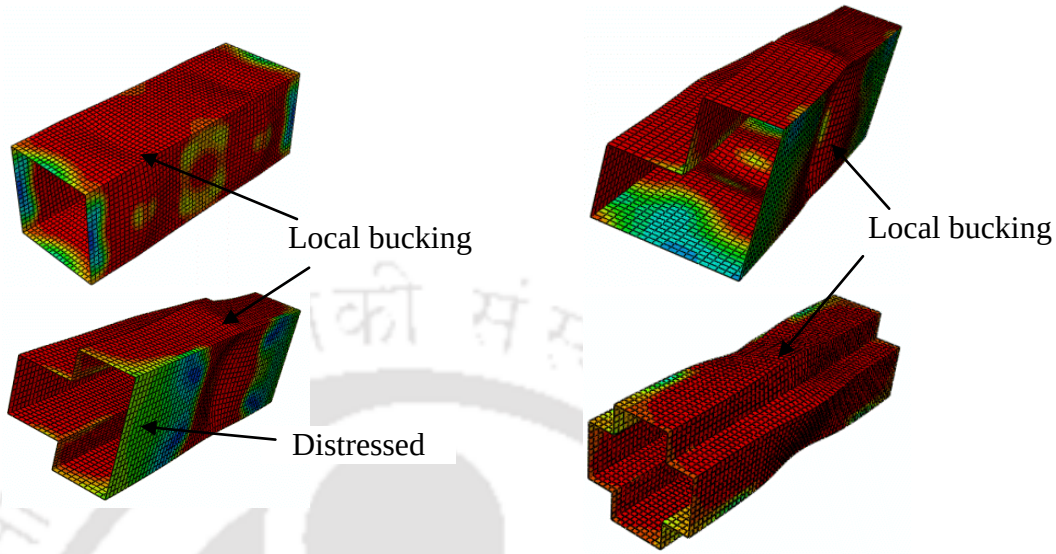

Figure 4.8: Von-Mises stress (superimposed on deformed shape) corresponding to deformation at 2xδ_u for Class 3 NRSs and representative square section (L = 300 mm).

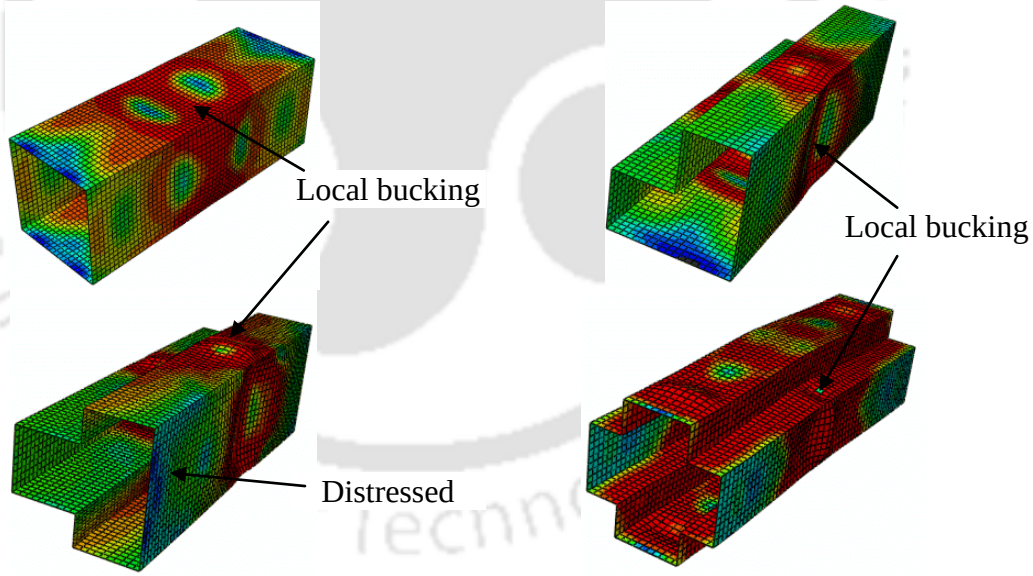

Figure 4.9: Von-Mises stress (superimposed on deformed shape) corresponding to deformation at 2xδ_u for Class 4 NRSs and representative square section (L = 300 mm).

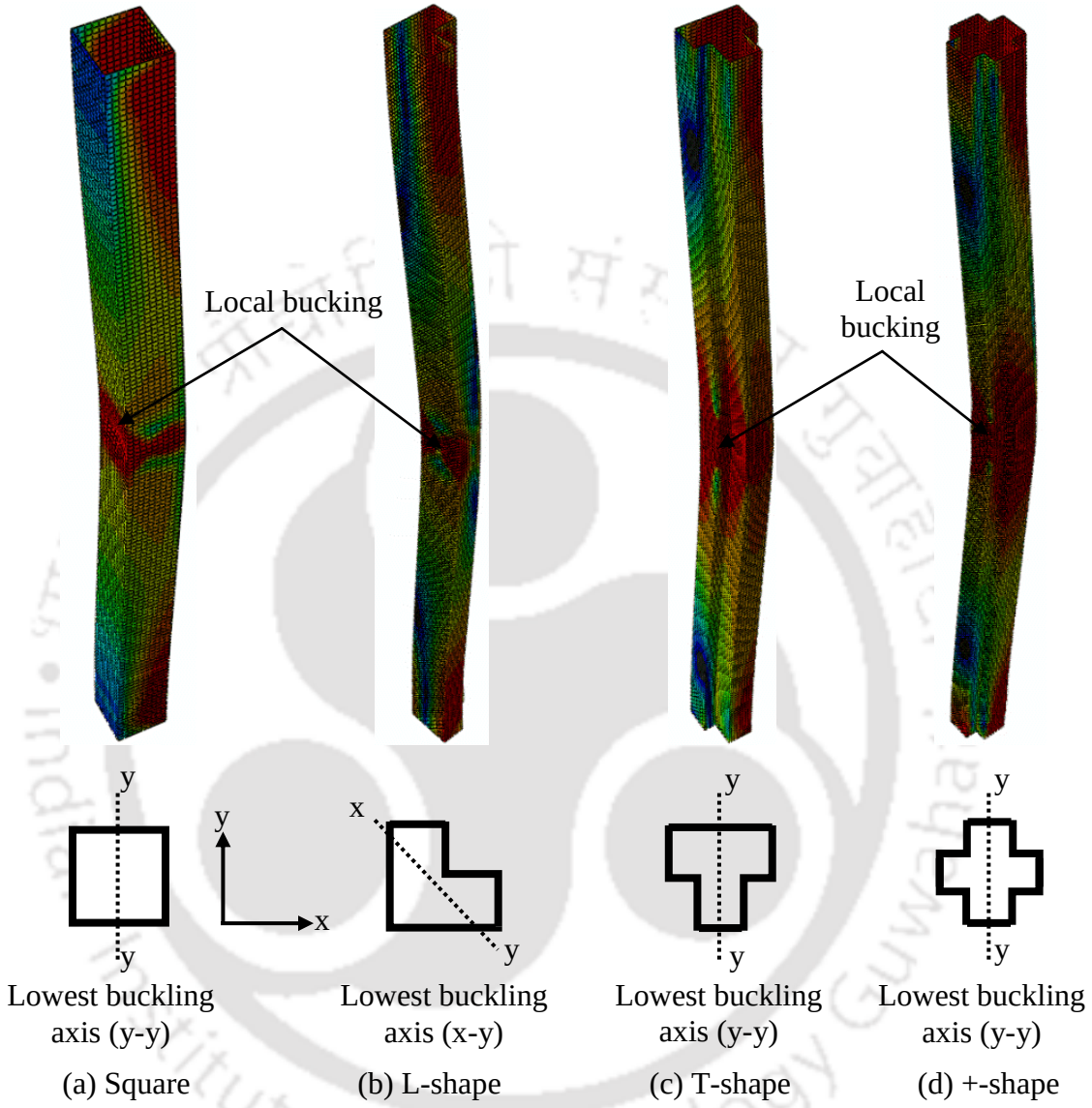

Figure 4.10: Von-Mises stress (superimposed on deformed shape) corresponding to deformation at 1.5xδ_u for Class 3 NRSs and representative square section (L = 3000 mm).

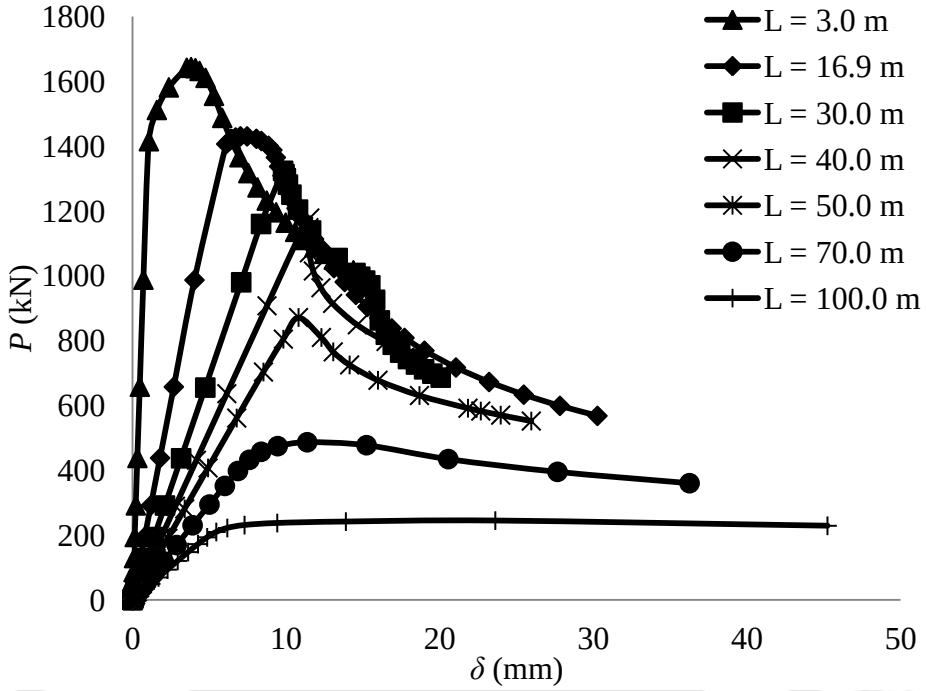

Figure 4.11: Typical variation of P with δ with varying lengths (Class 3 SHC).

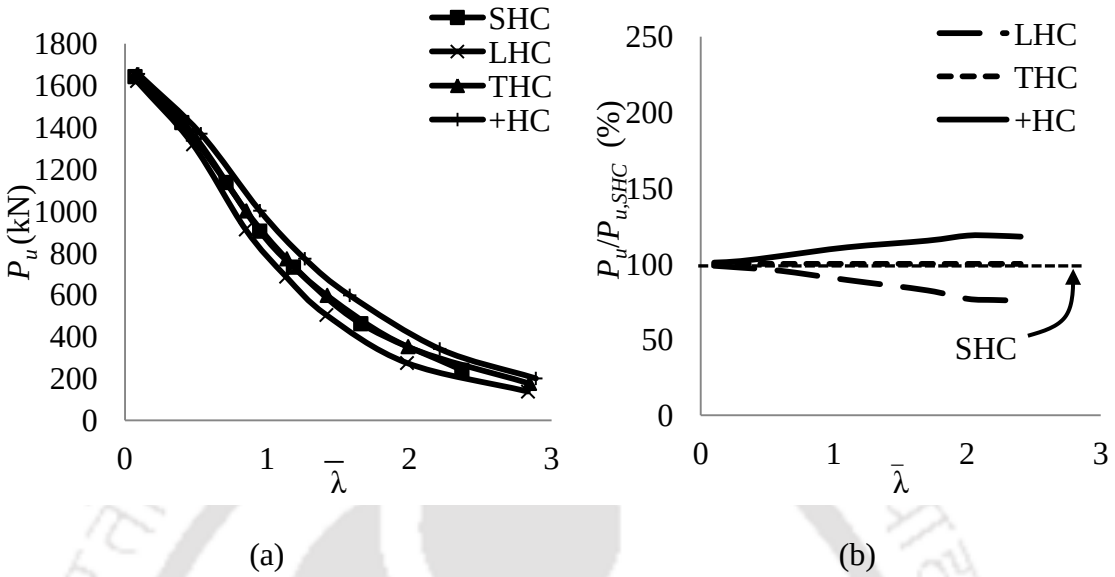

Figure 4.12: (a) Variation of P_u with $\bar{\lambda}$ and (b) $P_u/P_{u(SHC)}$ with $\bar{\lambda}$ for Class 3 sections.

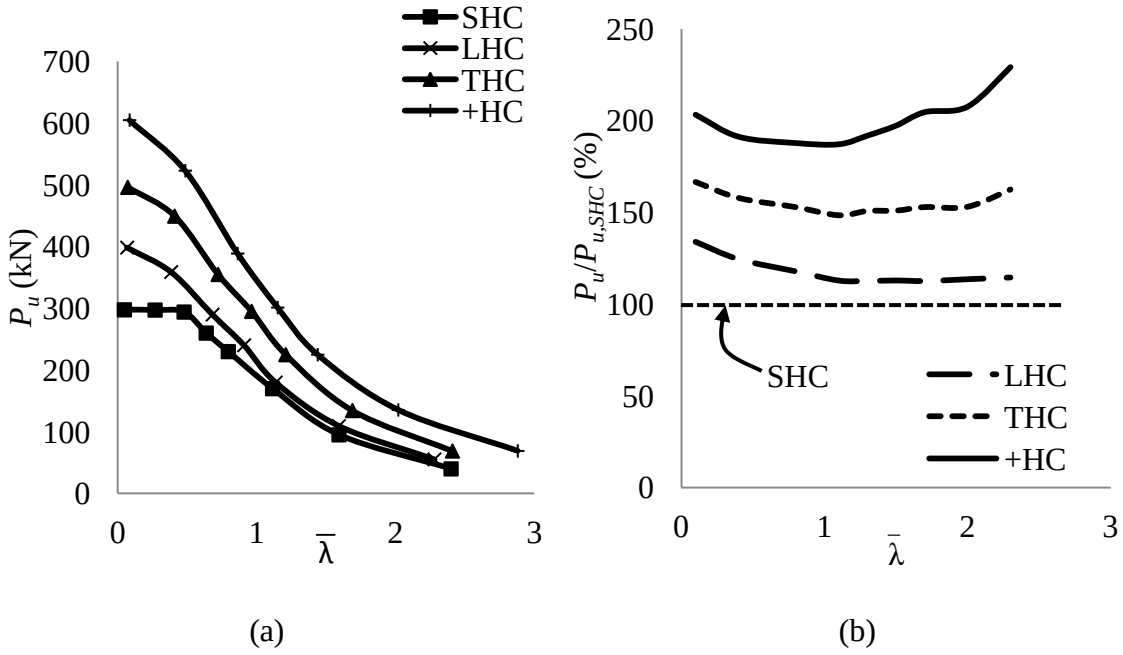

Figure 4.13: (a) Variation of P_u with $\bar{\lambda}$ and (b) $P_u/P_{u(SHC)}$ with $\bar{\lambda}$ for Class 4 sections.

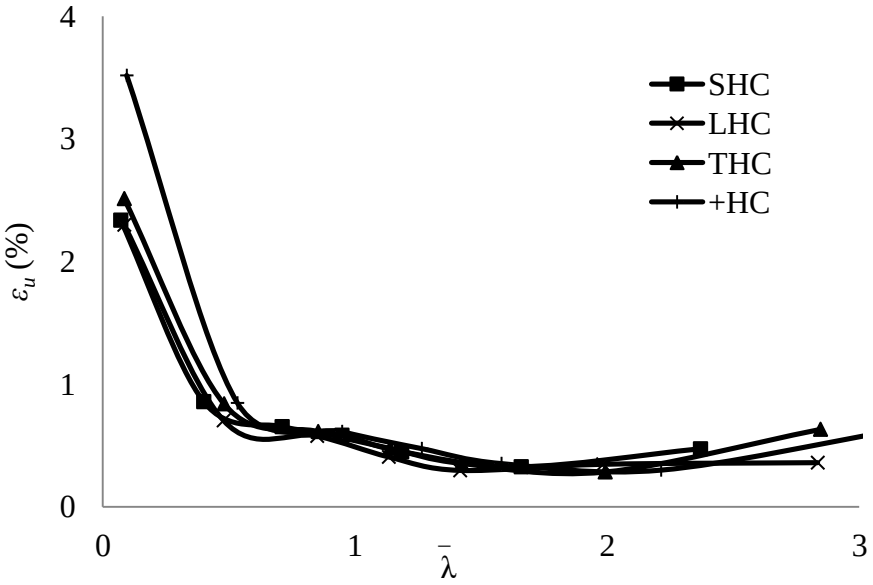

Figure 4.14: Variation of ε_u with $\bar{\lambda}$ for Class 3 sections.

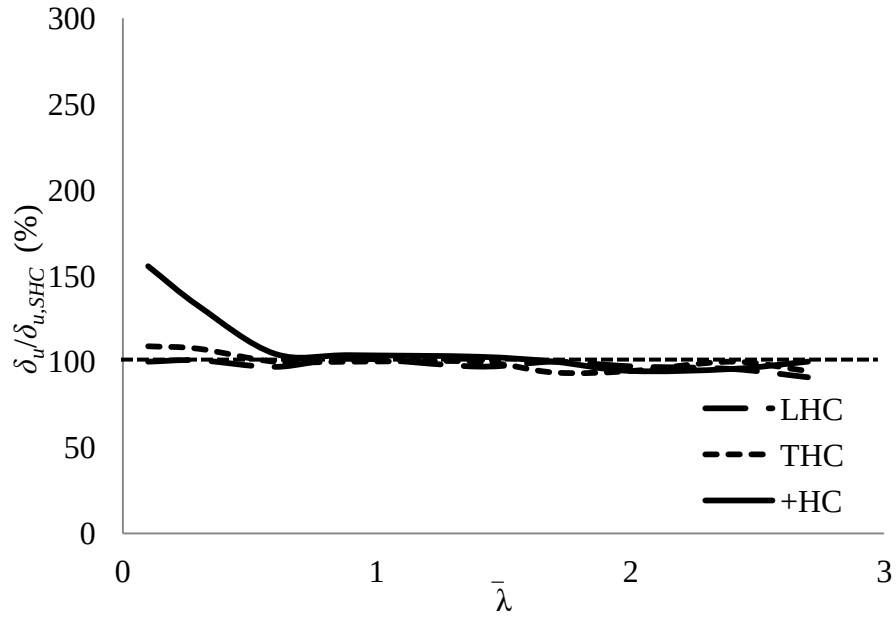

Figure 4.15: Variation of $\delta_u/\delta_{u,SHC}$ with $\bar{\lambda}$ for Class 3 sections.

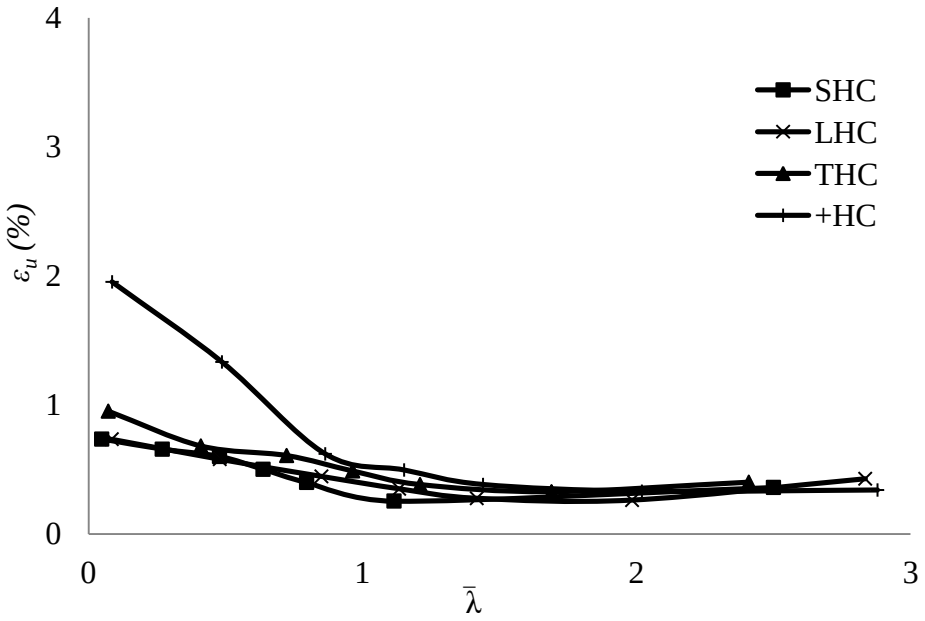

Figure 4.16: Variation of ε_u with $\bar{\lambda}$ for Class 4 sections.

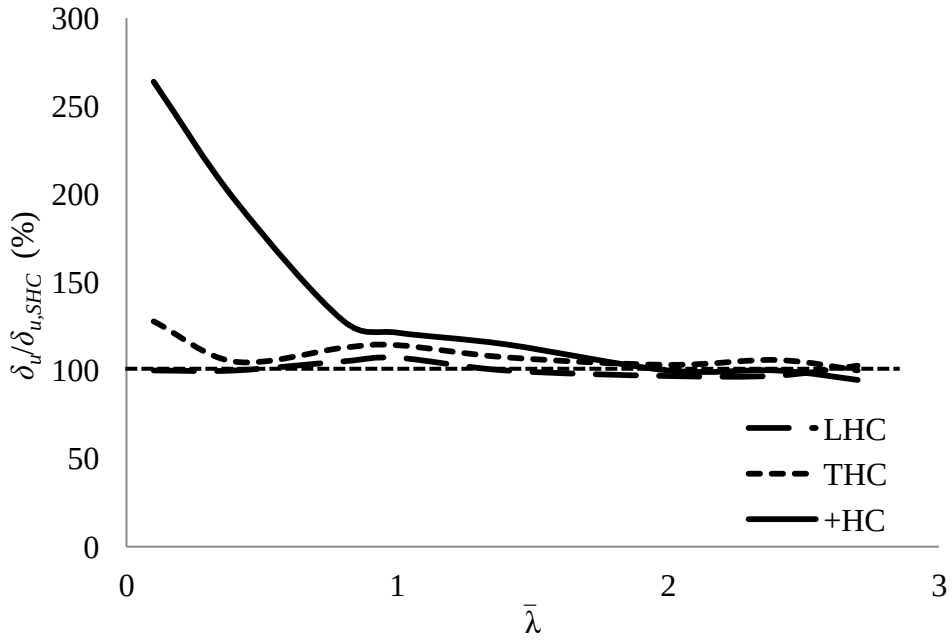

Figure 4.17: Variation of $\delta_u/\delta_{u,SHC}$ with $\bar{\lambda}$ for Class 4 sections.

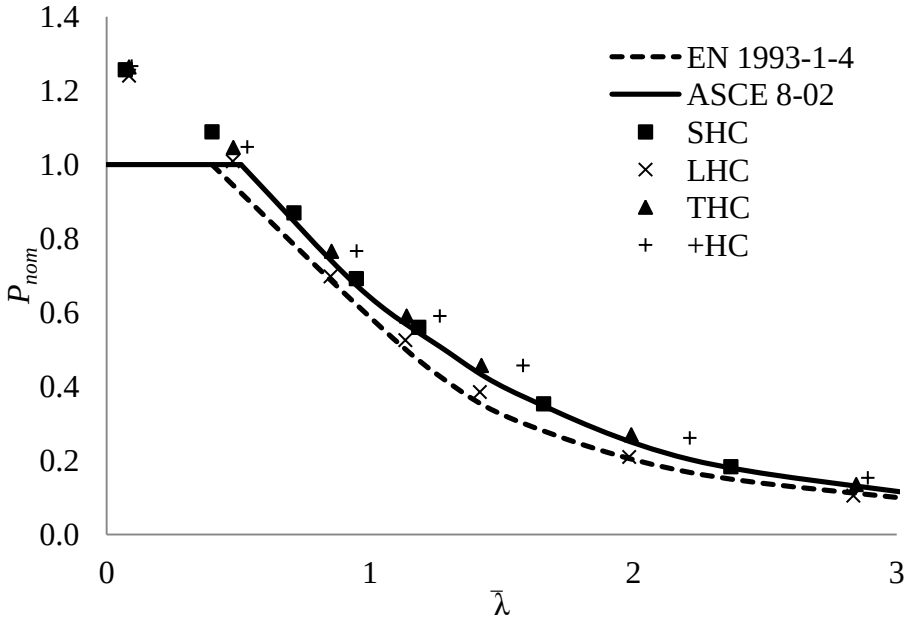

Figure 4.18: Variation of P_{nom} with $\bar{\lambda}$ for Class 3 sections.

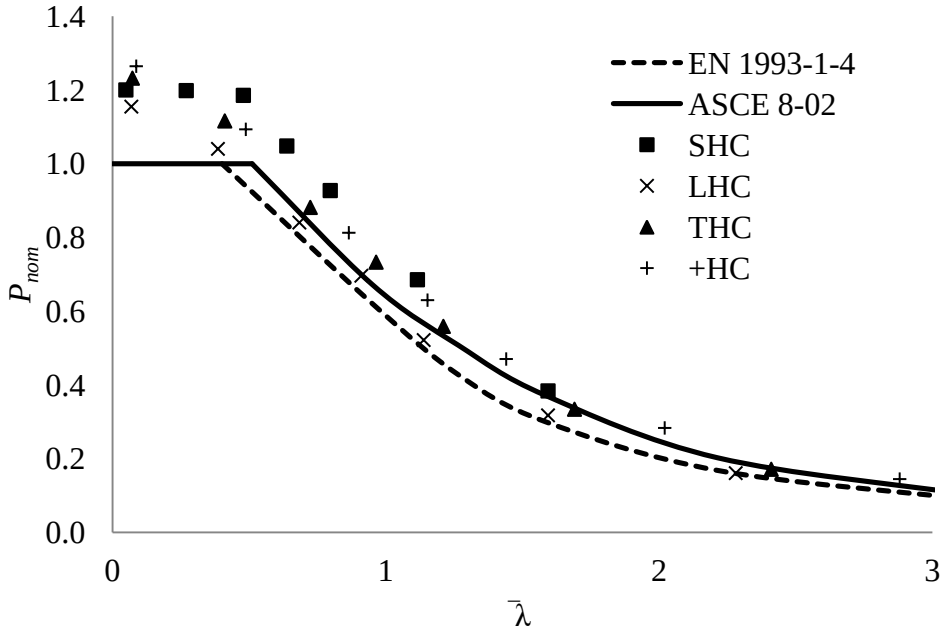

Figure 4.19: Variation of P_{nom} with $\bar{\lambda}$ for Class 4 sections.

CHAPTER 5

NUMERICAL MODELLING OF CONCRETE-FILLED LEAN DUPLEX STAINLESS STEEL STUB COLUMNS

5.1 INTRODUCTION

This chapter describes a series of numerical investigation on the behavior and strength of Concrete-Filled Lean Duplex Slender Stainless steel Tubular (CFDSST) stub columns under pure axial compression. The main objective of this study is to explore and compare the structural behaviours such as the load and deformation capacities and to see the effect of the LDSS tube thickness and concrete strength on the structural behavior of the CFDSST stub columns with NRSs and the representative square sections, but noting that all these column types have equal LDSS material cross-sectional areas as followed in Chapters 3 and 4, thus resulting in reduction of concrete core area by 36 % for NRSs compared to the representative square section. The FE results were compared with the currently available design standards for stainless steel, such as the European specification (EN 1994-1-1, 2004) and the American specification (ASCE 8-02, 2002), to assess their applicability in the design of concrete-filled LDSS hollow tubular stub columns. Reliability analysis of the design standards was also carried out based on the FE studies.

5.2 FE MODELLING

The development of an appropriate FE model requires a correct representation of the corresponding material characteristics as inaccurate representation of the material behavior, such as the LDSS and the concrete core material in the CFDSST columns, will overshadow the performance of even the most refined FE models. Gardner and Ashraf (2006) model is used to describe the LDSS material, as also validated through experimental test performed on hollow tubular stub column by Theofanous and Gardner (2009) and detailed in Section 3.3, in the FE modeling of CFDSST stub columns. In concrete-filled stainless steel tubular columns, small *D/t* ratios provide high considerable confinement for the concrete; hence, an equivalent uniaxial stress-strain relationship for confined concrete should be used. Whereas, high *D/t* ratios of concrete-filled stainless steel tubular columns provide inadequate confinement for the concrete, therefore the uniaxial stress-strain relationship for unconfined concrete can be used. As discussed in Section 2.6.2, Mander *et al*. (1988) defined the limiting *D/t* ratio between confined and unconfined concrete to be approximately equal to 29.2. In the present study of CFDSST stub columns with NRSs and the representative square sections, the uniaxial stress-strain relationship for the unconfined concrete was adopted as *D/t* ratio of the entire specimens lie in the range 30.0 to 80.0. The following sub-section presents further discussions on the steps followed to achieve an accurate FE model representation of the CFDSST stub columns.

5.2.1 Boundary conditions and analysis technique

The CFDSST stub columns considered had fixed ends which is similar to the approach followed for hollow tubular stub column FE models as discussed in Section 3.2.1. Figure 5.1 shows a typical geometry of a square CFDSST stub column. Similar analysis technique as mentioned in Section 3.2.1was followed, and the modified RIKS method was used in the nonlinear analyses of the CFDSST stub column FE models in line with

several other researchers (e.g. Dai and Lam, 2010; Hassanein, 2010; Hassanein *et al*., 2013).

5.2.2 FE mesh

S4R elements were used for representing the LDSS tube as detailed in Section 3.2.2. For the concrete core, a three-dimensional eight-noded solid element with reduced integration (C3D8R) having three translation degrees-of-freedom at each node was used. C3D8R is known to give an accurate representation of the concrete material, as also verified by various researchers (e.g. Ellobody and Young, 2006; Hassanein, 2010; Tao *et al*., 2011; Hassanein *et al*., 2013). A slightly coarse mesh was used throughout the FE study of CFDSST stub columns as the mesh refinement has very little influence on the numerical results (Hassanein, 2010). Accordingly, a mesh of an approximate global size ranging from 40 to 60 mm is used in the current modeling for the LDSS tube and concrete core. The aspect ratio of the element is kept at ~1.0 in all the FE models (see Figure 5.1).

5.2.3 Concrete core material model

The stress-strain curve development of the concrete core in the CFDSST stub columns is detailed in Section 2.7.2. Due to the thin nature of the LDSS tube adopted in the FE models (i.e. D/t > 29.2); inadequately confined concrete material model was adopted. Detailed modelling of the inadequately confined concrete core in the CFDSST stub column FE models through the Drucker-Prager (D-P) yield criterion model available in Abaqus (2009) and its potential in simulating the constitutive behavior of the concrete core is presented in Appendix C.

5.2.4 Modelling of concrete-LDSS tube interface

The contact between the LDSS tube and the concrete is modeled using interface elements which consist of two matching contact faces of LDSS tube and concrete elements. The mechanical property of the contact interaction is defined along normal and tangential directions to the interface respectively. The tangential mechanical property of the contact interaction is simulated by an isotropic Coulomb friction model, and the friction between the two faces is maintained as long as the surfaces remained in contact.

Dai and Lam (2010) studied different coefficient of friction (μ) (i.e. in the tangential direction), from 0.1 to 0.5, between the two interacting faces of the outer concrete core surface and the LDSS tube inner surface. It was found that there was little effect on the axial resistance when different friction factors were used, but using a smaller friction factor induced a convergent problem with large deformation. Therefore a μ of 0.2 to 0.3 is suggested to achieve a quick convergence and to obtain accurate results in the FE analyses of concrete-filled tubular columns. Hence, in the present FE studies of LDSS concrete-filled tubular stub columns, μ is taken as 0.25, in agreement with other researchers (e.g. Ellobody and Young, 2006; Hassanein, 2010; Hassanein *et al*., 2013). The 'Hard contact' relation in Abaqus (2009) is selected as normal mechanical property with no penetration allowed between the concrete core and the LDSS tube, which is to transfer the confinement effect of the LDSS hollow tubular sections to the concrete core, but is allowed to separate (e.g. Dai and Lam, 2010; Hassanein, 2010; Hassanein *et al*., 2013).

The effect of initial local imperfections on the CFDSST stub columns were neglected because the strength reduction is not significant compared to thin-walled hollow tubes owing to the delaying effect of steel tube local buckling by the core concrete (Tao *et al*., 2009).

5.3 VERIFICATION OF THE FE MODELS

In order to check the validity of the CFDSST stub column with NRSs and the representative square section for accurate representation of the concrete core strengths, similar experimental test conducted with $D/t > 29.2$ (i.e. the hollow tubular sections providing inadequately confinement to the concrete core) by Ellobody and Young (2006), Zuo *et al*., (2012) and Yang *et al*. (2010) for concrete-filled steel tubular stub columns with a square, L-shape, and T-shape sections, respectively, have been considered as the benchmark for verification. The measured dimensions and the steel material properties for the concrete-filled steel tubular stub columns with a square, L-shape, and T-shape sections are given in Figure 5.2 and Table 5.1.

Figure 5.3 shows a comparison of experimental results (Ellobody and Young, 2006; Zuo *et al*., 2012 and Yang *et al*., 2010) and FE results for concrete-filled steel tubular stub columns with a square, L-shape, and T-shape sections, and good agreement can be seen (see Figure 5.4). Also, in order to check the current FE models capability of simulating different concrete strengths, a comparison is made with the FE results by Hassanein (2010) for a rectangular CFDSST stub column with concrete compressive strengths of 25 MPa and 85 MPa (see Figure 5.4e). From Figure 5.4e, it can be seen that very good agreement was achieved. Hence, similar constitutive modeling of inadequately confined concrete stress-strain curve (as detailed in Appendix C) and the steps followed in the verification of FE models have been taken up in the subsequent FE analyses.

5.4 CONCRETE-FILLED TUBULAR STUB COLUMN MODELLING

5.4.1 Introduction

As a part of the study, a series of FE models to investigate the behaviour and strength of CFDSST stub columns are presented in this chapter. CFDSST stub columns of NRSs and

representative square section with compressive concrete strengths varying from 25 MPa to 100 MPa were analysed for the parametric study. The principle target was to build a knowledge basis for the mechanical behavior of this type of columns, which has not yet been investigated.

5.4.2 Development of the FE models

A total of 72 CFDSST stub columns along with 12 LDSS hollow tubular stub columns of NRSs and representative square sections with compressive concrete strengths varying from 25 MPa to 100 MPa were analysed for the parametric study. The dimensions as well as material properties of the LDSS hollow tubular and CFDSST stub columns are summarized in Table 5.2 (also see Figure 5.5). The LDSS cross-sectional areas of all the CFDSST stub columns are kept equal, to have the same steel material consumption, thus resulting in reduction of the concrete core area by 36 % for NRSs compared to the representative square section. LDSS hollow tubular and CFDSST stub columns are labeled such that the cross-sectional shape and concrete compressive strength can be identified from the label. For example, the label 'L1C0'and 'L2C25' defines the LDSS hollow tubular and CFDSST stub columns, respectively, with L-shape section of 7.5 mm and 9.0 mm thickness indicated by the letter "L1 and L2", respectively, and the letter "C0 and C25" defines the LDSS hollow tube and concrete compressive strength in MPa (25 MPa).

The length of all the stub columns (L) was chosen to be three times the overall depth of the sections to avoid the effects of flexural buckling and end conditions, as followed by several researchers (Dabaon *et al*., 2009, Hassanein, 2010, Uy *et al*., 2001, Young & Ellobody, 2006, Zuo *et a*l., 2012, Zhang & Yang, 2012). In line with other researchers (Hassanein, 2010, Zhang & Yang, 2012, Zuo *et a*l., 2012), the corners of the CFDSST stub columns of NRSs and representative square section are assumed herein to be exact 90^0 (i.e. corner radii are not considered).

Based on the thickness of the steel tube in the current investigation, which were taken as 7.5 mm, 9.0 mm and 10 mm, the lateral confining pressure (σ_{lat}) imposed by the current LDSS tubes were found to be negligible in all the models, as the *D/t* ratios of all the plate elements for the NRSs and representative square section considered are found to be greater than 29.2 (Mander *et al*., 1988). And hence, inadequately confined concrete models were considered in the FE models as discussed in the Section 2.7.2 and supplemented by Appendix C.

5.5 RESULTS AND DISCUSSION

5.5.1 Introduction

The results of the FE analysis for the CFDSST stub columns were presented in terms of variation in the load and deformation capacities along with the failure modes with change in the cross-sectional shape and thickness of the LDSS tube. The FE results of the CFDSST stub columns were compared with the currently available design standards for stainless steel, such as, the European (EN1994-1-1, 2004) and American (ASCE 8-02, 2002) specifications for their applicability in the design of the CFDSST stub columns. Reliability analyses of these design standards were also discussed based on the FE studies.

5.5.2 Deformed shapes of NRSs and square section

Figures 5.6a-f show typical von-mises stress superimposed over deformed shapes (or failure modes) at P_u for square, L, T, and +-shape sections. It can be seen that only slight overall out-of-plane deformation of the entire four faces, two faces, and one face (i.e at the longer faces of 600 mm wide) can be seen for the square, L-shaped and T-shaped sections, respectively, at P_u, for all the thickness considered (see Figure 5.6a-e), except for +-shaped section and at the shorter faces of L- and T-shape sections (i.e 300 mm side

width) where no local buckling is seen at P_u (see Figure 5.6b-f). Thus, it can seen that the initiation of local buckling can be delayed by decreasing the width-to-thickness ratio of the LDSS tube.

Figures 5.6g-l show typical von-mises stress superimposed over deformed shapes at 3xδ_u for square, L, T, and +-shape sections. The post peak failure modes in all the CFDSST stub columns are mainly through localized outward buckling of the wider faces of the LDSS tube (i.e local outward buckling at mid-height for the square and T-shape sections and near the two ends for L- and +-shape sections) followed by local buckling of the remaining shorter faces (i.e alternate local inward and outward buckling at mid-height for the L- and T-shape sections (see Figure 5.6)), and compression crushing of the concrete core. However, for +-shape section, no significant local buckling is not seen at the shorter faces (150 mm side width) of the LDSS tube which may be attributed to enhanced cross-section stability due to shorter sides and increased number of corners (similar to the observations made for hollow tubular stub columns), which further delays local buckling of the LDSS tube.

5.5.3 Load-axial deformation profile

Figure 5.7 shows typical variation of P with δ for CFDSST stub columns (square section and +-shape section) along with variation of von-mises stress distribution (over deformed shaped) at pre-peak (location S1), peak (location S2) and post-peak loads (location S3 and S4).). S1 marks the stage at which a profound change in the curve is seen, which approximately occurs at around ~ 0.75 P_u for all the CFDSST stub columns, as also observed by other researchers (e.g. Ren *et al*., 2011). S2 defines the ultimate strength capacity of the CFDSST stub column, and depends on the concrete cubic strength (see Figures 5.7a&b), cross-sectional shapes, and the LDSS tube thicknesses. Figure 5.8 shows the effect of concrete core strength on the P versus ε curve of CFDSST stub columns and found to be typical for all the thicknesses studied. Hence, only the LDSS tube thickness of 10.0 mm was plotted. It can be seen from Figure 5.8 that filling the

LDSS tube with concrete greatly enhances the strength capacity of the CFDSST stub columns, however, at the cost of decreasing ε_u (i.e. ε at Pu) with increasing concrete strengths. And with change in the cross-section from square → L → T → + shape, the better the section becomes in achieving more strain hardening and delay strain softening due to the increased confinement provided to the concrete core by the steel tube (see Figures 5.7a&c and Figure 5.7d). Thus, achieving a higher axial deformation capacity by the concrete-filled tubular stub column with NRSs compared to the representative square section (see Figure 5.8). At the location S3 of the post-peak (i.e taken at 0.85 P_u), there is local buckling of the steel tube and consequently reduces the confining pressure on the concrete. With change in the concrete strength as well as cross-section from square → L → T → + shape, the difference in the crushing strain of S2 and S3 gets wider and post peak curve from S2 to S3 gets milder due to the delay in localized buckling of the LDSS tube (see Figures 5.7 and 5.8), as also explained in Section 5.5.2. At S4, there is total failure of the CFDSST stub columns, as seen is Figures 5.7 and 5.8, where there is no increase in the P with further increase of ε. However, there is still a redundant strength (which may be coming from the combined effect of the LDSS tube and the confined crushed concrete) as also observed by several other researchers (e.g. Tao *et al*., 2011, Zuo *et al*., 2012,, Yang *et al*., 2010), of about 1.5 to 2 times that of the strength of the hollow tubular stub columns (see Figure 5.8).

5.5.4 Influence of the LDSS tube

Figures 5.9a&b show a plot of $P_u/P_{u,hollow}$ (%) versus f_{ck} for the CFDSST stub columns with NRSs and representative square section. It can be seen form Figures 5.9a&b that the influence of the LDSS tube alone (excluding the involvement of the concrete core and the confinement effect) on the P_u decreases with increasing concrete strength and increases with increasing thickness of the steel tube. Also, it can be readily seen that the contribution of the LDSS tube on the P_u becomes more effective as the cross-sectional shape changes from square → L → T → +-shape section. This may attributed to the

delay in the local buckling offered by the NRSs. Based on the findings of the study it was found that on filling the LDSS tube with concrete, there is an increase in the P_u by about 70 % to 435 %, 63 % to 299 %, 35 % to 283 %, and 20 % to 181% for square, L, T, and +-shape sections, respectively.

Figures 5.9c&d show a plot of $\delta_u/\delta_{u,hollow}$ (%) versus f_{ck} for the CFDSST stub column with NRSs and representative square section. It can be seen from Figures 5.9c&d that the influence of the LDSS tube on the δ_u increases with increasing thickness of the LDSS tube (i.e influence of local buckling on the LDSS tube decreases with increasing thickness) and increasing concrete strength (i.e as concrete strengths increases, it becomes less ductile, thereby, the main contribution on δ_u comes from the LDSS tubes).

Hence, a simple change of cross-section provides effective utilization of the steel tube material which in turn improves the strength and deformation capacities of CFDSST stub columns.

5.5.5 Strength capacity of concrete-filled NRSs and square section

Figure 5.10 shows the variation of P_u with f_{ck} for CFDSST stub columns of NRSs and representative square section with LDSS tube thickness of 10.0 mm. Only the results corresponding to 10.0 mm was plotted as similar behavior has been observed for both the thicknesses of 7.5 mm and 9.0 mm. It can be seen from Figure 5.10 that P_u linearly increases with increasing f_{ck} from 25 MPa to 100 MPa. The rate of increase in the load capacities with increasing f_{ck} for square section is higher compared to NRSs, where, the all the NRSs showed a similar rate. From Figure 5.10, it can also be observed that for normal concrete strength ($f_{ck} \leq 40$ MPa), NRSs appears to have similar or slightly enhanced P_u, in comparison with square section. At higher f_{ck} (> 40 MPa), L-, T-, and +-shape sections predicted lower values of P_u (for $f_{ck} = 100$ MPa) by about 18 %, 15 % and 12 %, respectively, compared to the representative square section. Thus, it indicates that there appears to have certain tangible benefit in using NRSs for normal concrete as

compared to the representative square section, this is in addition to the 36% area reduction in concrete core (leading to lighter sections). But in the case of high strength concrete core, NRSs are clearly at disadvantage as far as the values of P_u is concerned, however as the NRSs are lighter by 36%, they still offers an attractive options for the designers.

In order to examine the effect of concrete strength on the CFDSST stub columns, the efficiency of the cross-sections expressed as $P_u/P_{u,C25}$ was calculated, where $P_{u,C25}$ is the FE ultimate strength for the CFDSST stub columns with f_{ck} = 25 MPa. Figure 5.11 plots the efficiency with respect to f_{ckI} for LDSS tube thicknesses of 7.5 mm and 10.0 mm. Simply, it can be noticed that by increasing the strength of the concrete core, for all the NRSs and representative square section, there is a linear increase in the strength for the range of concrete strengths investigated herein (25–100 MPa). Also, it can be seen that the square section shows a higher increasing rate compared to the NRSs for the same LDSS tube thickness.

Figures 5.12a&b show a typical plot of P_u versus t and f_{ck}, respectively, for CFDSST stub columns. It can be seen from Figure 5.12(a) that on increase in thickness of the LDSS tube for all the CFDSST stub columns from 7.5 mm to 9.0 (20 % increase) and 10.0 mm (33% increase), the average increase in strengths are 14-19 % and 25-30 %, respectively. On increase in concrete strength from 40 MPa to 48 MPa (20 % increase) and 53 MPa (33% increase), the average increase in strengths are 6 - 9 % and 10 - 15 %, respectively (see Figure 5.12b). Hence increasing the thickness of the LDSS tube is more beneficial in increasing the strength of the CFDSST stub columns rather than the concrete strength.

5.5.6 Deformation capacity of concrete-filled NRSs and square section

Figure 5.13a shows variation of δ_u with f_{ck} for CFDSST stub columns. It shows that in CFDSST stub columns, δ_u decreases with increasing concrete strengths, but increases as the sections changes from Square → L → T → +-shape. The drop in δ_u with increasing

concrete strength may be related to increasing compression stiffness of the concrete core. Further, lower values of δ_u for the representative square section may be attributed to early buckling of the LDSS tube thus providing less confinement on the concrete core as compared to the NRSs.

Figure 5.13b shows variation of δ_u with t for CFDSST stub columns. It can be seen from Figure 5.13b that by increasing the steel tube thickness from 7.5 mm to 9.0 mm (20 % increase) and 10.0 mm (33 % increase), the average increase in δ_u for square section is 5.39 % and 10.16 %, L-shaped section is 7.01 % and 13.97 %, T-shaped section is 7.01 % and 13.97 %, and +-shaped section is 3.24 % and 7.17 %, respectively.

5.5.7 Comparison with design codes

The FE results were compared with the unfactored design strengths as per the European (EN 1993-1-1, 2004) and American (ASCE 8-02, 2002) specifications. A sample cross-section resistance calculation of a square CFDSST stub column with the two design standards is given in Appendix D. The design standards are based on the stainless steel material and hence their applicability on LDSS is assessed through the FE results.

5. 5.7.1 Effective area determination

The effective width concept as detailed in Section 3.5.7.1 given in EN 1993-1-4 (2006) to account for the effect of local buckling on the LDSS tube was considered in the design strengths of the CFDSST stub columns. In the present study of the CFDSST stub columns, all the cross-sections considered lies under Class 4 section, and Figure 5.14 shows the location of B_e for the Class 4 sections of NRSs and the representative square section.

5. 5.7.2 Cross-section resistance

The CFDSST stub columns were designed as concentrically loaded compression members. The design strengths as per EN 1994-1-1 (2004) and ASCE 8-02 (2002) specifications are defined by Equation 5.1 and 5.2, respectively. The plastic resistance of the concrete-filled stainless steel tubular columns should be calculated by adding the plastic resistance of the steel tube material and the concrete core, in the case no reinforcement was used, as in the current finite element specimens, as follows:

$$P_{EN1994\text{-}1\text{-}1} = A_s f_y + A_c f_c \quad (5.1)$$

$$P_{\text{ASCE 8-02}} = A_s f_n + A_c f_c \quad (5.2)$$

where A_s is the cross-sectional area of steel and determined as given in Section 3.5.7.1, A_c is the cross-sectional area of concrete, and f_c is the design value of the cylinder compressive strength of concrete.

5. 5.7.3 Comparison of FE strengths with design strengths

Figures 5.15 - 5.18 show a comparison of FE results with the design standards and plot the variation of P_u versus f_{ck} for CFDSST stub columns of NRSs and representative square section. It can be seen from Figure 5.15 - 5.18 that a linearly increasing P_u with increasing f_{ck} is seen from both the FE analysis and codal predictions through EN 1994-1-1 (2004) and ASCE 8-02 (2002) specifications. FE strengths over predicts the EN 1994-1-1 (2004) specification by about in average 21 %, 19%, 14 % and 4 % for the square, L, T, and +-shape sections, respectively, whereas, ASCE 8-02 (2002) specification gives a slightly conservative prediction in average of about 16 %, 10%, 8 % and 1 % for the square, L, T, and +-shape sections, respectively.

5.5.7.4 Reliability analysis of the codes

The reliability analysis of the EN 1993-1-1 (2004) and ASCE 8-02 (2002) specifications based on the FE results is carried out as detailed in Section 3.6.6.4 of Chapter 3. Reliability indices are tabulated in Tables 5.3, 5.4 and 5.5 for 7.5 mm, 9.0 mm, and 10.0 mm thickness, respectively.

Based on the reliability analyses it can be seen that except for CFDSST stub columns with +-shape section, both the codes show $\beta_0 \geq 2.5$ when compared with the present FE results. Considering the lower limit of β_0 = 2.5 suggested by ASCE 8-02 (2002) specification for structural members, it can be inferred that both specifications can be adopted for all the design of CFDSST stub columns except for CFDSST stub columns with +-shape section, wherein a suitable modification may be employed after systematic studies (including experiments). However, for CFDSST stub columns, design based on the American specification tends to be slightly more reliable compared to the European specification.

5.6 CONCLUSIONS

A comprehensive FE analysis of CFDSST stub columns with NRSs and representative square section for various concrete compressive strengths ranging from 25 MPa to 100 MPa has been carried out in this work to understand the cross-sectional shape effect on the ultimate load and deformation characteristics. As the steel material being relatively expensive compared to concrete, the steel material cross-sectional area for the NRSs and representative square section are kept equal, giving a reduction in the concrete core area of about 36 % for the NRSs. The following conclusions are drawn within the limitation of this study:

1) Out-of-plane deformation (seen only at the longer faces) of the entire four faces, two faces, and one face can be seen for the square, L-shaped and T-shaped sections,

respectively, at P_u, except for +-shaped section and at the shorter faces of L- and T-shape sections where no local buckling is seen at P_u.

2) On filling the LDSS tube with concrete, there in an increase in the P_u by about 70 % to 435 %, 63 % to 299 %, 35 % to 283 %, and 20 % to 181% for square, L, T, and +-shape sections, respectively.

3) The influence of the LDSS tube on the δ_u increases with increasing thickness of the LDSS tube and increasing concrete strength.

4) For normal concrete strength ($f_{ck} \leq 40$ MPa), NRSs appears to have similar or slightly enhanced P_u, in comparison with square section. At higher f_{ck} (> 40 MPa), L-, T-, and +-shape sections predicted lower values of P_u (for f_{ck} = 100 MPa) by about 18 %, 15 % and 12 %, respectively, compared to the representative square section.

5) Increasing the strength of the concrete core, for all the NRSs and representative square section, there is a linear increase in the strength for the range of concrete strengths investigated herein (25–100 MPa). Also, it can be seen that the square section shows a higher increasing rate compared to the NRSs for the same LDSS tube thickness.

6) On increase in thickness of the LDSS tube for all the CFDSST stub columns from 7.5 mm to 9.0 (20 % increase) and 10.0 mm (33% increase), the average increase in strengths are 14-19 % and 25-30 %, respectively. On increase in concrete strength from 40 MPa to 48 MPa (20 % increase) and 53 MPa (33% increase), the average increase in strengths are 6 - 9 % and 10 - 15 %, respectively. Hence increasing the thickness of the LDSS tube is more beneficial in increasing the strength of the CFDSST stub columns rather than the concrete strength.

7) In CFDSST stub columns, δ_u decreases with increasing concrete strengths, but increases as the sections changes from Square → L → T → +-shape.

8) FE strengths over predicts the EN 1994-1-1 (2004) specification by about in average 21 %, 19%, 14 % and 4 % for the square, L, T, and +-shape sections, respectively, whereas, ASCE 8-02 (2002) specification gives a slightly conservative prediction by about in average 16 %, 10%, 8 % and 1 % for the square, L, T, and +-shape sections, respectively.

9) Based on the reliability analyses it can be inferred that both specifications can be adopted for all the design of CFDSST stub columns except for CFDSST stub columns with +-shape section, wherein a suitable modification may be employed after systematic studies (including experiments). However, for CFDSST stub columns, design based on the American specification tends to be slightly more reliable compared to the European specification.

Table 5.1: Measured dimensions of concrete-filled stub columns.

Specimen	L (mm)	B (mm)	H (mm)	t (mm)	Material Properties		Tested by
					Concrete strength, f_c (MPa)	Steel tube, f_y (MPa)	
S9	299	100	100	4.10	97.20	333	Ellobody & Young (2006)
C1	1200	400	400	6.00	47.60	465	Zuo *et al.*, (2012)
T-4	900	330	270	3.49	23.20	315	Yang *et al.* (2010)

Table 5.2: Details of LDSS hollow tubular and CFDSST stub columns of NRSs and the representative square sections.

Specimen	Dimensions and Cross-sectional areas						% deduction in A_c	Material properties	
	D (mm)	B (mm)	t (mm)	L (mm)	A_s (mm^2)	A_c (mm^2)		$\sigma_{0.2}$ (MPa)	f_{ck} (MPa)
S1C0 S2C0 S3C0	600	600	7.5 9.0 10.0	1800	17775 21276 23600	-	-	657	-
L1C0 L2C0 L3C0	600	600	7.5 9.0 10.0	1800	17775 21276 23600	-	-	657	-
T1C0 T2C0 T3C0	600	600	7.5 9.0 10.0	1800	17775 21276 23600	-	-	657	-
+1C0 +2C0 +3C0	600	600	7.5 9.0 10.0	1800	17775 21276 23600	-	-	657	-
S1C25 to S1C100 S2C25 to S2C100 S3C25 to S3C100	600	600	7.5 9.0 10.0	1800	17775 21276 23600	336400	Nil	657	25 to 100
L1C25 to L1C100 L2C25 to L2C100 L3C25 to L3C100	600	600	7.5 9.0 10.0	1800	17775 21276 23600	246400	36.0	657	25 to 100
T1C25 to T1C100 T2C25 to T2C100 T3C25 to T3C100	600	600	7.5 9.0 10.0	1800	17775 21276 23600	246400	36.0	657	25 to 100
+1C25 to +1C100 +2C25 to +2C100 +3C25 to +3C100	600	600	7.5 9.0 10.0	1800	17775 21276 23600	246400	36.0	657	25 to 100

Table 5.3: Comparison of FE strengths with codal design strengths for 7.5 mm thickness of the steel tube.

Concrete cubic strength, f_{ck} (MPa)	$P_{FE}/P_{EN\ 1993\text{-}1\text{-}1}$				$P_{FE}/P_{ASCE\ 8\text{-}02}$			
	SHC	LHC	THC	+HC	SHC	LHC	THC	+HC
25	1.399	1.408	1.309	1.143	1.287	1.265	1.194	1.087
40	1.277	1.278	1.214	1.112	1.201	1.175	1.128	1.066
55	1.215	1.204	1.149	1.076	1.158	1.124	1.081	1.038
70	1.154	1.143	1.126	1.052	1.109	1.078	1.068	1.019
85	1.120	1.106	1.091	1.029	1.083	1.051	1.042	1.001
100	1.102	1.086	1.083	1.015	1.070	1.039	1.039	0.990
Mean, P_m	1.211	1.204	1.162	1.071	1.152	1.122	1.092	1.034
COV, V_p	0.085	0.092	0.068	0.042	0.065	0.070	0.050	0.033
Reliability index, β_0	2.81	2.77	2.71	2.46	2.92	2.82	2.76	2.59

Table 5.4: Comparison of FE strengths with codal design strengths for 9.0 mm thickness of the steel tube.

Concrete cubic strength, f_{ck} (MPa)	$P_{FE}/P_{EN\ 1993\text{-}1\text{-}1}$				$P_{FE}/P_{ASCE\ 8\text{-}02}$			
	SHC	LHC	THC	+HC	SHC	LHC	THC	+HC
25	1.416	1.358	1.248	1.103	1.281	1.209	1.132	1.047
40	1.300	1.262	1.185	1.061	1.205	1.148	1.093	1.015
55	1.229	1.188	1.147	1.068	1.157	1.096	1.070	1.027
70	1.182	1.149	1.110	1.037	1.124	1.072	1.045	1.002
85	1.150	1.147	1.081	1.019	1.101	1.079	1.025	0.988
100	1.130	1.102	1.049	1.004	1.087	1.044	1.000	0.976
Mean, P_m	1.235	1.201	1.137	1.049	1.159	1.108	1.061	1.009
COV, V_p	0.082	0.071	0.062	0.038	0.058	0.051	0.051	0.034
Reliability index, β_0	2.89	2.82	2.64	2.39	2.96	2.81	2.66	2.50

Table 5.5: Comparison of FE strengths with codal design strengths for 10.0 mm thickness of the steel tube.

Concrete cubic strength, f_{ck} (MPa)	$P_{FE}/P_{EN\ 1993\text{-}1\text{-}1}$				$P_{FE}/P_{ASCE\ 8\text{-}02}$			
	SHC	LHC	THC	+HC	SHC	LHC	THC	+HC
25	1.429	1.339	1.231	1.085	1.282	1.189	1.115	1.029
40	1.323	1.251	1.167	1.038	1.216	1.133	1.073	0.992
55	1.250	1.183	1.126	1.056	1.167	1.086	1.047	1.014
70	1.202	1.146	1.095	1.035	1.134	1.064	1.027	0.999
85	1.165	1.118	1.081	1.009	1.108	1.046	1.020	0.976
100	1.143	1.101	1.063	0.995	1.094	1.037	1.009	0.965
Mean, P_m	1.252	1.19	1.127	1.036	1.167	1.093	1.048	0.996
COV, V_p	0.085	0.071	0.059	0.044	0.057	0.055	0.054	0.044
Reliability index, β_0	2.92	2.79	2.62	2.34	22.99	2.75	2.61	2.44

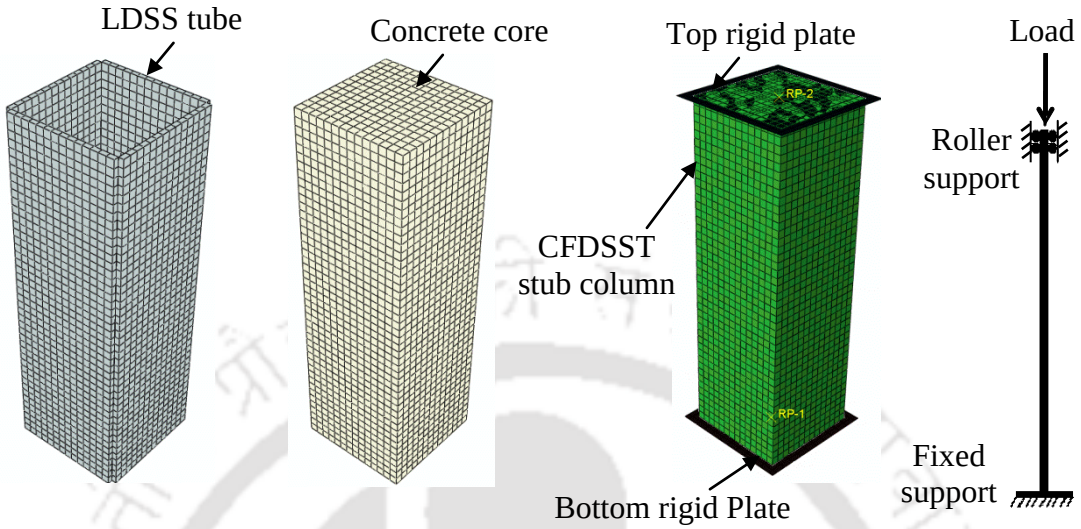

Figure 5.1: Typical Boundary conditions applied to CFDSST stub column FE models.

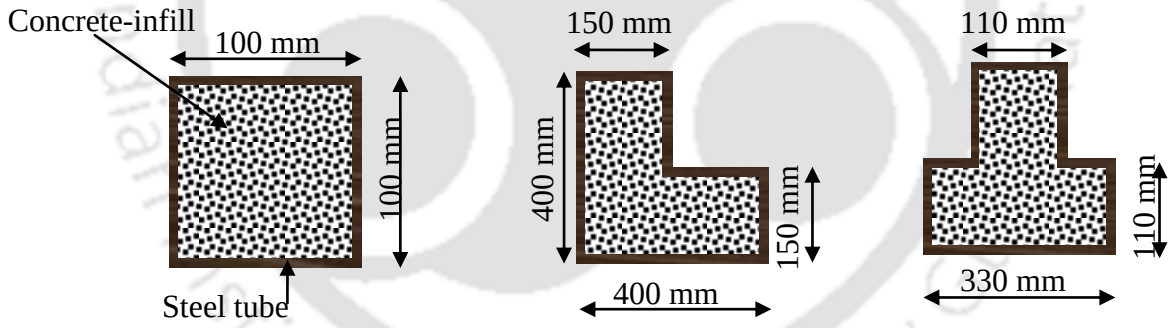

(a) S9 (Ellobody and Young, 2006)

(b) C1 (Zou *et al*., 2012)

(c) T-4 (Yang *et al*., 2012)

Figure 5.2: Concrete-filled steel tubular stub column specimens.

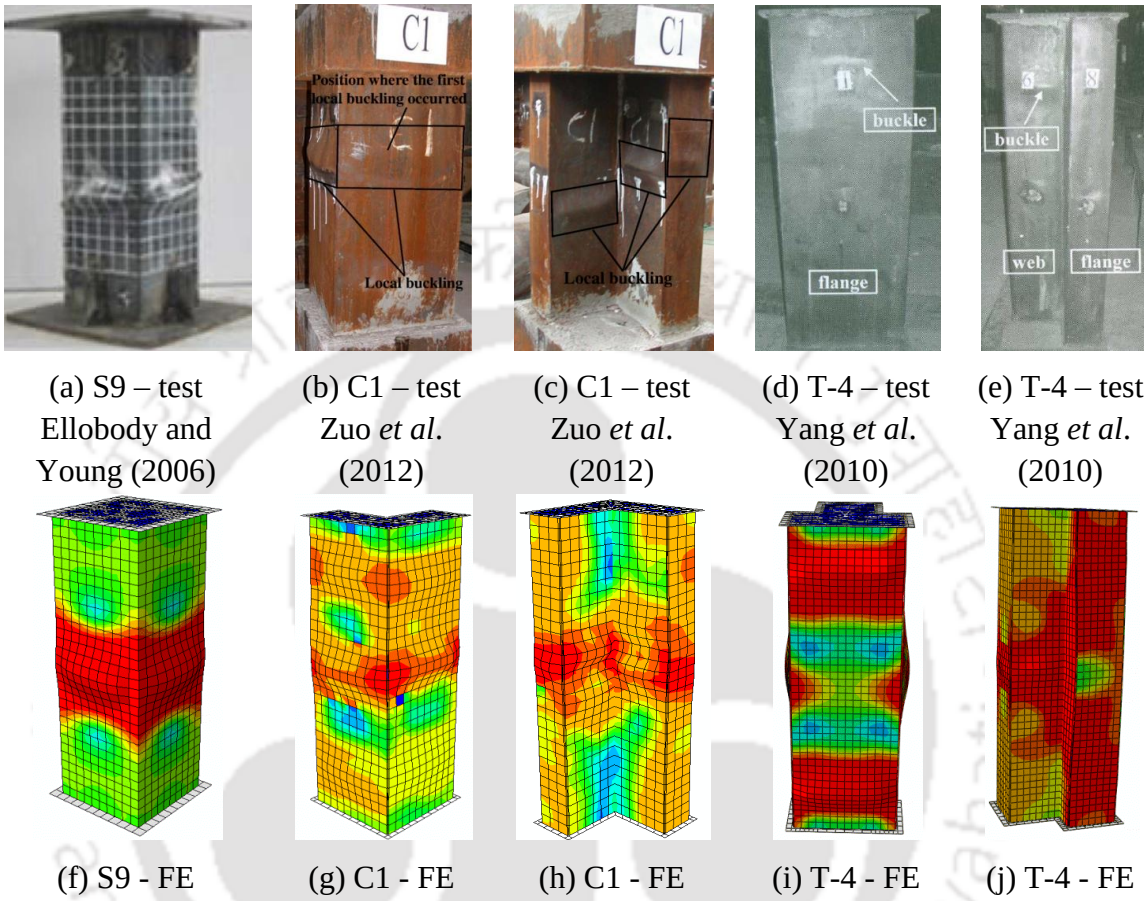

(a) S9 – test Ellobody and Young (2006) | (b) C1 – test Zuo *et al.* (2012) | (c) C1 – test Zuo *et al.* (2012) | (d) T-4 – test Yang *et al.* (2010) | (e) T-4 – test Yang *et al.* (2010)

(f) S9 - FE | (g) C1 - FE | (h) C1 - FE | (i) T-4 - FE | (j) T-4 - FE

Figure 5.3: Comparison of the experimental and FE failure modes for the concrete-filled steel tubular stub columns.

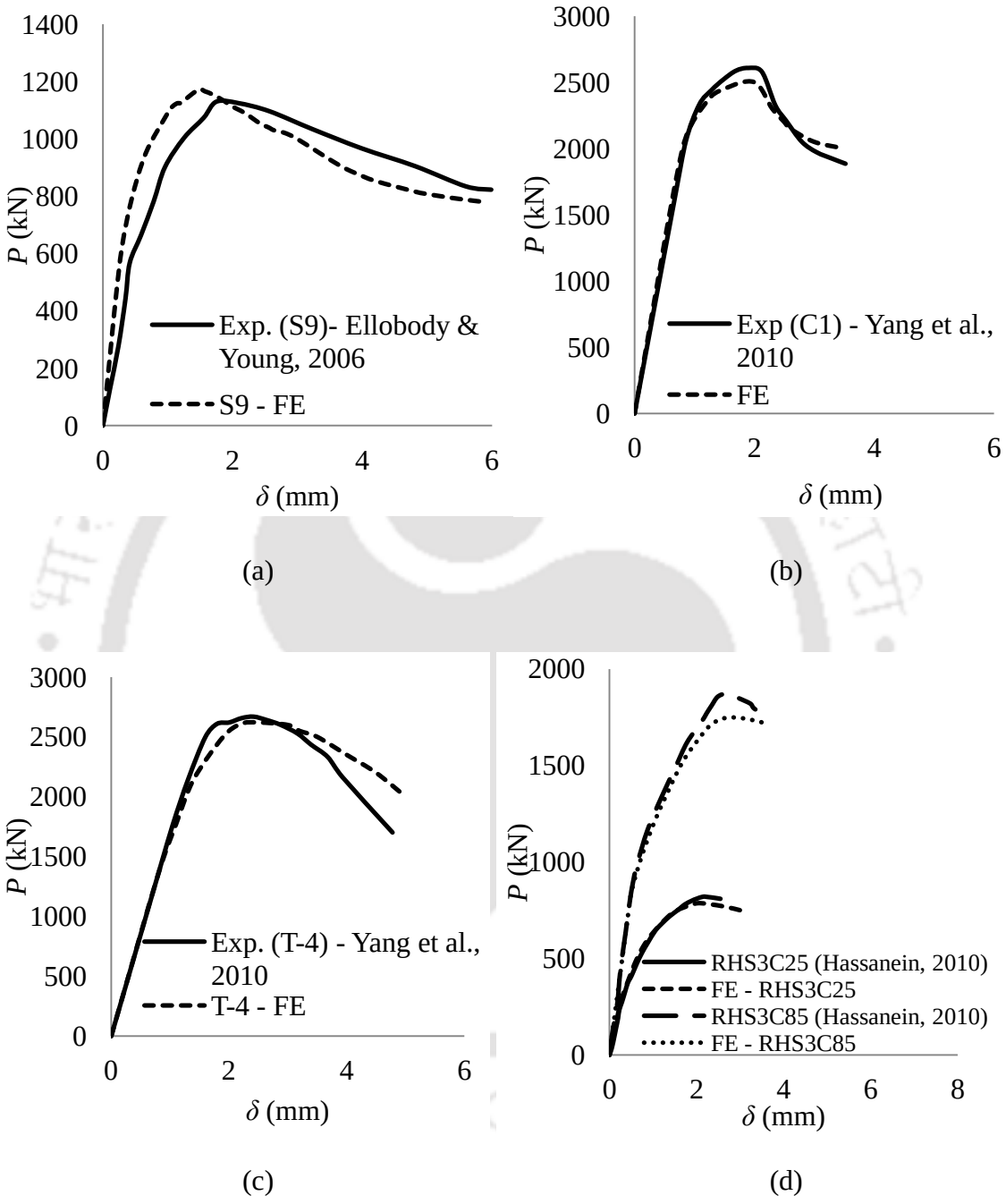

Figure 5.4: *P* versus δ plot for the concrete-filled tubular stub columns specimens.

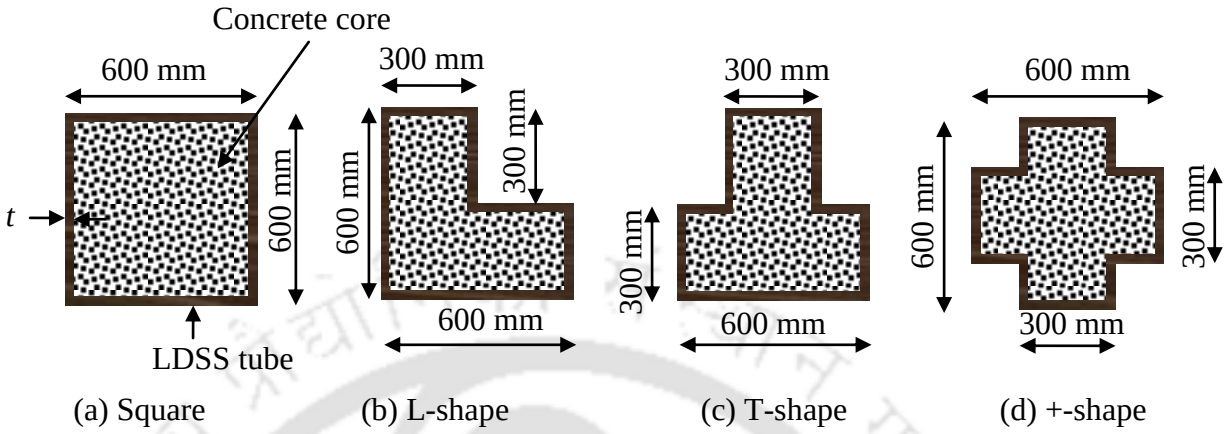

Figure 5.5: Numerical test specimens of CFDSST stub columns.

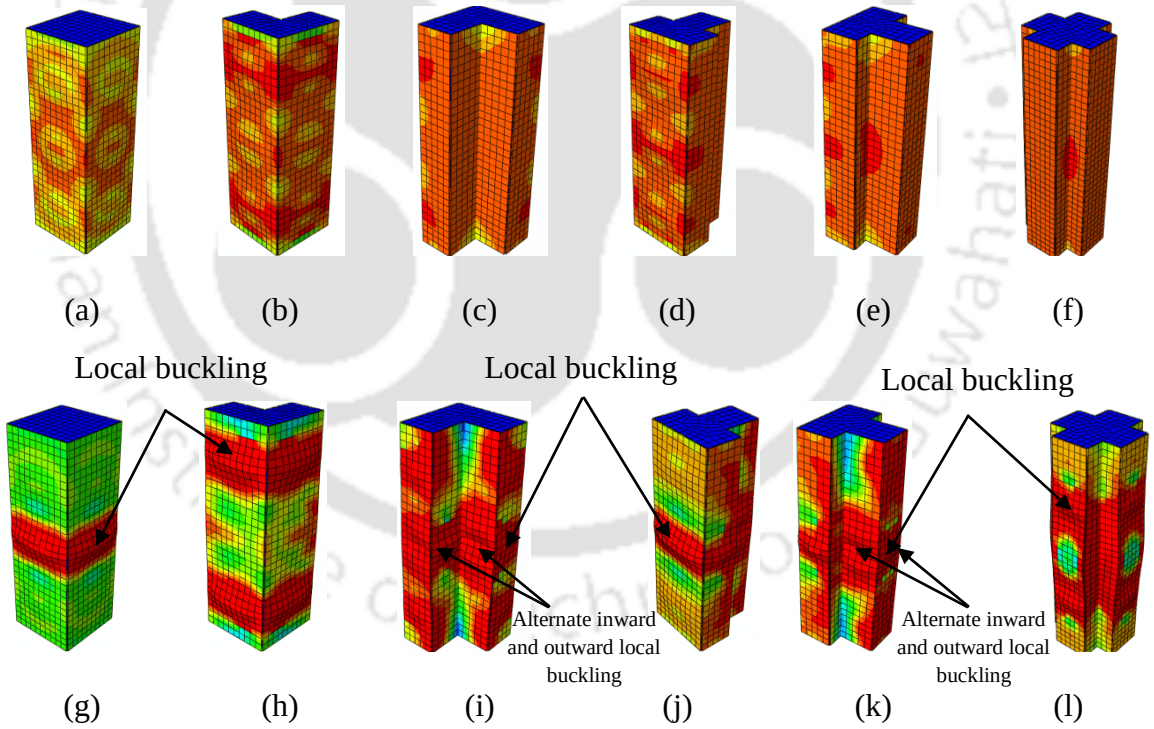

Figure 5.6: (a-f) Typical failure modes (von-Mises stress superimposed over deformed shape) at P_u and (g-l) 3 x δ_u the deformation at P_u for CFDSST stub columns of NRSs and representative square section.

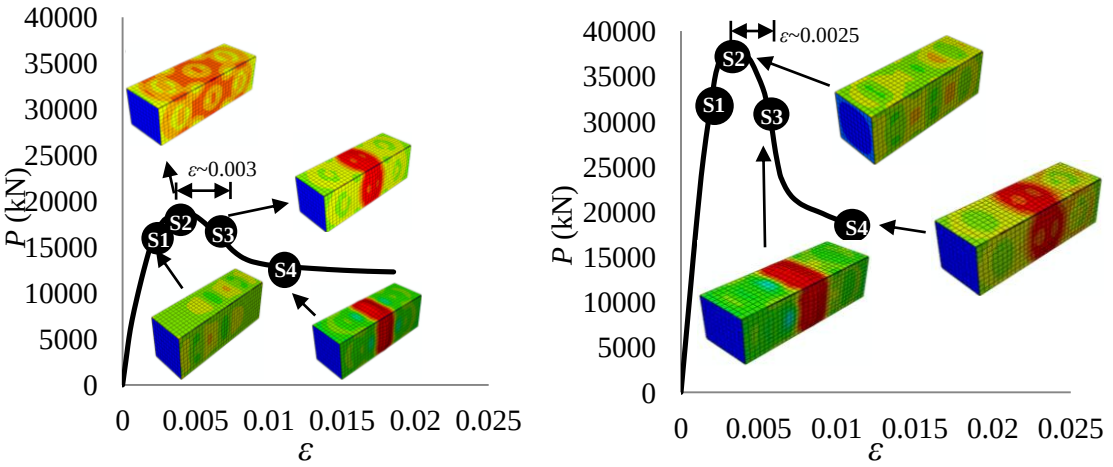

(a) 25 MPa concrete compressive strength (b) 85 MPa concrete compressive strength

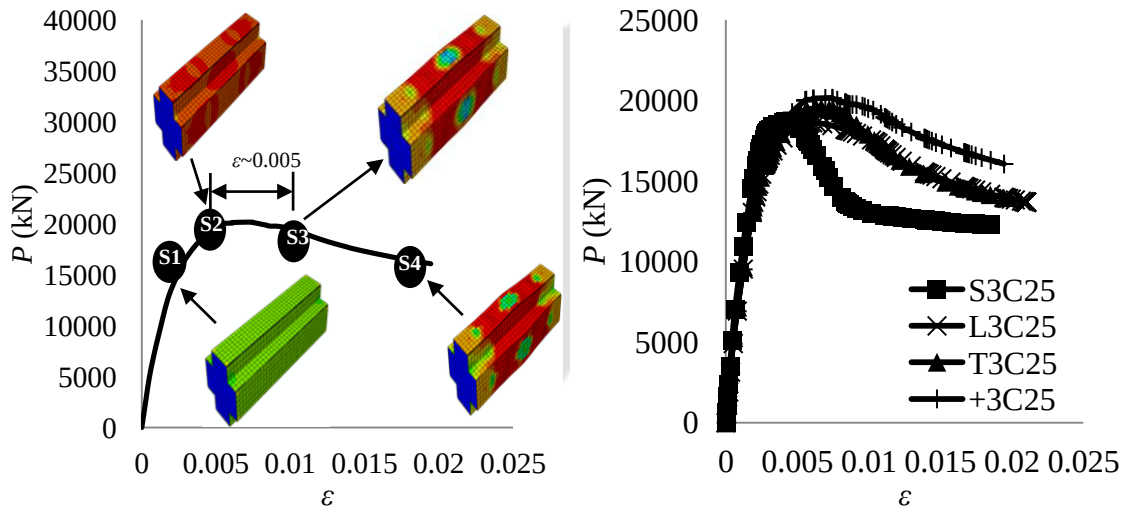

(c) 25 MPa concrete compressive strength (d) 25 MPa concrete compressive strength

Figure 5.7: Typical *P*- ε plot for CFDSST stub columns of (a&b) Square section, (c) +-shape section and (d) NRSs and representative square section.

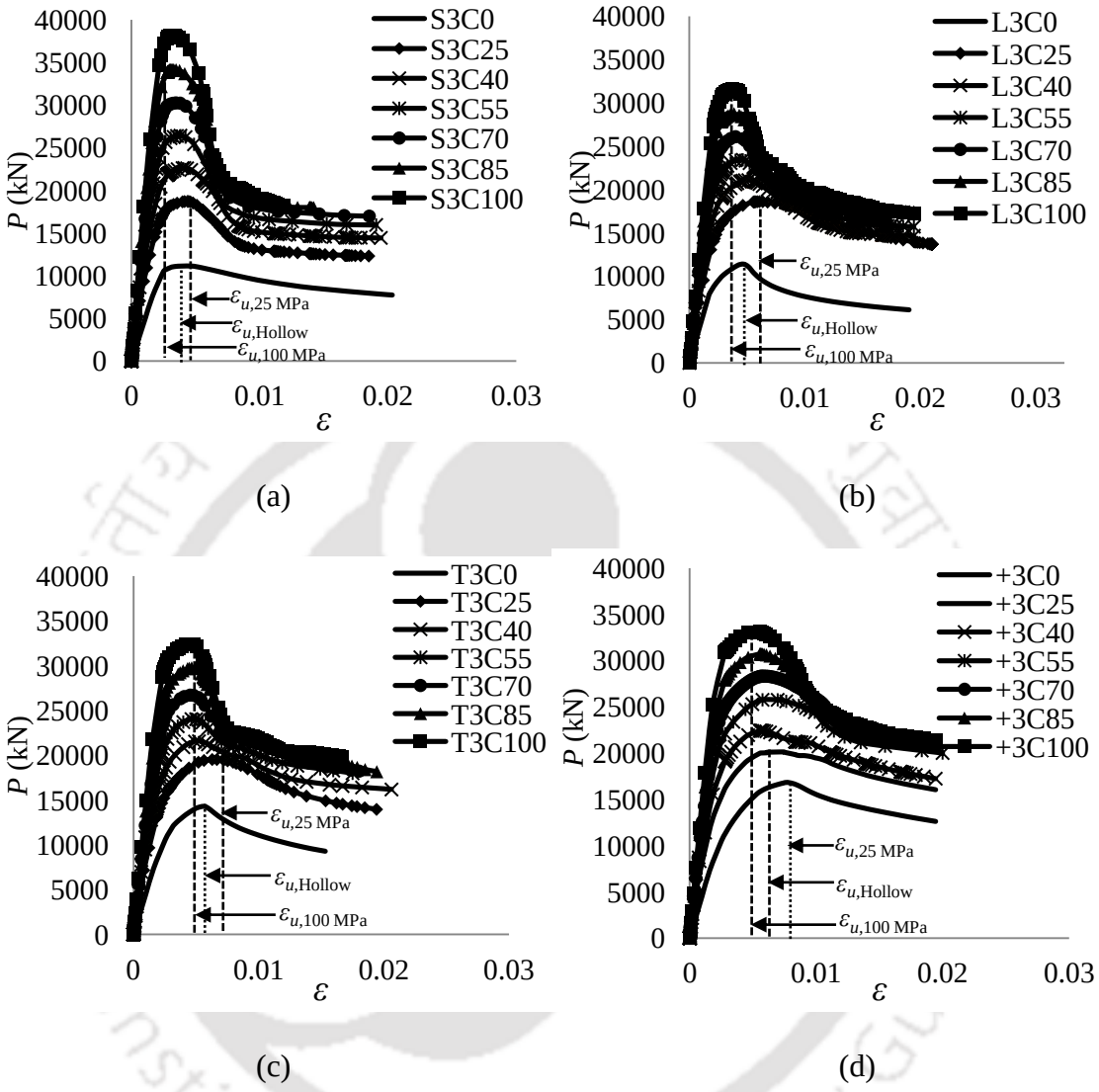

Figure 5.8: Typical *P*- ε plot for CFDSST stub columns with thickness of 10.0 mm.

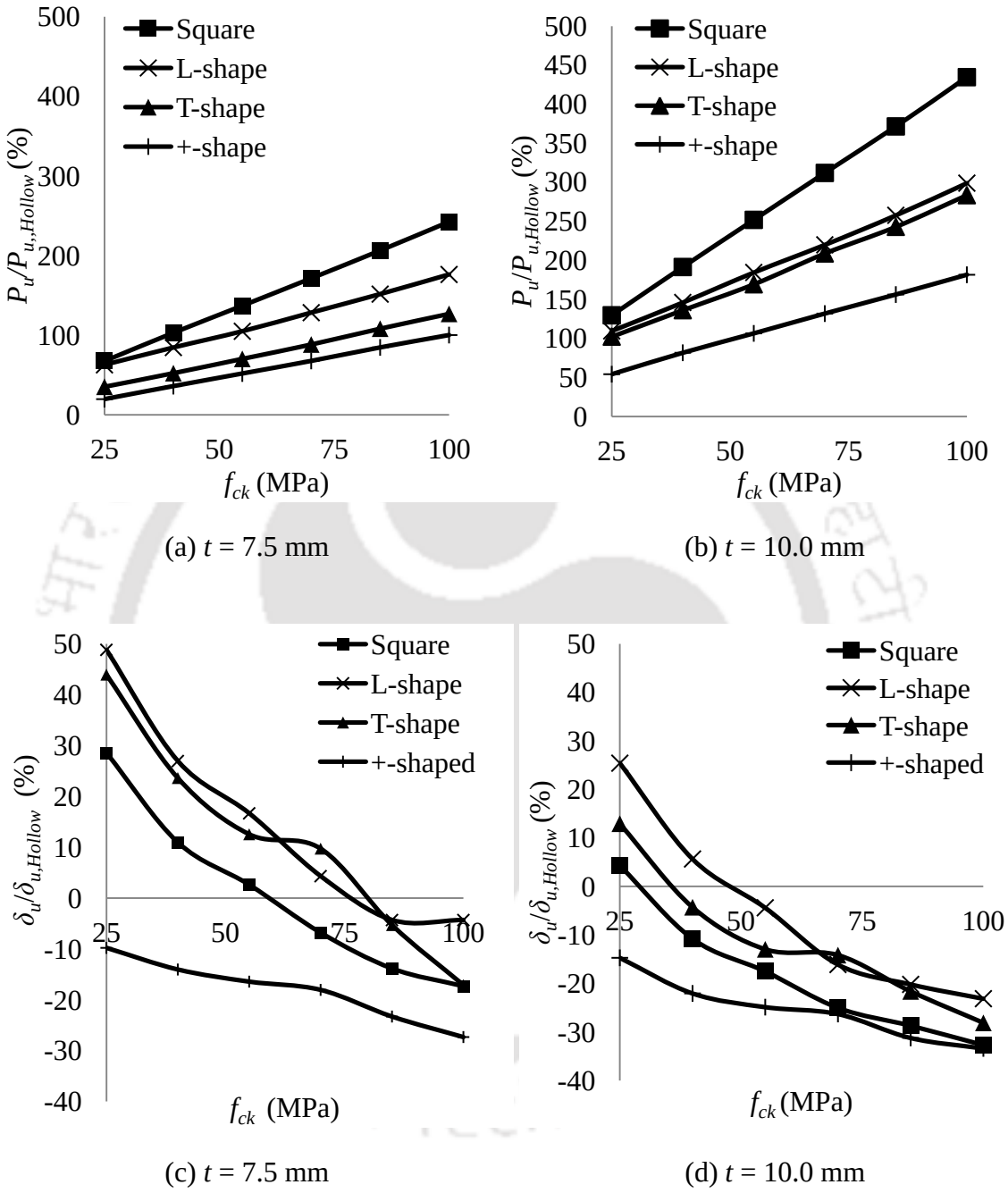

Figure 5.9: Effect of the steel tube on the load and deformation capacities of CFDSST stub columns.

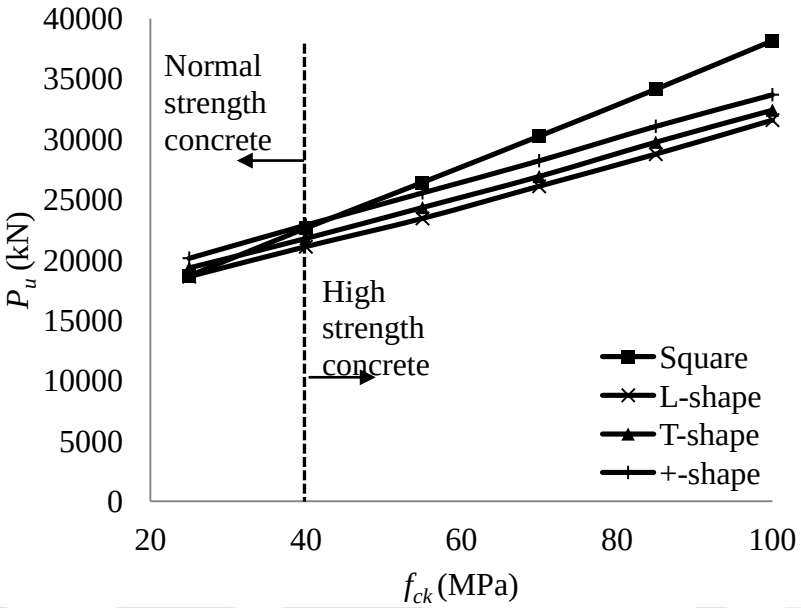

Figure 5.10: Typical plot of P_u versus f_{ck} for CFDSST stub columns (t = 10.0 mm).

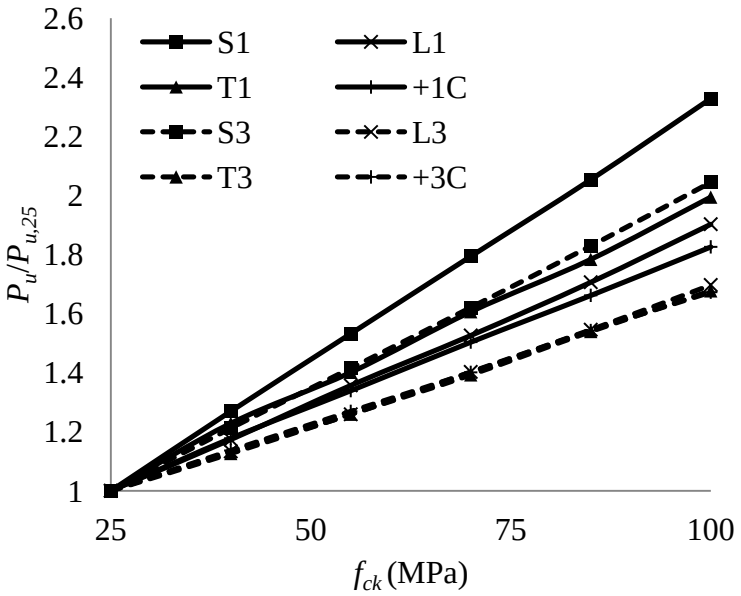

Figure 5.11: Efficiency of CFDSST stub columns for thicknesses of 7.5 mm and 10.0 mm.

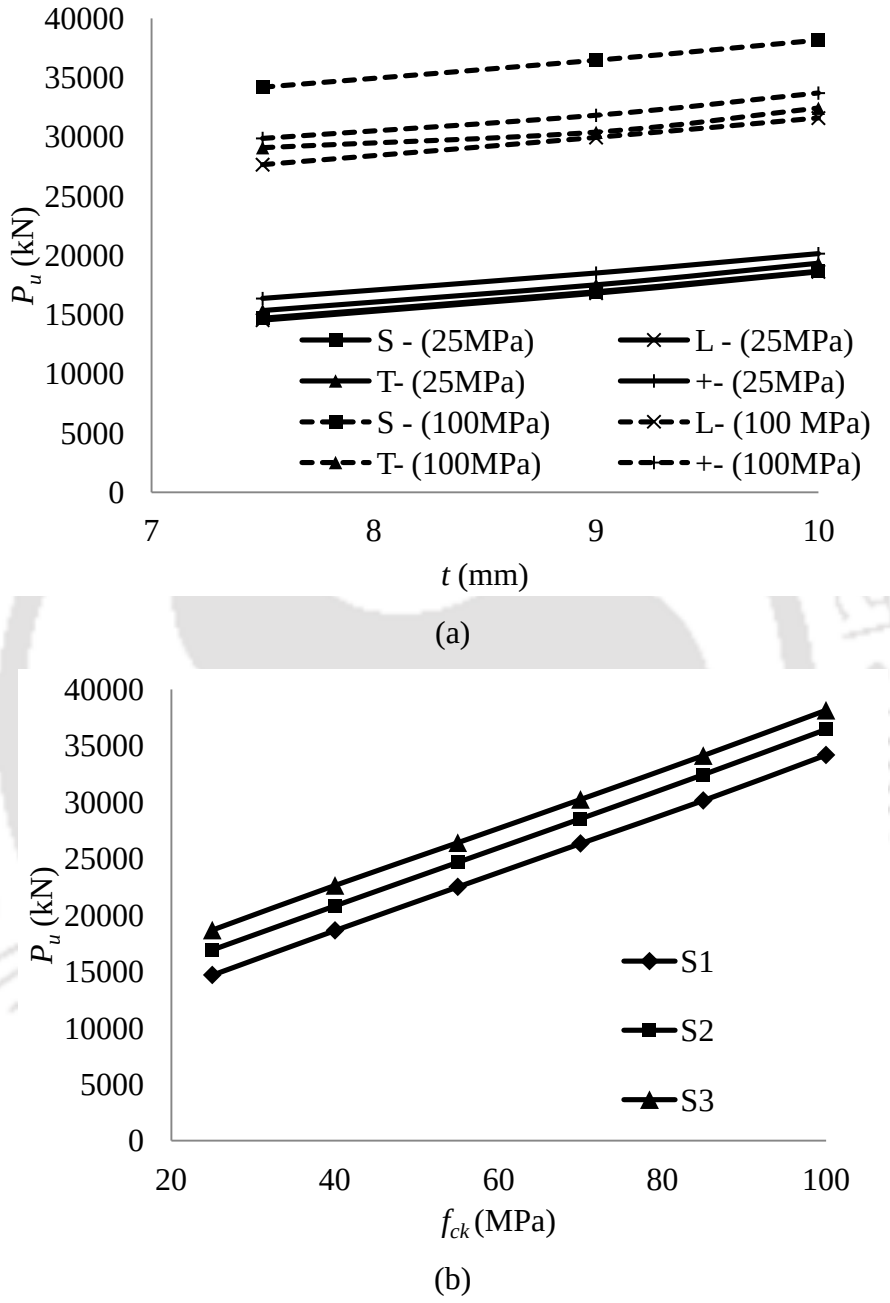

Figure 5.12: (a) P versus t for CFDSST stub columns; (b) Typical plot of P_u versus f_{ck} for CFDSST stub columns.

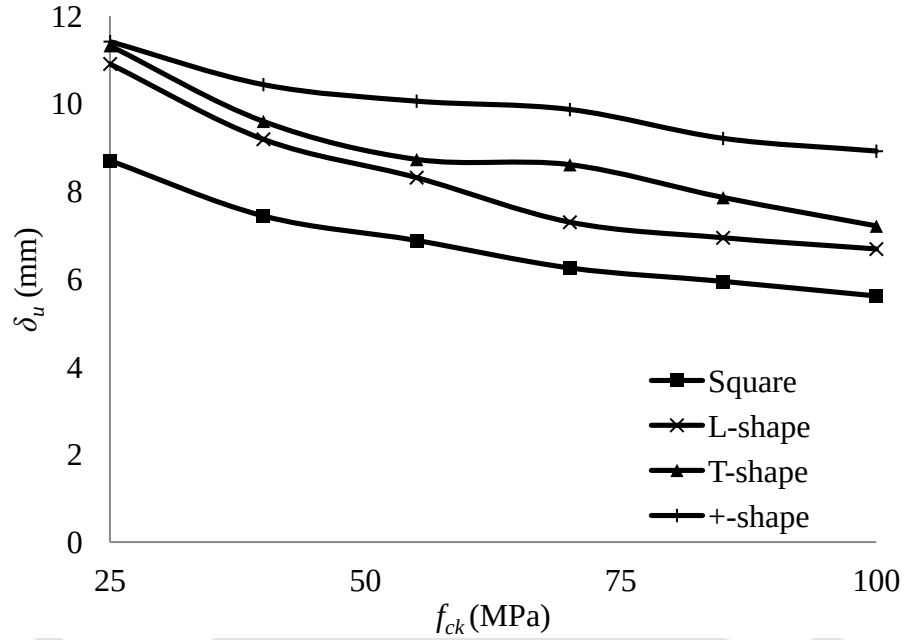

(a)

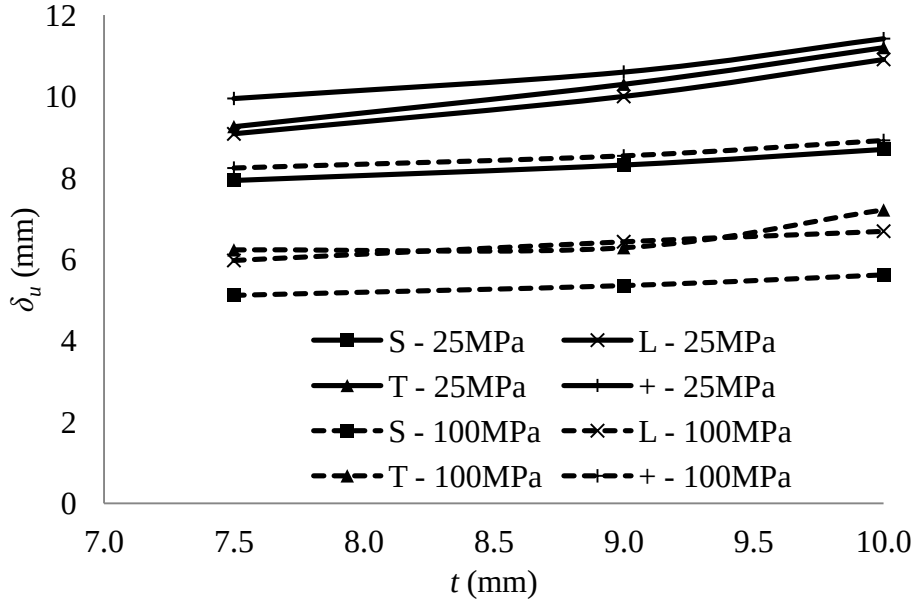

(b)

Figure 5.13: (a) Effect of shape on the δ_u versus f_{ck} for CFDSST stub columns; (b) Effect of t on the δ_u versus f_{ck} for CFDSST stub columns.

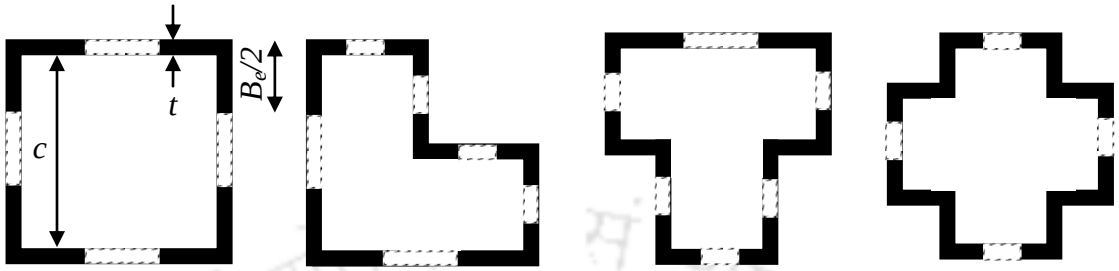

(a) Square (b) L-shape (c) T-shape (d) +-shape

Figure 5.14: Schematic diagams showing determination of B_e for the LDSS tube in CFDSST stub columns.

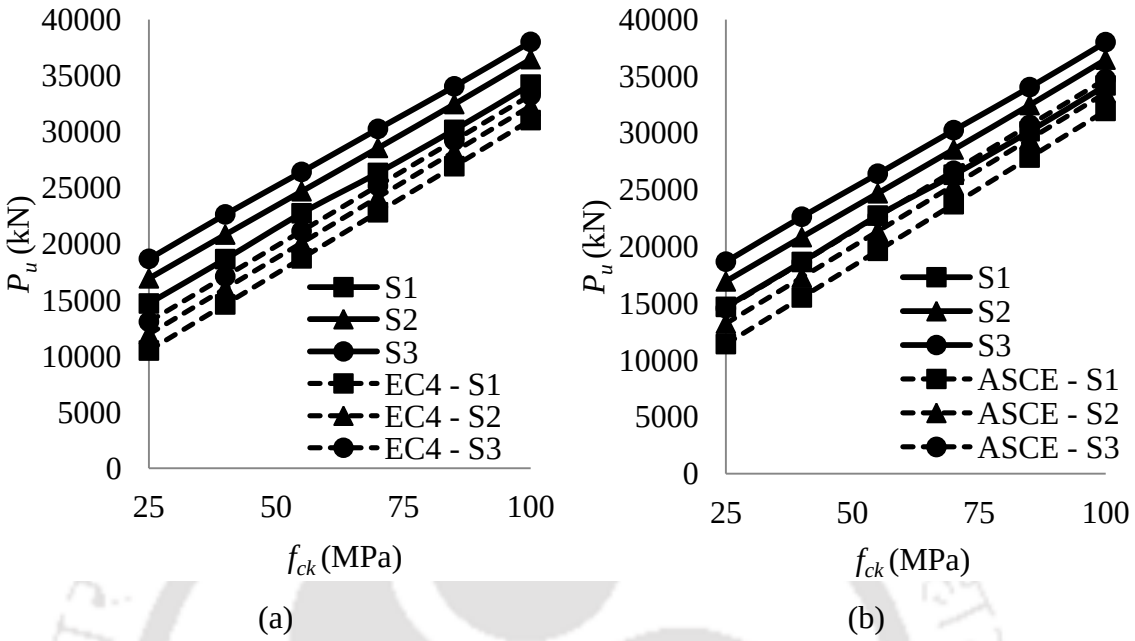

Figure 5.15: Comparison of P_u versus f_{ck} for square section with (a) European and (b) American specifications.

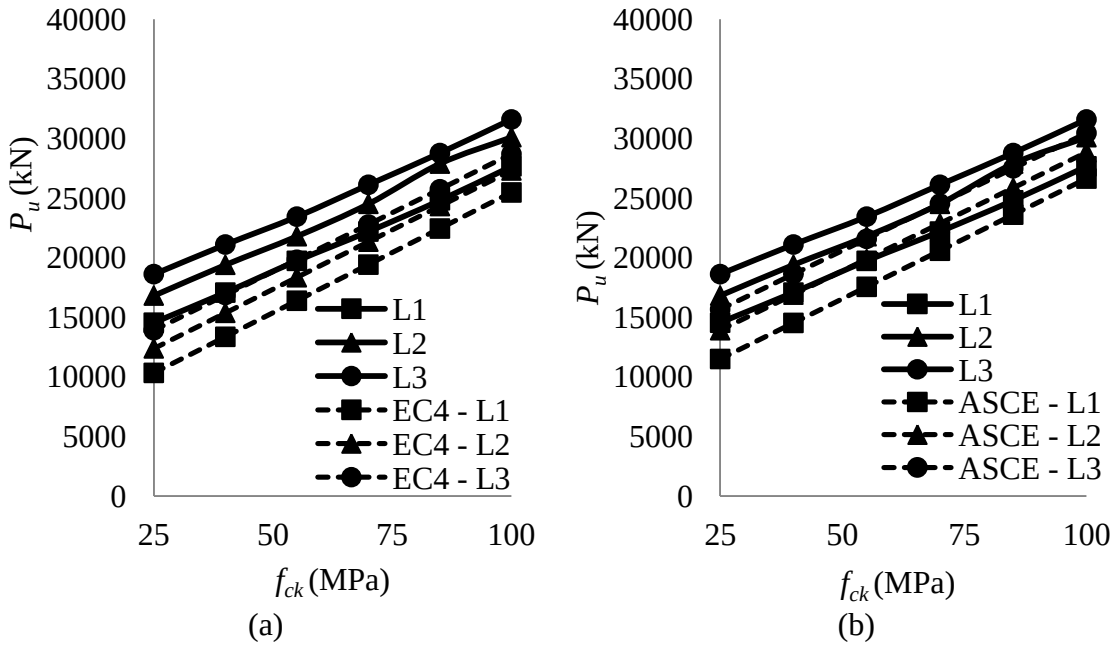

Figure 5.16: Comparison of P_u versus f_{ck} for L-shape section with (a) European and (b) American specifications.

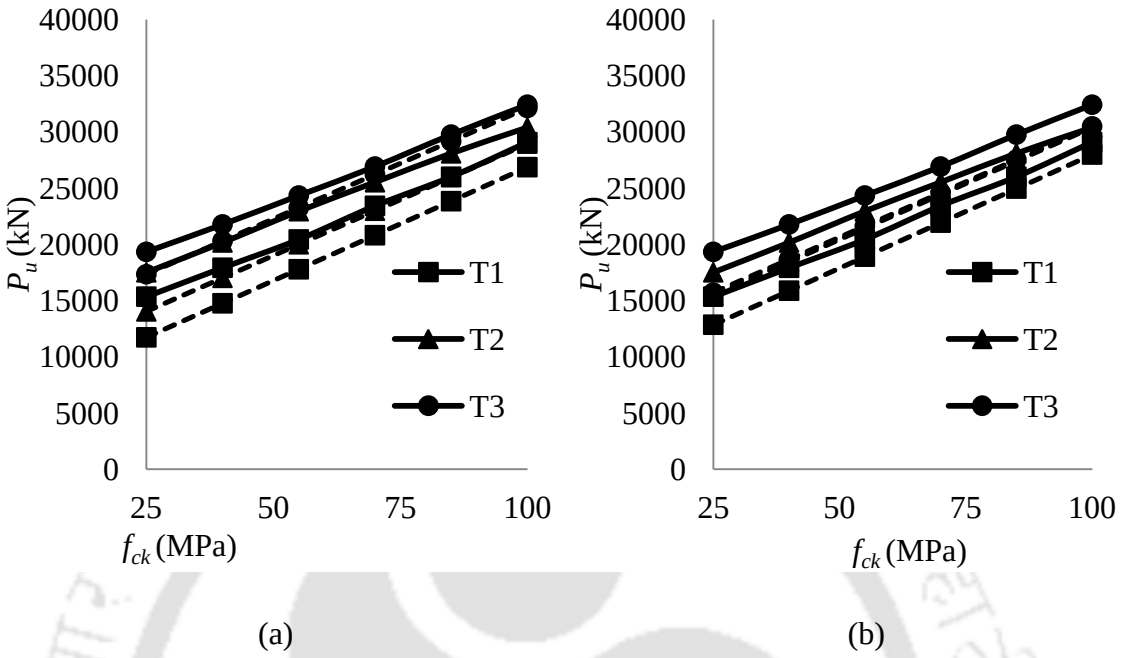

Figure 5.17: Comparison of P_u versus f_{ck} for T-shape section with (a) European and (b) American specifications.

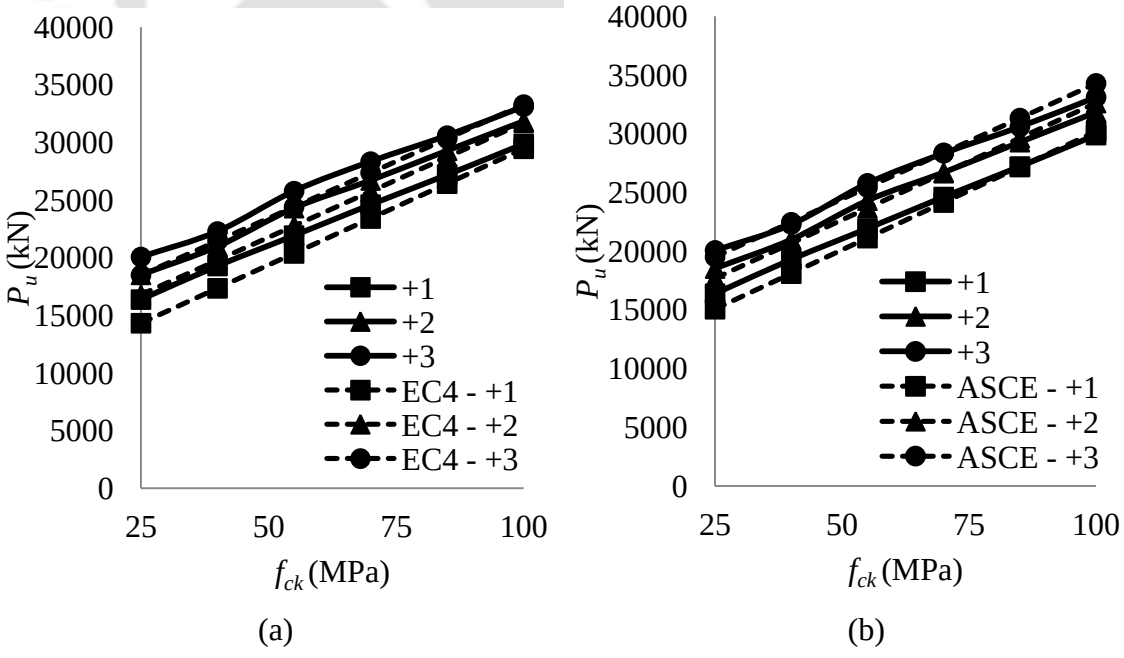

Figure 5.18: Comparison of P_u versus f_{ck} for +-shape section with (a) European and (b) American specifications.

CHAPTER 6

NUMERICAL MODELLING OF CONCRETE-FILLED LEAN DUPLEX STAINLESS SLENDER COLUMNS

6.1 INTRODUCTION

A detailed account of nonlinear FE analyses of CFDSST stub columns under pure axial compression is given in Chapter 5, where comparison of the load and deformation capacities of the CFDSST stub columns with NRSs and representative square section was made. In this chapter, extension of the CFDSST stub columns to fixed-ended CFDSST slender columns to explore their structural performances under axial compression at different lengths, where the NRSs having same LDSS cross-sectional area and 36 % reduction in the concrete core area as compared to the representative square section is presented. The main objective is to study the effects of cross-sectional geometries on the strength and behavior of the fixed-ended CFDSST slender columns with NRSs and representative square section. The currently available design standards on stainless steel, such as the European (EN 1994-1-1, 2004) and the American (ANSI/AISC 360-05, 2005) specifications, were assessed based on the FE results for their applicability in the design of fixed-ended CFDSST slender columns. Based on the FE results reliability analysis was then carried out.

6.2 FE MODELLING

The development of an accurate FE models representation for the fixed-ended CFDSST slender columns taking account of the appropriate representation of the corresponding material characteristics (i.e. LDSS and concrete core material) were similar to that detailed in Section 5.2. Similar analyses technique (i.e. the modified RIKS method), boundary conditions, concrete-LDSS tube interface properties, and the elements used for representation of the LDSS tube (S4R) and the concrete core (C3D8R) were adopted in the FE analyses for the fixed-ended CFDSST slender columns as discussed in detail in the previous chapters.

6.2.1 Concrete core material model

The stress-strain curve development of the concrete core in the fixed-ended CFDSST slender columns is detailed in Section 2.7.2. Due to the thin nature of the LDSS tube adopted in the FE models (i.e. $D/t > 29.2$); inadequately confined concrete material model was adopted similar to that followed in the analyses of CFDSST stub columns. In the CFDSST slender columns under pure axial compressive loading, the concrete core experiences compressive state at initial stage of loading and both tensile and compressive state at later stage due to flexural deformation of the column. Hence, the concrete damage plasticity (CDP) model provided in the material library of Abaqus (2009) is applied for describing the constitutive behavior of concrete core due to the inability of the Drucker-Prager yield criterion model adopted in Chapter 5 to simulate the concrete core under such tensile and compressive state. Detailed modelling of the inadequately confined concrete core in fixed-ended CFDSST slender column FE models through the CDP model is described in Appendix E.

6.2.2 Initial geometric imperfections

Linear elastic analysis technique was initially performed on the fixed-ended CFDSST slender column FE models to the global buckling mode shapes. The first global buckling mode shapes are then utilised as initial geometric imperfections pattern to perturb the geometry of the slender columns similar to that followed in Chapter 4 for the FE analyses of the fixed-ended hollow tubular slender columns.

The effect of local geometric imperfections on the fixed-ended CFDSST slender columns were neglected because the strength reduction is not significant compared to thin-walled hollow tubes owing to the delaying effect of steel tube local buckling by the concrete core (Tao *et al*., 2009). However, global geometric imperfections were considered as it is one of the main effect factors on the ultimate strength (Galambos, 1998). The global geometric imperfections of the concrete-filled tubular columns mainly come from initial out-of-straightness of the steel tubes. Thus, the global geometric imperfection magnitude in all the fixed-ended CFDSST slender column FE models was assumed as *L*/1500 similar to that adopted in the FE analyses of fixed-ended hollow tubular slender columns as discussed in Section 4.2.3. This imperfection magnitude was applied at the mid-span of the column in the plane of the weaker principal axis for all the fixed-ended CFDSST slender column FE models.

6.3 VERIFICATION OF THE FE MODEL

The validity of the fixed-ended CFDSST slender column FE models was established through comparison with various experimental test conducted on concrete-filled thin-walled stainless steel tubular slender columns of square and rectangular sections by Uy *et al*., 2011. Figure 6.2 shows a comparison of P_u with *L/D* ratio for the concrete-filled thin-walled stainless steel tubular slender columns. It can be seen from Figure 6.2 that good agreement was achieved between the developed FE models and the experimental test

results. Hence, the steps followed in the verification of FE models was used in subsequent FE analysis of fixed-ended CFDSST slender columns.

6.4 CONCRETE-FILLED TUBULAR SLENDER COLUMN MODELLING

6.4.1 Introduction

As part of the study, a series of FE models to investigate the structural behaviour of fixed-ended CFDSST slender columns with NRSs and representative square section subjected to pure axial compression over a range of column lengths having normal concrete strength (i.e. 25 MPa) were reported. The effects of column lengths and cross-sectional shapes on the buckling strength of these columns were analysed.

6.4.2 Development of the FE models

Fixed-ended CFDSST columns with NRSs and the representative square section with lengths varying from 1.8 - 70.0 m which provided a range of $\bar{\lambda}$, defined through by Equation 6.1, in accordance with EN1993-1-4 (2006), from 0.05 to 2.0, were considered for the parametric studies.

$$\bar{\lambda} = \sqrt{\frac{N_0}{N_{cr}}} \tag{6.1}$$

where;

$N_o = A_s f_y + A_c f_c$ as per EN1994-1-1(2004) (6.2)

$N_o = A_s f_n + A_c f_c$ as per ANSI/AISC 360-05 (2005) (6.3)

$$N_{cr} = \frac{\pi^2 \left(E_s I_s + 0.6 E_c I_c\right)}{L_e^2}$$ as per EN1994-1-1(2004) (6.4)

$$N_{cr} = \frac{\pi^2 \left(E_s I_s + E_c I_c \left(0.6 + 2 \frac{A_s}{A_{sc}} \right) \right)}{L_e^2} \text{ as per ANSI/AISC 360-05 (2005)} \quad (6.5)$$

$$A_{sc} = A_s + A_c \quad (6.6)$$

where N_{cr} is the nominal Euler load for concrete-filled tubular columns representing the ultimate strength of an ideal elastic columns under pure axial compression, and I_s and I_c are the moment of inertia for steel tube and concrete core, respectively.

The dimensions and material properties of the CFDSST columns are summarized in Table 6.2 (also see Figure 6.3). The fixed-ended CFDSST slender columns are labeled such that the cross-sectional shape, concrete cube strength as well as the column lengths can be identified from the label. For example, the label 'SC25L36000' and 'LC25L36000' defines the square and L-shaped LDSS columns indicated by the first letter 'S and L', respectively, and the letter 'C25' and 'L36000' defines the concrete cube strength in MPa (25 MPa) and length of 36000 mm, respectively. Similar to the work of other researchers (e.g. Hassanein, 2010, Zuo *et al*., 2012, Zhang *et al*., 2012), the corners of the CFDSST slender columns are assumed herein to be exact 90^0 (i.e corner radii are not considered).

Based on the thickness of the LDSS tube of 10.0 mm considered in the current investigation, the width-to-thickness ratios of the LDSS tube in all the cross-sections considered are all greater than 29.2. Hence, inadequately confined concrete model was adopted in the fixed-ended CFDSST slender column FE models as discussed in the previous chapters, considering the thin-walled mature of the LDSS tube.

6.5 RESULTS AND DISCUSSIONS

6.5.1 Introduction

The results of the FE analysis for the fixed-ended CFDSST slender columns were presented in terms of variation in the load and deformation capacities along with the failure modes with change in the cross-sectional shapes. The FE results were compared with the currently available design standards for stainless steel, such as, the European (EN1994-1-1, 2004) and American (ANSI/AISC 360-05, 2005) specifications for their applicability in the design of fixed-ended CFDSST slender columns. Reliability analyses of these design standards were also discussed based on the FE studies.

6.5.2 Deformed shapes of concrete-filled NRSs and square section

Figure 6.4 shows the failure modes of fixed-ended LDSS hollow tubular and CFDSST slender columns. It can be seen from Figure 6.4 that only overall buckling is seen for both the hollow tubular and CFDSST columns at P_u. At post ultimate load, LDSS hollow tubular members fails through overall buckling and thereafter accompanied by local buckling of the LDSS tube at mid-height sections (see Figure 6.4e-h). However, local buckling of the LDSS tube is prevented due to the concrete core in CFDSST columns (see Figure 6.4i-l).

6.5.3 Load-axial deformation profile

Figures 6.5 and 6.6 show a typical P versus δ as well as u_{mu} (i.e. mid-height deflection at P_u) for fixed-ended CFDSST and the reference LDSS hollow tubular slender columns. As similar nature of P versus δ and P versus u_{mu} are also observed for other CFDSST's and the reference LDSS hollow tubular slender columns, only square and +-shape columns are plotted.

It can be seen from Figure 6.5 that the P_u of CFDSST columns is higher than that of the reference hollow steel tubular columns because of increased flexural rigidity provided by the concrete core, thereby achieving higher u_{mu} by the CFDSST columns (see Figure 6.6). However, δ_u of CFDSST column is lower than that of the reference LDSS hollow tubular column because of higher compression stiffness offered by the concrete core. It can be seen from Figure 6.6 that the larger the column length, the smaller the peak load is for both the CFDSST and the reference LDSS hollow tubular columns due to the failure of longer columns governed principally by flexure and failing to reach the yield load. Also, with increasing column length, the post-peak curve becomes milder for both the hollow and CFDSST column.

6.5.4 Strength capacity of NRSs and square section

Figure 6.7 shows the effect of cross-sectional shapes for fixed-ended CFDSST slender columns on the P_u versus $\overline{\lambda}$ curves. It can be seen from Figure 6.7 that for all the sections analysed P_u decreases with increasing $\overline{\lambda}$. Also, +-shape and T-shape sections showed a higher P_u for all the $\overline{\lambda}$, however, L-shape section showed a similar P_u at lower $\overline{\lambda}$ and a lower P_u at higher $\overline{\lambda}$ compared to that of the representative square section.

Figure 6.8 shows the efficiency of fixed-ended concrete-filled CFDSST slender columns of NRSs to identify the type of relationship with change in the cross-sectional shape from square section to NRSs. Simply, it can be seen from Figure 6.8 that, for $\overline{\lambda} \sim < 0.5$, +-shape showed a 7 % higher strength and L- and +-shape showed similar strengths compared to the representative square section. For $0.5 \leq \overline{\lambda} \geq 1.5$, a linear increasing trend in strength is seen with increasing $\overline{\lambda}$. However, for $\overline{\lambda} > 0.5$, T- and +-shape showed a 10 % and 25 % more strength and L-shape showing a 10 % lower strength compared to the representative square section. Thus, in fixed-ended CFDSST slender columns, change of

cross-sectional shape from square section to NRSs is significant, especially for T-shape and +-shape sections, and can promote the application of thin-wall LDSS tube.

6.5.5 Deformation capacity of NRSs and square section

Figure 6.9 shows the effect of cross-sectional shapes on the ε_u versus $\overline{\lambda}$ curves for fixed-ended CFDSST slender columns. It can be seen that the influence of the cross-sectional shapes on the ε_u becomes less significant with increasing $\overline{\lambda}$, but becomes increasingly significant with decreasing $\overline{\lambda}$. Also, it can be seen that, the NRSs shows a higher ε_u for all $\overline{\lambda}$ considered compared to the representative square section, with +-shape section showing the highest ε_u.

6.5.6 Comparison with design codes

The results from the FE analyses were compared with the unfactored design strengths predicted using the European (EN1994-1-1, 2004) and American (ANSI/AISC 360-05, 2005) specifications. A sample design strength calculation for the fixed-ended square CFDSST slender column with the two design standards is given in Appendix F. As the current design standards are based on stainless steel material, the applicability of these codes in the design of fixed-ended CFDSST slender columns are assessed through the FE studies. A detail comparison between the FE results and the design standard predictions are discussed in the following sub-sections.

6.5.6.1 Effective area determination

In the present study of fixed ended CFDSST slender columns, all the cross-sections considered lies under Class 4 section, hence, the effective width concept as detailed in Section 3.5.7.1 given in EN 1993-1-4 (2006) to account for the effect of local buckling on

the LDSS tube was considered in the design strengths of the fixed-ended CFDSST slender columns.

6.5.6.2 Design strengths

The design strengths for the fixed-ended CFDSST columns were considered as concentrically loaded compression members and L_e was assumed to be $L/2$. The design strengths based on the EN1994-1-1 (2004) and ANSI/AISC 360-05 (2005) specifications are defined by Equation 6.7 and Equations 6.8 and 6.9, respectively.

$$P_{u,EN1994\text{-}1\text{-}1} = \chi N_o \tag{6.7}$$

$$P_{u,ANSI/AISC\ 360\text{-}05} = 0.658^{\left(\frac{N_o}{N_{cr}}\right)} N_o \qquad \text{for } N_{cr} \geq 0.44\ N_o \tag{6.8}$$

$$P_{u,ANSI/AISC\ 360\text{-}05} = 0.877 N_{cr} \qquad \text{for } N_{cr} < 0.44\ N_o \tag{6.9}$$

6.5.6.3 Comparison of FE strengths with design strengths

Figures 6.10 to 6.12 show a plot of P_u versus L/D for fixed-ended CFDSST slender columns with NRSs and the representative square section. It is found that both the design standards showed over conservative results for square and L-shape sections and conservative for T-shape and +-shape sections. However, the European specification gives a conservative estimation of strengths compared to the American specification for square and L-shape sections, and vice versa in case of T-shape and +-shape sections.

6.5.6.4 Reliability analysis of the codes

The reliability analysis of the EN 1993-1-1 (2004) and ANSI/AISC 360-05 (2005) specifications based on the FE results is carried out as detailed in Section 3.5.7.4. Reliability indices are tabulated in Table 6.3.

Based on the reliability analyses it can be seen that, except for L-shape section, both the design standards show $\beta_0 \geq 2.5$ when compared with the FE results. Considering the lower limit of $\beta_0 = 2.5$ suggested by ASCE 8-02 (2002) specification for structural members, it can be inferred that both specifications can be adopted for all the design of fixed-ended CFDSST slender columns, except for the L-shape section, wherein a suitable modification may be employed after systematic studies (including experiments). For the design of fixed-ended CFDSST slender columns of square and L-shape sections, American specification tends to be more reliable compared to the European specification and vice versa in the design for the fixed-ended CFDSST slender columns of T-shape and +-shape sections.

6.6 CONCLUSIONS

The FE modeling of fixed-ended CFDSST slender columns of NRSs and representative square sections subjected to pure axial compressive loading are discussed in this Chapter. Variations in buckling strength with changes in the cross-sectional shapes were studied by considering equal LDSS material cross-sectional areas (or equal LDSS material consumption), thereby giving a reduction in the concrete core area of the NRSs by about 36 % compared to the representative square section, over a range of column lengths. The following conclusions are drawn within the limitation of this study:

1) At P_u, only overall buckling is seen for both the hollow tubular and CFDSST columns. At post P_u, LDSS hollow tubular members fails through overall buckling and thereafter accompanied by local buckling of the LDSS tube at mid-height sections. However, local buckling of the LDSS tube is prevented due to the concrete core in CFDSST columns.

2) The P_u of CFDSST columns is higher than that of the reference hollow steel tubular columns because of increased flexural rigidity provided by the concrete core, thereby achieving higher u_{mu} by the CFDSST columns. However, the δ_u of CFDSST column is lower than that of the reference LDSS hollow tubular column because of a higher elastic compression stiffness of the latter due to concrete core

3) For all the section analysed the P_u decreases with increasing $\overline{\lambda}$. Also, +-shape and T-shape sections show a higher P_u for all the $\overline{\lambda}$, however, L-shape section showed a similar P_u at lower $\overline{\lambda}$ and a lower P_u at higher $\overline{\lambda}$ compared to that of the representative square section.

4) For $\overline{\lambda} \sim < 0.5$, +-shape showed a 7 % higher strength and L- and +-shape showed similar strengths compared to the representative square section. For $0.5 \leq \overline{\lambda} \geq 1.5$, a linear increasing trend in strength is seen with increasing $\overline{\lambda}$. However, for $\overline{\lambda} > 0.5$, T- and +-shape showed a 10 % and 25 % more strength and L-shape showing a 10 % lower strength compared to the representative square section.

5) In fixed-ended CFDSST slender columns, change of cross-sectional shape from square section to NRSs is significant, especially for T-shape and +-shape sections, and can promote the application of thin-wall LDSS tube.

6) The influence of the cross-sectional shapes on the ε_u becomes less significant with increasing $\overline{\lambda}$, but becomes increasingly significant with decreasing $\overline{\lambda}$. Also, NRSs shows a higher ε_u for all $\overline{\lambda}$ considered compared to the representative square section, with +-shape section showing the highest ε_u.

7) The design standards show over conservative results for square and L-shape sections and conservative for T-shape and +-shape sections. However, the European specification gives a conservative estimation of strengths compared to the American

specification for square and L-shape sections and vice versa in case of T-shape and +-shape sections.

8) Based on the reliability analyses both specifications can be adopted for all the design of fixed-ended CFDSST slender columns, except for the L-shape section, wherein a suitable modification may be employed after systematic studies (including experiments). For the design of fixed-ended CFDSST slender columns of square and L-shape sections, American specification tends to be more reliable compared to the European specification and vice versa in the design for the fixed-ended CFDSST slender columns of T-shape and +-shape sections.

Table 6.1: Concrete-filled steel stub and slender column dimensions and material properties.

Specimen	Dimensions			Material properties		Authors
	D (mm)	t (mm)	L (mm)	Steel tube $f_y/\sigma_{0.2}$(MPa)	Concrete strength (MPa)	
S9	100	4.10	299	333	97.20	Ellobody and Young (2006)
S1-1a S1-2a S1-3a	100.3	2.76	300 1200 2400	390.3	36.3	Uy *et. al*. (2011)
C1	400	6.0	1200	465	47.60	Yang *et. al*. (2006)
T-4	330	3.49	315	315	23.2	Yang *et. al*. (2009)
RHS3C25	180	2.0	540	530	25.0	Hassanein (2010)
RHS3C85					85.0	
R1-1a R1-2a R1-3a	99.5	1.93	300 600 1200	363.3	36.3	Uy *et. al*. (2011)

Table 6.2: Details of the fixed-ended CFDSST slender columns.

Specimen	Dimensions and Cross-sectional areas						% deduction in A_c	Material properties	
	D (mm)	B (mm)	t (mm)	L/D (mm)	A_s (mm^2)	A_c (mm^2)		$\sigma_{0.2}$ (MPa)	f_c (MPa)
SC25	600	600	10.0	3.0 to 100	23600	336400	Nil	657	25
LC25	600	600	10.0	3.0 to 100	23600	246400	36.0	657	25
TC25	600	600	10.0	3.0 to 100	23600	246400	36.0	657	25
+C25	600	600	10.0	3.0 to 100	23600	246400	36.0	657	25

Table 6.3: Comparison of FE strengths with codal design strengths for fixed-ended CFDSST columns.

L/*D*	$P_{FE}/P_{EN\ 1993\text{-}1\text{-}1}$				$P_{FE}/P_{ANSI/AISC\ 360\text{-}05}$			
	SHC	LHC	THC	+HC	SHC	LHC	THC	+HC
10	1.42	1.29	1.17	1.08	1.44	1.31	1.17	1.08
15	1.43	1.27	1.20	1.11	1.44	1.29	1.16	1.07
20	1.41	1.26	1.23	1.13	1.42	1.32	1.17	1.06
30	1.29	1.11	1.26	1.11	1.37	1.27	1.23	1.09
40	1.19	1.00	1.23	1.12	1.31	1.14	1.14	1.06
50	1.12	0.96	1.20	1.12	1.25	1.05	1.09	1.03
60	1.10	0.94	1.18	1.11	1.18	0.97	1.06	1.01
70	1.08	0.96	1.15	1.09	1.10	0.94	1.01	0.97
80	1.10	0.97	1.15	1.11	1.07	0.93	0.99	0.98
90	1.09	0.97	1.14	1.09	1.02	0.93	0.97	0.95
Mean, P_m	1.222	1.074	1.19	1.107	1.26	1.116	1.099	1.029
COV, V_p	0.116	0.129	0.032	0.013	0.122	0.145	0.075	0.048
Reliability index, β_0	2.74	2.26	2.86	2.61	3.04	2.55	2.73	2.55

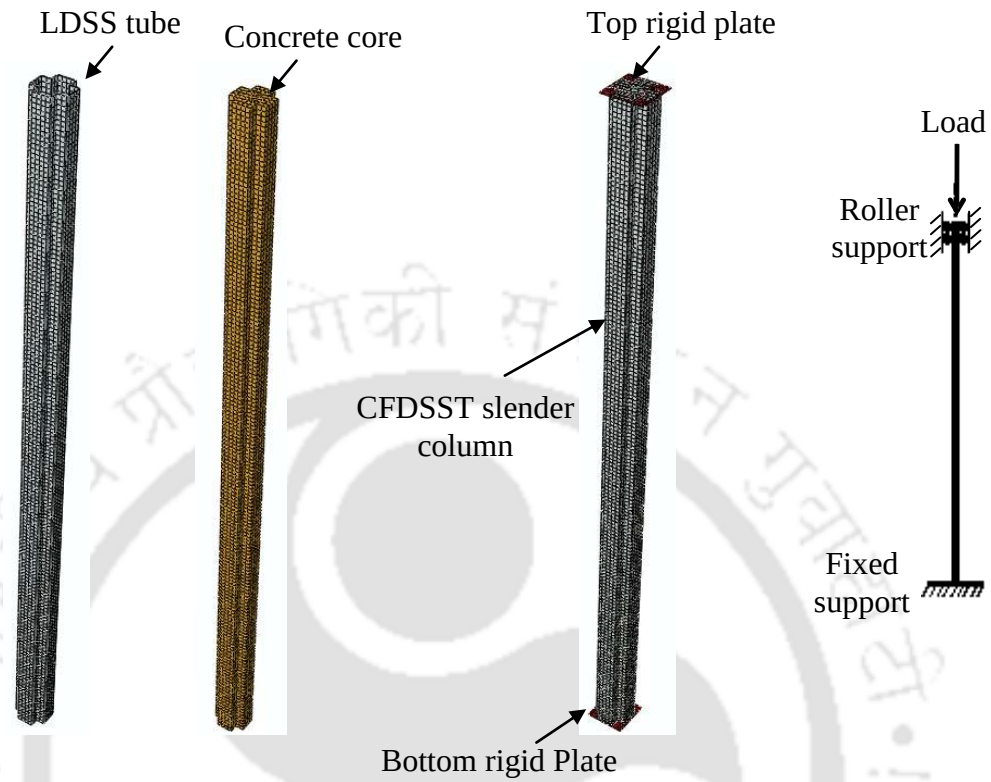

Figure 6.1: Typical boundary conditions applied to fixed-ended CFDSST slender columns FE models.

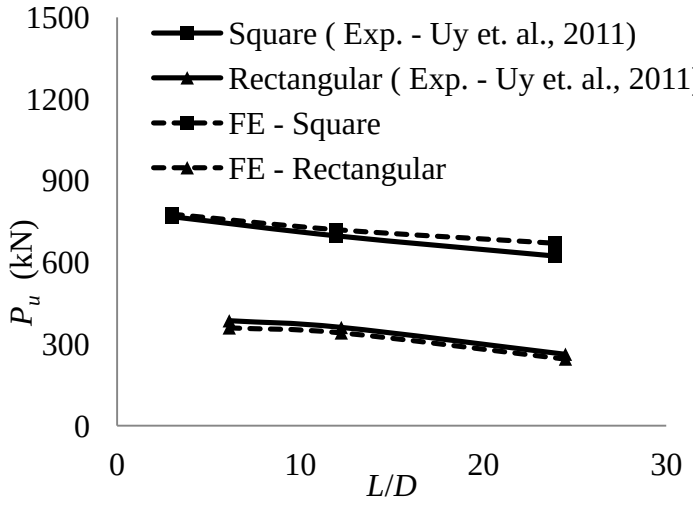

Figure 6.2: Plot of P_u versus L/D ratio for concrete-filled thin-walled stainless steel slender columns.

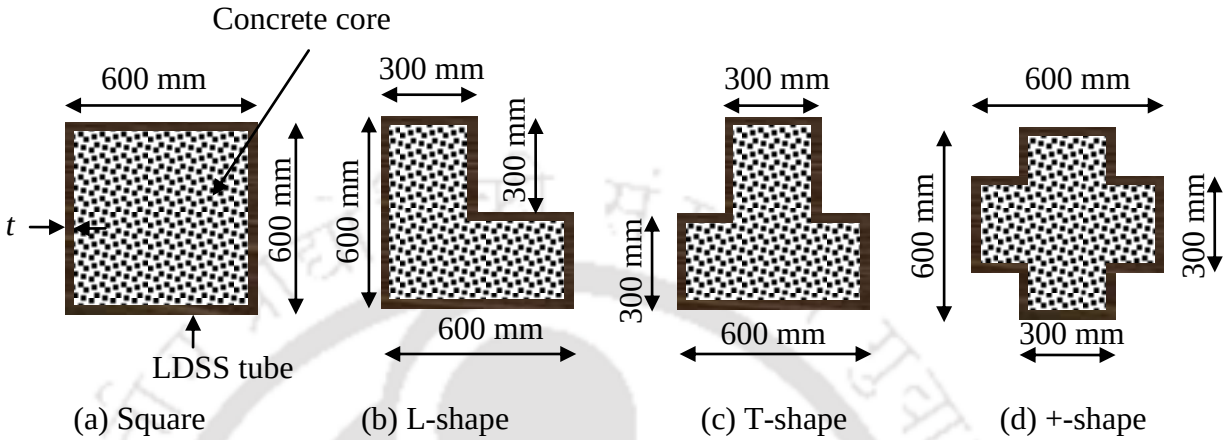

Figure 6.3: Numerical test specimens of the fixed-ended CFDSST slender columns.

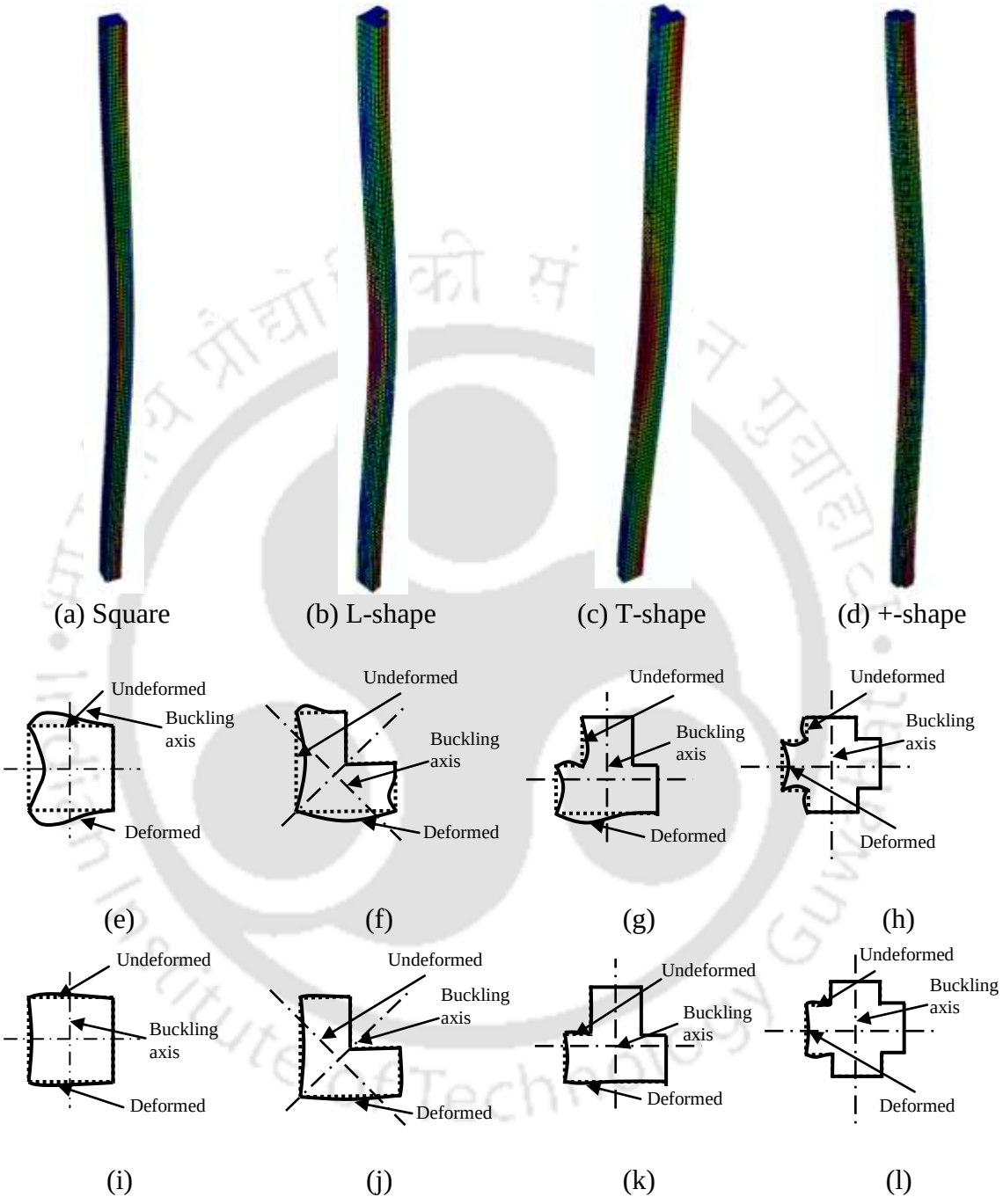

Figure 6.4: (a-d)Schematic failure modes of fixed-ended CFDSST slender columns; (e-h) Typical midspan failure shapes of hollow tubular columns and (i-l) CFDSST slender columns.

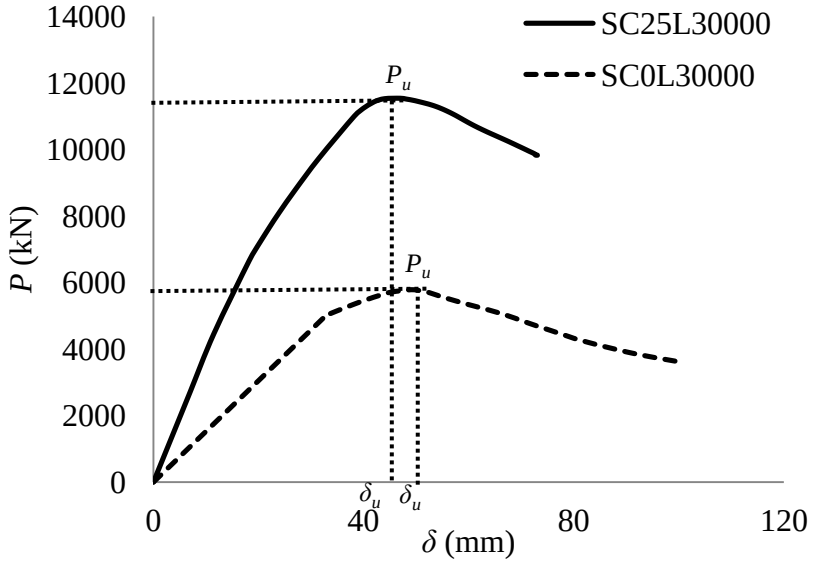

Figure 6.5: Typical P versus δ curves for the fixed-ended hollow tubular and CFDSST slender columns.

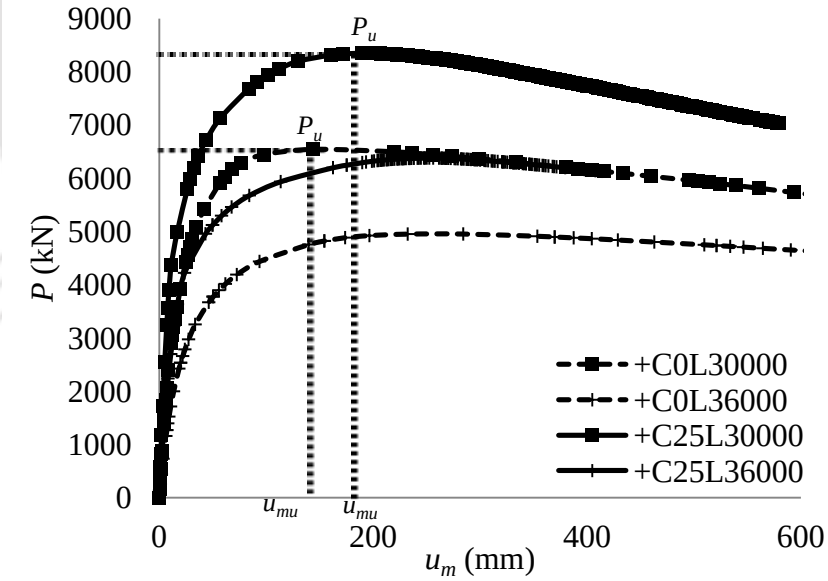

(b)

Figure 6.6: Typical P versus u_m curves for the fixed-ended hollow tubular and CFDSST slender columns.

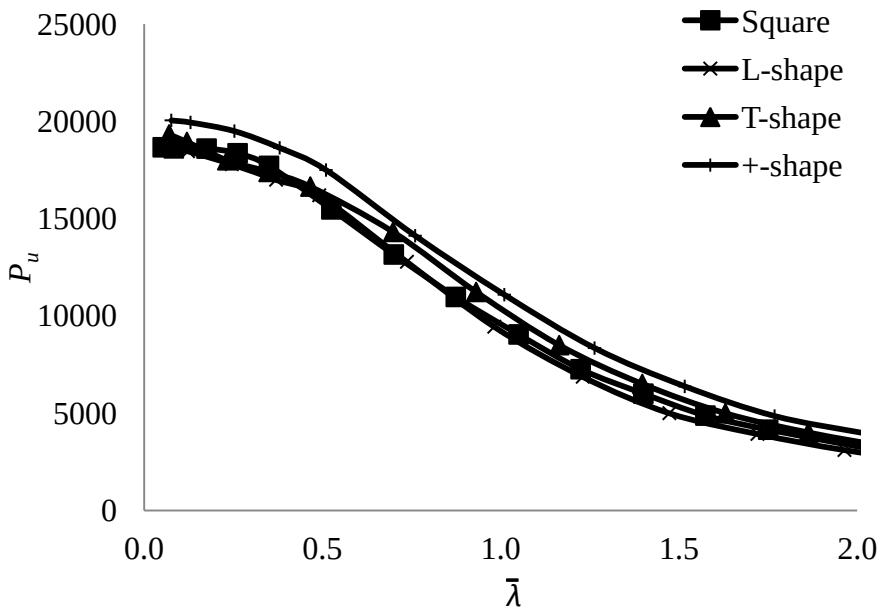

Figure 6.7: Effect of cross-sectional shape on the P_u versus $\bar{\lambda}$ curves of fixed-ended CFDSST slender column.

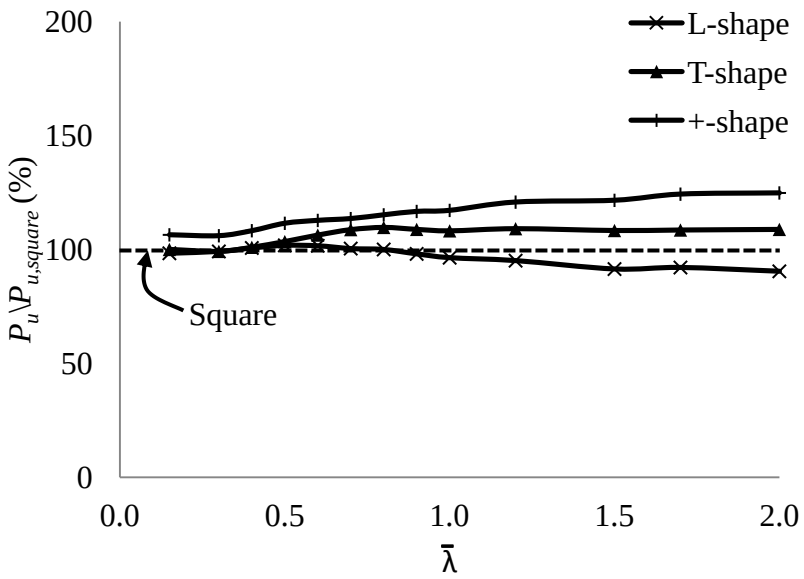

Figure 6.8: Efficiency of the fixed-ended concrete-filled CFDSST slender columns of NRSs.

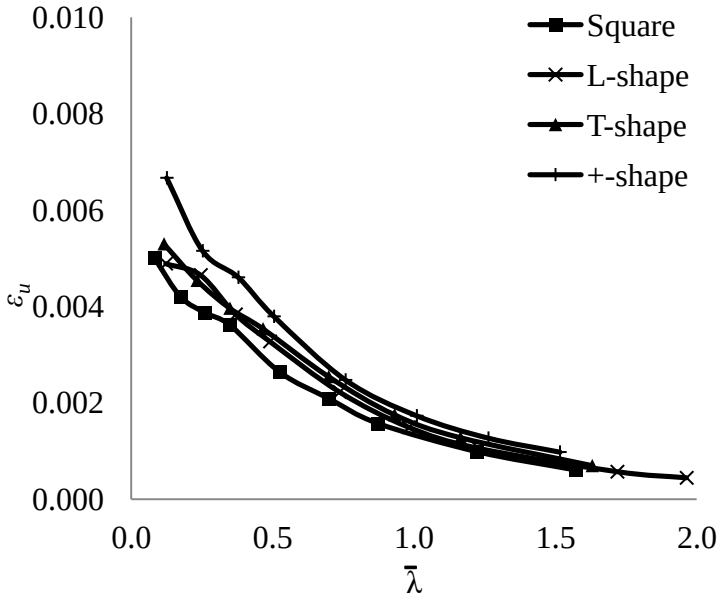

Figure 6.9: Effect of cross-sectional shape on the ε_u versus $\bar{\lambda}$ curves of fixed-ended CFDSST slender columns.

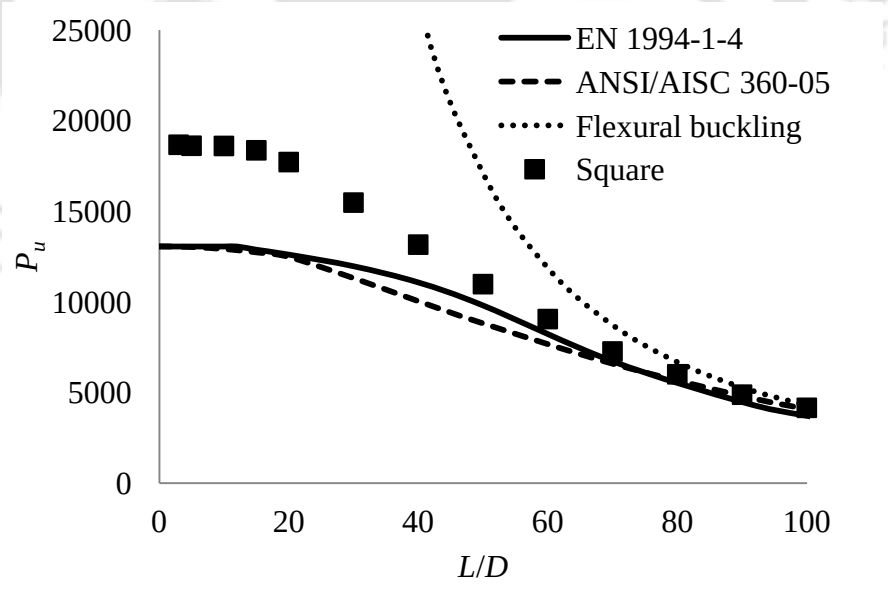

Figure 6.10: Comparison of P_u with L/D for fixed-ended CFDSST slender columns for square section.

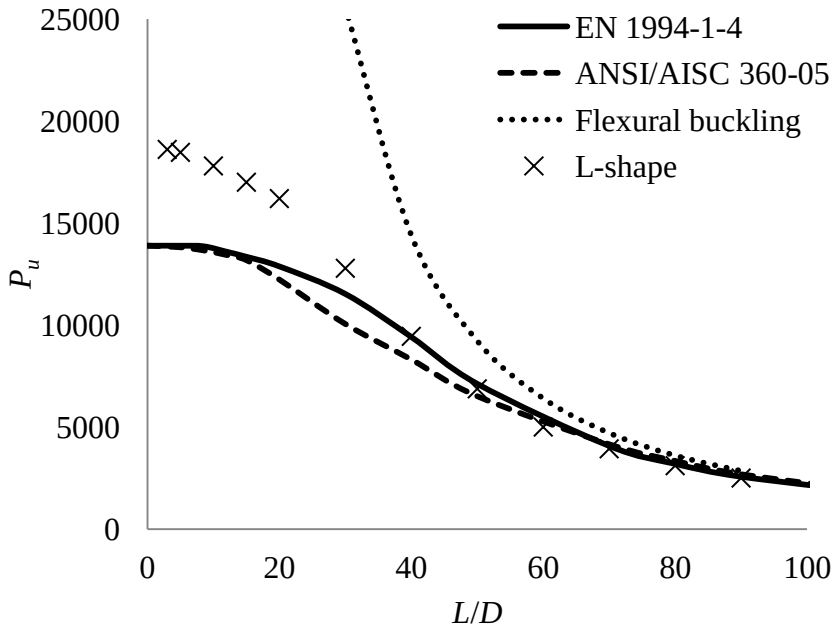

Figure 6.11: Comparison of P_u with L/D for fixed-ended CFDSST slender columns for L-shape section.

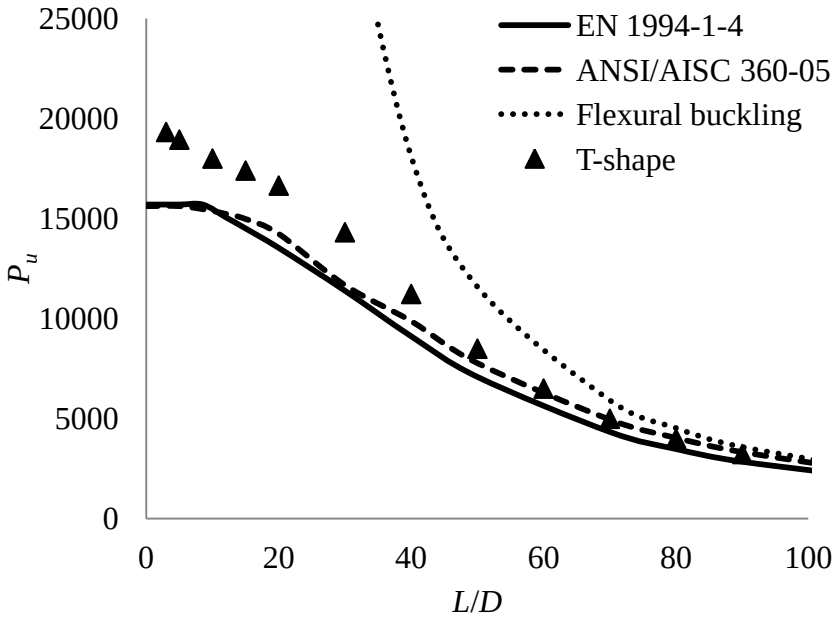

Figure 6.12: Comparison of P_u with L/D for fixed-ended CFDSST slender columns for T-shape section.

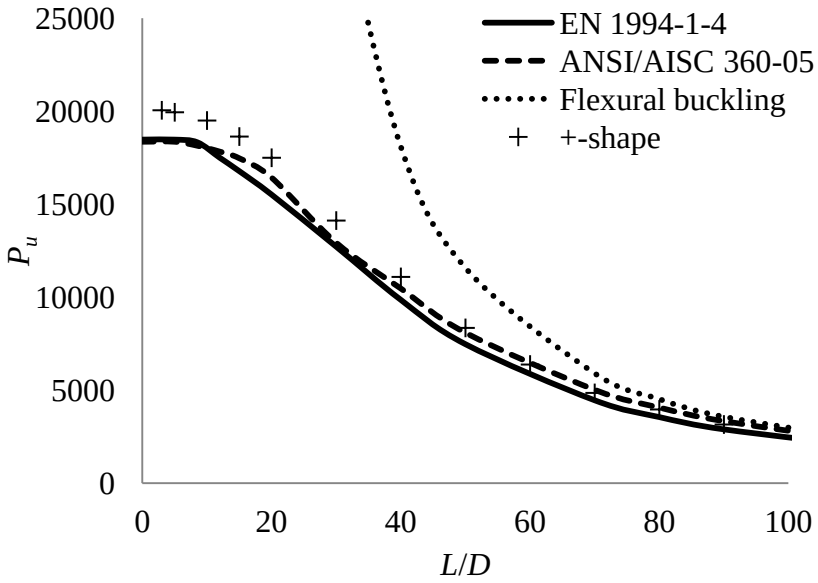

Figure 6.13: Comparison of P_u with L/D for fixed-ended CFDSST slender columns for +-shape section.

CHAPTER 7

CONCLUSIONS AND SUGGESTIONS FOR FURTHER WORK

7.1 CONCLUSIONS

The present research was undertaken to investigate the structural behavior of LDSS hollow tubular and concrete-filled tubular columns under pure axial compression using FE software package Abaqus. The aim was to compare the load and deformation characteristics as well as the failure modes of such columns with NRSs over those of the representative square sections having equal LDSS cross-sectional area and an attempt has been made to draw meaningful conclusions from the FE results generated. Further, effort has been made to compare the FE results with the current existing codes on stainless steel material to assess their applicability on the design of structural LDSS. Based on the study following conclusions are identified:

7.1.1 Hollow tubular stub columns of NRSs and square section

1) As the section goes from square → L → T → +-shape (i.e number of sides in a section increases), more effective the section becomes in controlling local buckling due to increase in the stiffness of the section.

2) For NRSs, there is approximately a linear increase of P_u with increasing LDSS tube thicknesses, whereas, for the representative square section, a milder increase of P_u is seen at lower thickness and linear increase at higher LDSS tube thicknesses.

3) For LDSS tube thickness < 30 mm, NRSs shows a higher strength capacity compared to the representative square section, with +-shaped section having the highest strengths. However at LDSS tube thicknesses ≥ 30 mm, all the sections considered gave similar strengths.

4) For changes in the cross-sectional shape from square to + shape, the increase in P_u are ~ 136%, 109%, 72%, 26%, 9% for 5mm, 10, mm, 15 mm, 20 mm and 25 mm, respectively, showing that the increase in P_u is more effective at thinner sections.

5) The gain in P_u with change in the cross-sectional shape from square to L, T and +-shape are in the range 120%-150%, 130%-170%, 140%-230%, respectively, at lower thicknesses of the steel tube (< 20 mm). Thus, it can be seen that by switching over to + shape sections, significant gain in ultimate strength can be obtained for all the thicknesses considered, with thinner sections giving more pronounced gain.

6) NRSs have notably better deformation capacity compared to the representative square section, with +-shape section estimating a much higher deformation capacity. Also, the deformation capacity increases with increasing thickness for all the hollow tubular stub columns analysed.

7) Both the current design specifications are generally capable of predicting the LDSS hollow tubular column strengths. For stocky sections, FE strengths over predicts both the codal strengths (European and American specifications) by about 28 % for all the section studied. For slender sections, at lower thicknesses of the steel tube (i.e t ~ < 20 mm), FE strengths over predicts the European specification by 28 %, 26 %, 21 % and 23 % for SHC, LHC, THC and +HC, respectively, and American specification by 5%, 6%, 9% and 17 % for SHC, LHC, THC and +HC, respectively. Based on the FE studies it can be inferred that, for slender sections, the American specification

provides closer values as compared to the European specification, thus, providing a significant material saving through design by the American specification.

8) Based on the reliability analyses it can be inferred that both specifications can be adopted for all the design of LDSS hollow tubular stub columns. However, for LDSS hollow tubular stub columns, design based on European specification tends to be slightly more reliable compared to the American specification, except for +-shape section, where the American specification tends to be more reliable.

7.1.2 Hollow tubular slender columns of NRSs and square section

1) Hollow tubular slender column fail first by overall flexural buckling followed by local buckling at mid-height of the column, irrespective of the cross-sectional shape considered, and is seen to be typical for both the Class 3 and 4 sections.

2) The buckling strength of the fixed-ended hollow tubular slender columns (both Class 3 and Class 4 sections) decreases with increasing lengths due to reduction in the stiffness of the columns, with very slender columns failing by elastic instability failure where the P_u is mainly dominated by flexural rigidity.

3) For Class 3 sections:

   a) For $\bar{\lambda} \leq 0.5$ and at high $\bar{\lambda}$, all the sections exhibit similar structural capacities. The reason being, at lower $\bar{\lambda}$, regardless of the cross-sectional shapes, all the sections experiences hardening above the global yielding load without any occurrences of local buckling at ultimate load; and the failure for high slender columns are governed principally by member stiffness rather than the cross-sectional shape.

   b) For $0.5 < \bar{\lambda} \geq 2.0$, there is a nearly linear variation in strengths (increasing trend for +HC, similar trend for THC and decreasing trend for LHC), with stabilization beyond $\bar{\lambda} > 2.0$. For $\bar{\lambda} > 2.0$, P_u for +HC showed ~ 30% higher; THC showed

similar strength; and LHC showed ~20% lower than the corresponding value for SHC, indicating that +HC has an improved ultimate strength for all the ranges of $\bar{\lambda}$.

c) At lower $\bar{\lambda}$ < ~ 0.50, the values of ε_u are found to be highest for +HC, whilst SHC, LHC and THC predicted similar values. However, at higher $\geq$ 0.50, ε_u values lies in the range of ~ 0.2 – 0.6 % for all the section analysed.

4) For Class 4 sections:

a) In contrast to Class 3 sections, cross-sectional shape becomes increasingly significant with decreasing $\bar{\lambda}$, however, the cross-sectional shape becomes insignificant for very high $\bar{\lambda}$ as also the case for Class 3 sections.

b) The average strength enhancement as compared to the representative square section are ~ 10 %, 50 %, and 90 % higher for LHC, THC, and +HC, respectively.

c) Similar to Class 3, +HC predicted higher deformation at peak load, as compared to SHC, LHC and THC, at lower values of $\bar{\lambda}$ (< ~ 1.0). At higher slenderness ($\bar{\lambda}$ > ~ 1.0), ε_u values also lies in the range of ~ 0.2 – 0.5 % for all the section analysed.

5) A higher $\bar{\lambda}$, for both the Class 3 and Class 4 sections, European specification gives a conservative estimation of strengths compared to the American specification, which gives slightly conservative value, in the design of LDSS hollow tubular slender columns. However, the design of hollow tubular slender column with L-shape section through the American specification tends to be critical where it over predicts the FE strengths.

6) Based on the reliability analyses it is recommended that both the specifications can be adopted for all the design of fixed-ended LDSS hollow tubular slender columns except for Class 3 LHC, wherein a suitable modification may be employed after systematic studies (including experiments). For the design of Class 3 sections,

European specification tends to be more reliable compared to the American specification and vice versa in the design of Class 4 sections.

7.1.3 Concrete-filled tubular stub columns of NRSs and square section

1) Out-of-plane deformation (seen only at the longer faces) of the entire four faces, two faces, and one face can be seen for the square, L-shaped and T-shaped sections, respectively, at P_u, except for +-shaped section and at the shorter faces of L- and T-shape sections where no local buckling is seen at P_u.

2) On filling the LDSS tube with concrete, there in an increase in the P_u by about 70 % to 435 %, 63 % to 299 %, 35 % to 283 %, and 20 % to 181% for square, L, T, and +-shape sections, respectively.

3) The influence of the LDSS tube on the δ_u increases with increasing thickness of the LDSS tube and increasing concrete strength.

4) For normal concrete strength ($f_{ck} \leq 40$ MPa), NRSs appears to have similar or slightly enhanced P_u, in comparison with square section. At higher f_{ck} (> 40 MPa), L-, T-, and +-shape sections predicted lower values of P_u (for $f_{ck} = 100$ MPa) by about 18 %, 15 % and 12 %, respectively, compared to the representative square section.

5) Increasing the strength of the concrete core, for all the NRSs and representative square section, there is a linear increase in the strength for the range of concrete strengths investigated herein (25–100 MPa). Also, it can be seen that the square section shows a higher increasing rate compared to the NRSs for the same LDSS tube thickness.

6) On increase in thickness of the LDSS tube for all the CFDSST stub columns from 7.5 mm to 9.0 (20 % increase) and 10.0 mm (33% increase), the average increase in strengths are 14-19 % and 25-30 %, respectively. On increase in concrete strength from 40 MPa to 48 MPa (20 % increase) and 53 MPa (33% increase), the average increase in strengths are 6 - 9 % and 10 - 15 %, respectively. Hence increasing the

thickness of the LDSS tube is more beneficial in increasing the strength of the CFDSST stub columns rather than the concrete strength.

7) In CFDSST stub columns, δ_u decreases with increasing concrete strengths, but increases as the sections changes from Square → L → T → +-shape.

8) FE strengths over predicts the EN 1994-1-1 (2004) specification by about in average 21 %, 19%, 14 % and 4 % for the square, L, T, and +-shape sections, respectively, whereas, ASCE 8-02 (2002) specification gives a slightly conservative prediction by about in average 16 %, 10%, 8 % and 1 % for the square, L, T, and +-shape sections, respectively.

9) Based on the reliability analyses it can be inferred that both specifications can be adopted for all the design of CFDSST stub columns except for CFDSST stub columns with +-shape section, wherein a suitable modification may be employed after systematic studies (including experiments). However, for CFDSST stub columns, design based on the American specification tends to be slightly more reliable compared to the European specification.

7.1.4 Concrete-filled tubular slender columns of NRSs and square section

1) At P_u, only overall buckling is seen for both the hollow tubular and CFDSST columns. At post P_u, LDSS hollow tubular members fails through overall buckling and thereafter accompanied by local buckling of the LDSS tube at mid-height sections. However, local buckling of the LDSS tube is prevented due to the concrete core in CFDSST columns.

2) The P_u of CFDSST columns is higher than that of the reference hollow steel tubular columns because of increased flexural rigidity provided by the concrete core, thereby achieving higher u_{mu} by the CFDSST columns. However, the δ_u of CFDSST column

is lower than that of the reference LDSS hollow tubular column because of a higher elastic compression stiffness of the latter due to concrete core

3) For all the section analysed the P_u decreases with increasing $\overline{\lambda}$. Also, +-shape and T-shape sections show a higher P_u for all the $\overline{\lambda}$, however, L-shape section showed a similar P_u at lower $\overline{\lambda}$ and a lower P_u at higher $\overline{\lambda}$ compared to that of the representative square section.

4) For $\overline{\lambda} \sim < 0.5$, +-shape showed a 7 % higher strength and L- and +-shape showed similar strengths compared to the representative square section. For $0.5 \leq \overline{\lambda} \geq 1.5$, a linear increasing trend in strength is seen with increasing $\overline{\lambda}$. However, for $\overline{\lambda} > 0.5$, T- and +-shape showed a 10 % and 25 % more strength and L-shape showing a 10 % lower strength compared to the representative square section.

5) In fixed-ended CFDSST slender columns, change of cross-sectional shape from square section to NRSs is significant, especially for T-shape and +-shape sections, and can promote the application of thin-wall LDSS tube.

6) The influence of the cross-sectional shapes on the ε_u becomes less significant with increasing $\overline{\lambda}$, but becomes increasingly significant with decreasing $\overline{\lambda}$. Also, NRSs shows a higher ε_u for all $\overline{\lambda}$ considered compared to the representative square section, with +-shape section showing the highest ε_u.

7) The design standards show over conservative results for square and L-shape sections and conservative for T-shape and +-shape sections. However, the European specification gives a conservative estimation of strengths compared to the American specification for square and L-shape sections and vice versa in case of T-shape and +-shape sections.

8) Based on the reliability analyses both specifications can be adopted for all the design of fixed-ended CFDSST slender columns, except for the L-shape section, wherein a

suitable modification may be employed after systematic studies (including experiments). For the design of fixed-ended CFDSST slender columns of square and L-shape sections, American specification tends to be more reliable compared to the European specification and vice versa in the design for the fixed-ended CFDSST slender columns of T-shape and +-shape sections.

7.2 SUGGESTIONS FOR FURTHER WORK

Even though a considerable understanding have been obtained in the present work for the structural behavior of LDSS hollow tubular and concrete-filled tubular columns with NRSs and representative square section under pure axial compression, significant amount of work may be identified and suggestions for further work are presented under the following sub-sections.

7.2.1 Loading Conditions

The present study is limited to structural members under pure axial compression. Extension of the present work to cover different loading scenarios form an important part of promoting hollow and concrete-filled tubular NRSs. Hollow and concrete-filled tubular NRSs under following loading conditions may be studied:

1) Behavior of LDSS hollow and concrete-filled tubular NRSs under uniaxial and bi-axial loading conditions.
2) Structural behavior of hollow and concrete-filled tubular NRSs under cyclic loading condition.
3) Effect of impact/blast on LDSS hollow and concrete-filled tubular NRSs.
4) Studies on LDSS hollow and concrete-filled tubular NRSs at elevated temperatures.

7.2.2 In-fill Materials

Different types of material or a combination of materials can be filled inside the hollow steel tubes, in which the present study was focused mainly on plain concrete in-fill with varying concrete strengths. The following presents a various in-fill materials which may be investigated:

1) Use of fly-ash concrete material.
2) The strength and ductility enhancement in the use of steel reinforcement inside the concrete-infill of NRSs need to be examined.
3) Possible use of very high strength concrete such as fiber reinforced concrete material.

7.2.3 Other Suggestions

Apart from the two main categories mentioned in Section 8.1 & 8.2, exploitation on the use of hollow and concrete-filled tubular NRSs are mentioned below:

1) Possibilities on the application of concrete-filled NRSs to beams.
2) The effect of perforations on the structural capacities of hollow and concrete-filled tubular NRSs.
3) Comparison in the structural behavior of concrete-filled tubular NRSs to that of reinforced concrete columns of such sections.
4) Studies may be done on the doubly skin hollow and concrete-filled tubular NRSs.
5) Investigation can also be done on the tapered hollow and concrete-filled tubular NRSs.
6) Effect of confinement on the concrete-filled tubular NRSs.

REFERENCES

Abaqus, 2009. Hibbitt, Karlsson & Sorensen, Inc. Abaqus/Standard user's manual volumes I-III and ABAQUS CAE manual. Version 6.9-EF1, Pawtucket, USA.

ACI, 1999. Building code requirement for structural concrete and commentary. ACI; American concrete Institute; USA.

AISI, 1968. Specification for the design of light gauge cold-formed stainless steel structural members. American Iron and Steel Institute. Washington, D.C.

AISI, 1974. Stainless steel cold-formed structural design manual. American Iron and Steel Institute. Washington, D.C.

An, Y.F., Han, L.H. & Zhao, X.L., 2012. Behaviour and design calculations on very slender thin-walled CFST columns. Thin-Walled Structures; 53: 161-175.

ANSI/AISC 360-05, 2005. Specification for structural steel buildings. Chicago (IL, USA).

ASCE, 1982. ASCE task committee on concrete and masonry structure, state of the art report on finite element analysis of reinforced concrete, American Society of Civil Engineering; New York.

ASCE, 1990. Specification for the design of cold-formed stainless steel structural members. ANSI/ASCE 8-90. American Society of Civil Engineering. New York.

ASCE 8-02, 2002. Specification for the design of cold-formed stainless steel structural members. SEI/ASCE 8-02. American Society of Civil Engineering. New York.

Ashraf, M., 2006. Structural stainless steel design: Resistance based on deformation capacity. PhD. thesis. Department of Civil and Environmental Engineering, Imperial College London, UK.

Ashraf, M., Gardner, L. & Nethercot, D.A., 2006. Finite element modeling of structural stainless steel cross-sections. Thin-Walled Structures; 44: 1048-1062.

Ashraf, M., Gardner, L. & Nethercot, D.A., 2008. Resistance of stainless steel CHS columns based on cross-section deformation capacity. Journal of Constructional Steel Research; 64: 962–970.

Attard, M. M. & Setung, S., 1996. Stress-Strain Relationship of Confined and Unconfined Concrete, ACI, Materials Journal; 93-M49: 432-442.

Aust/NZS, 2001. Cold-formed stainless steel structures. Australian/ New Zealand Standard AS/NZS 4673:2001. Sydney, Australia: Standards Australia.

Baddoo, N.R., Burgan, R. & Ogden, R., 1997. Architects' guide to stainless steel. SCI-P-179, UK: The Steel Construction Institute.

Baddoo, N.R., 2008. Stainless steel in construction: a review of research, applications, challenges and opportunities. Journal of Constructional Steel Research; 64: 1199-1206.

Bearley, H., 1989. Harry Bearley: Stainless pioneer. British steel stainless and the Kelham island industrial museum, Sheffield (eds.), McCann-Erickson Central Solihull, West Midlands.

Bjorhovde, R., 1972. Deterministic and probabilistic approaches to the strength of steel columns. Bethlehem (PA): Lehigh University.

Boyd, F. P., Cofer, W. F. & McLean, D., 1995. Seismic performance of steel-encased concrete column under flexural loading. ACI Structural Journal; 92(3): 355–365.

Bradford, M. A., 1996. Design strength of slender concrete-filled rectangular steel tubes. ACI Structural Journal; 93(2): 229–235.

Bradford, M. A., Loh, H. Y. & Uy, B., 2002. Slenderness limits for filled circular steel tubes. Journal of Constructional Steel Research; 58(2): 243–252.

BS EN 10088-1, 1995. Stainless steels – Part 1: List of stainless steels. British Standards Institution.

BSSA. British Stainless Steel Association. http://www.bssa.org.uk/topics.php?article=125.

Buijs, N.W., 2008. The role and signifance of nickel. http://www.innomet.nl/docs/SSWtechHastelloy.pdf.

CIDECT, 1984. Construction with hollow steel sections. British Steel plc, Corby, Northants, U.K., ISBN 0-9510062-0-7.

Chan, T.M. & Gardner L., 2008. Compressive resistance of hot-rolled elliptical hollow sections. Engineering Structures; 30(2): 522–532.

Chen, Y.N. & Kempner, J., 1976. Buckling of oval cylindrical-shell under compression and asymmetric bending. AIAA Journal; 14(9): 1235–1240.

Cheng, T. & Thomas, H., 1989. T-shaped reinforced concrete members under biaxial and axial compression. ACI Structural Journal; 86(4): 2576-2595.

Chou, S.M., Chai, G.B. & Ling, L., 2000. Finite element technique for design of stub columns. Thin-Walled Structures; 37: 92-112.

Cusson, D. & Paultre, P., 1994. High Strength Concrete Columns Confined by Rectangular Ties, Journal of Structural Engineering Division, ASCE, No. 3; 120: 783-804.

Dabaon, M.A., El-Boghdadi, M.H. & Hassanein, M.F., 2009. A comparative experimental study between stiffened and unstiffened stainless steel hollow tubular stub columns. Thin-Walled Structures; 47: 73–81.

Dawson, R. G. & Walker, A. C., 1972. Post-buckling of geometrically imperfect plates. Journal of the Structural Division, ASCE; 98: ST1, 75-94.

Dai, X. & Lam, D., 2010. Numerical modeling on the axial compressive behavior of short concrete-filled elliptical columns. Journal of Constructional Steel Research; 66: 931-942.

Du, G.F., Xu, L.H., Wen, F. & Xu, H.R., 2008. Test study on behavior of T-shaped concrete-filled steel tubular short columns under axial compression. Journal of Huazhong University Science and Technology (Urban Science) 2008; 25(3):188–194 [in Chinese].

Dundar, C. & Sahin, B., 1993. Arbitrarily shaped reinforced concrete members subjected to biaxial bending and axial load. Computers and Structures; 49(4): 643-662.

Dutta, D., Würker, K.G, 1988. Handbuch Hohlprofile in Stahlkonstruktionen, Verlag TÜV Rheinland GmbH, Köln, Germany, ISBN 3-88585-528-3.

Ellobody, E., 2007. Buckling analysis of high strength stainless steel stiffened and unstiffened slender hollow section columns. Journal of Constructional Steel Research; 63: 145-155.

Ellobody, E. & Young, B., 2005. Structural performance of cold-formed high strength stainless steel columns. Journal of Constructional Steel Research; 61: 1631-1649.

Ellobody, E. & Young, B., 2006a. Design and behaviour of concrete-filled cold-formed stainless steel tube columns. Engineering Structures; 28: 716–728.

Ellobody, E. & Young, B., 2006b. Nonlinear analysis of concrete-filled steel SHS and RHS columns. Thin-walled Structures; 44: 919-930.

Ellobody, E. & Young, B., 2011. Numerical simulation of concrete encased steel composite columns. Journal of Constructional Steel Research; 67: 211-222.

Ellobody, E., Young, B. & Lam, D., 2006. Behaviour of normal and high strength concrete-filled compact steel tube circular stub columns. Journal of Constructional Steel Research; 62(7): 706-15.

ENV1993-1-1, 1992. Design of steel structures, Part 1.1: General rules and rules for buildings.

ENV 1993-1-4, 1996. Eurocode 3: Design of steel structures-Part 1.4: General rules-Supplementary rules for stainless steel. CEN.

EN 1994-1-1, 2004. Design of composite steel and concrete structures, part 1.1: general rules and rules for building. British Standards Institution. London (UK).

EN 1993-1-4, 2006. Eurocode 3: Design of steel structures-Part 1.4: General rules-Supplementary rules for stainless steel. CEN.

EN 10088-4, 2009. Stainless steels_part 4: technical delivery conditions for sheet/plate and strip of corrosion resisting steels for general purposes. CEN.

Euro Inox, 1994. Design manual for structural stainless steel. NIDI. Toronto, Canada.

Furlong, R. W., 1967. Strength of steel-encased concrete beam columns. Journal of Structural Division, ASCE; 93 (5): 113–124.

Furlong, R. W., 1974. Concrete encased steel columns—Design tables.'' Journal of Structural Division, ASCE; 100(9): 1865–1882.

Galambos, T.V., 1998. Guide to stability design criteria for metal structures. 4th Edition. New York: John Wiley and Sons Inc.

Galinsky. Inland Steel, Chicago. http://www.galinsky.com/buildings/inlandsteel/, Retrieved on September 2013.

Gao, D.X., Ke, J. & Wang, L.H., 2005. Seismic behavior analysis of special-shaped column frame structure. Journal of Xi'an University of Technology; 21(3): 285-288 [in Chinese].

Gardner, L., 2002. A new approach to structural stainless steel design. PhD. Thesis. Structures Section, Dept of Civil and Environmental Engineering; Imperial College London, UK.

Gardner, L., 2005a. Structural behaviour of oval hollow sections. International Journal of Advanced Steel Construction;1(2): 29–54.

Gardner, L., 2005b. The use of stainless steel in structures. Progress in Structural; 7(2): 45-55.

Gardner, L., 2013. Proposed Amendment to include Lean Duplexes , Evolution Group for EN 1993-1-4, (Personal communication).

Gardner, L. & Ashraf, M., 2006. Structural design for non-linear metallic materials. Engineering Structures; 28: 925-936.

Gardner, L. & Chan, T.M., 2007. Cross-section classification of elliptical hollow sections. Steel Composite Structures;7(3):185–200.

Gardner, L., Insausti, A., Ng, K.T. & Ashraf, M., 2010. Elevated temperature material properties of stainless steel alloys. Journal of Constructional Steel Research; 66: 634-647.

Gardner, N. J. & Jacobson, E. R., 1967. Structural Behavior of Concrete Filled Steel Tubes. ACI Journal; 64 (7): 404-413.

Gardner, L. & Ministro, A., 2004. Testing and numerical modelling of structural steel oval hollow sections. In: Department of Civil and Environmental Engineering, Structural section. Imperial College, UK: London.

Gardner, L. & Nethercot, D.A., 2002. Numerical modelling of cold-formed stainless steel sections. In: NSCC 2001 proceedings: NSCC 2001 ninth Nordic steel constructional conference, Helsinki, Finland. 781–790.

Gardner, L. & Nethercot, D.A., 2004a. Experiments on stainless steel hollow sections-Part 1: Material and cross-sectional behavior. Journal of Constructional Steel Research; 60: 1291–1318.

Gardner, L. & Nethercot, D.A., 2004b. Experiments on stainless steel hollow sections-Part 2: Member behaviour of columns and beams. Journal of Constructional Steel Research; 60: 1319–1332.

Gardner, L. & Nethercot, D.A., 2004c. Numerical modeling of stainless steel structural components-A consistent approach. Journal of Structural Engineering, ASCE; 130(10): 1586-1601.

GB50017-2003, 2003. Code for design of steel structures. Beijing: China Planning Press; 2003 [in Chinese].

Ge, H. B. & Usami, T., 1992. Strength of concrete-filled thin-walled steel box columns: Experiment.'' Journal of Structural Engineering; 118(11): 3036–3054.

Ge, H. B. & Usami, T., 1994. Strength analysis of concrete-filled thin-walled steel box columns.'' Journal of Constructional Steel Research; 30(3): 259–281.

Gedge, G., 2008. Structural uses of stainless steel-buildings and civil engineering. Journal of Constructional Steel Research; 64(11): 1194-1198.

Geograph. London Gatwick North Terminal. http://www.geograph.org.uk/photo/3177511, Retrieved on September 2013.

Gho, W and Liu, D., 2004. Flexural behaviour of high-strength rectangular concrete-filled steel hollow sections. Journal of Constructional Steel Research; 60 (11): 1681-1696.

Giakoumelis, G. & Lam, D., 2004. Axial capacity of circular concrete-filled tube columns. Journal of Constructional Steel Research; 60(7):1049–68.

Grigorenko, Y.M. & Rozhok, L.S., 2002. Stress analysis of hollow elliptic cylinders with variable eccentricity and thickness. International journal of applied mechanics; 38(8): 954–966.

Hajjar, J. F. & Gourley, B. C., 1996. Representation of concrete-filled steel tube cross-section strength. Journal of Structural Engineering; 122(11): 1327–1336.

Hammer, E.W.Jr. & Petersen, R.E., 1955. Column curves for type 301 stainless steel. Aeronautical Engineering Review; 14: 12, 33-39 and 48.

Han, L.H., 2007. Concrete filled steel tubular structures. 2nd Edition. Beijing: China Science Press; [in Chinese].

Han, L.H. & yao, G.H., 2004. Experimental behaviour of thin-walled hollow structural steel (HSS) columns filled with self-consolidating concrete (SCC). Thin-Walled Structures; 42: 1357-1377.

Hassanein, M.F., 2010. Numerical modelling of concrete-filled lean duplex slender stainless steel tubular stub columns. Journal of Constructional Steel Research; 66: 1057-1068.

Hassanein, M.F., 2011. Finite element investigation of shear failure of lean duplex stainless steel plate girders. Thin-Walled Structures; 49: 964-973.

Hassanein, M.F. & Silvestre N., 2013. Flexural behavior of lean duplex stainless steel girders with slender unstiffened webs. Journal of Constructional Steel Research; 85: 12-23.

Hassanein, M.F., Kharoob, O.F. & Liang, Q.Q., 2013. Behaviour of circular concrete-filled lean duplex stainless steel tubular short columns. Thin-Walled Structures; 68: 113-123.

Hill, H.N., 1944. Determination of stress-strain relations from ``offset" yield strength values. Technical Note No 927, Washington DC: National advisory committee for aeronautics.

Hong, S. & Varma, A.H., 2009. Analytical modeling of the standard fire behavior of loaded CFT columns. Journal of Constructional Steel Research; 65(1): 54–69.

Hu, H.T. & Schnobrich, W.C., 1989. Constitutive modeling of concrete by using nonassociated plasticity. Journal of Material Civil Engineering; 1 (4): 199-216.

Hu, H.T., Huang, C.S., Wu, M.H. & Wu, Y.M., 2003. Nonlinear analysis of axially loaded concrete-filled tube columns with confinement effect. Journal of Structural Engineering, ASCE; 129(10): 1322-1329.

Huang, Y. & Young, B., 2012. Material properties of cold-formed lean duplex stainless steel sections. Thin-Walled Structures; 54: 72-81.

Huang, Y. & Young, B., 2013. Tests of pin-ended cold-formed lean duplex stainless steel columns. Journal of Constructional Steel Research; 82: 203-215.

Jamaluddin, N., Lam, D., Dai, X.H. & Ye, J., 2013. An experimental study on elliptical concrete-filled columns under axial compression. Journal of Constructional Steel Research; 87: 6-16.

Joaquin, M., 1979. Design aids for L-shaped reinforced concrete columns. ACI Structural Journal; 76(49): 1197-1216.

Johansson, M., 2002. Composite action and confinement effects in tubular steel_concrete columns. Ph.D. thesis. Goteborg (Sweden): Chalmers University of Technology.

Johnson, A.L. & Winter, G., 1966. Behaviour of stainless steel columns and beams. Journal of the Structural Division, ASCE; ST5: 97-118.

Kato, B., 1996. Column curves of steel-concrete composite members. Journal of Constructional Steel Research; 39(2): 121-135.

Kempner, J. & Chen, Y.N., 1974. Buckling and initial post-buckling of oval cylindrical- shells under combined axial-compression and bending. Transactions of the New York Academy of Sciences; 36(2): 171–191.

Knowles, R. B. & Park, R., 1969. Strength of concrete filled steel tubular columns. Journal of the Structural Division, ASCE; 95 (12): 2565–2587.

Kupfer, H. B. & Gerstle,K.H., 1973. Behaviour of concrete under biaxial stresses. Journal of Engineering Mechanics Division; 99: 853-866.

Lam, D. & Gardner, L., 2008. Structural design of stainless steel concrete filled columns. Journal of Constructional Steel Research; 64(11): 1275–82.

Law, k.H. & Gardner, L., 2013. Buckling of elliptical hollow section members under combined compression and uniaxial bending. Journal of Constructional Steel Research; 86: 1-16.

Lee, J. & Fenves,G.L., 1998. Plastic-damage model for cyclic loading of concrete structures. Journal of Engineering Mechanics; 124(8): 892-900.

Liang, Q. Q. & Uy, B., 2000. Theoretical study on the post-local buckling of steel plates in concrete-filled box column. Computers and Structures; 75(5): 479–490.

Lin, Z.Y., Shen, Z.Y., Luo, J.H. & Zhang, J.C., 2009. Study on behavior of L-shaped concrete-filled steel tube stubs subjected to axial compression. Progress in Steel Building Structures; 11(6): 14–19 [in Chinese].

Lu, X., Li, X. & Wang, D., 2007. Modelling and experimental verification on concrete-filled steel tubular columns with L or T section. Frontiers of Architecture and Civil Eng in China; 1: 163-169.

Lubliner, J., Oliver, J., Oller, S. & Oñate,E., 1989. A Plastic-Damage Model for Concrete. International Journal of Solids and Structures; 25(3): 229–326.

Lui, Y. & Young, B., 2003. Buckling of stainless steel square hollow section compression members. Journal of Constructional Steel Research; 59: 165–177.

Maekawa, K., Pimanmas, A. & Okamura, H. 2003. Nonlinear mechanics of reinforced concrete. Spon Press.

Mallikarjuna & Mahadevappa, P., 1992. Computer aided analysis of reinforced concrete columns subjected to axial compression and bending-I L-shaped sections; Computers and Structures; 44(5): 1121-1138.

Mann, A.P., 1993. The structural use of stainless steel. Journal of Structural Engineering; 71(4):60–9.

Mander, J.B., Priestley, M.J.N. & Park, R., 1988. Theoritical stress-strain model for confined concrete. Journal of Structural Engineering, ASCE; 114(8): 1804-1826.

Mirambell, E. & Real, E., 2000. On the calculation of deflections in structural stainless steel beams: an experimental and numerical investigation. Journal of Constructional Steel Research; 54: 109-133.

Morino, S., 1998. Recent developments in hybrid structures in Japan-Research, design and construction. Engineering Structures, 20(4–6): 336–346.

Mursi, M. & Uy, B., 2003. Strength of concrete filled steel box columns incorporating interaction buckling. Journal of Structural Engineering, ASCE; 129(5): 626–639.

Nayal, R. & Rasheed, H.A., 2006. Tension stiffening model for concrete beams reinforced with steel and FRP bars. Journal of Materials in Civil Engineering; 18 (6): 831-841.

Nilsson, J.O., Chai, G. & Kivisäkk, U., 2008. Recent development of stainless steels. In: Proceedings of the sixth European stainless steel conference; 585-590.

Nowzartash, F. & Mohareb, M., 2009. Plastic interaction relations for elliptical hollow sections. Thin-Walled Structures; 47: 681-691.

Nowzartash, F. & Mohareb, M., 2011. Column curves for elliptical hollow section members. Journal of Structural Engineering; 67: 1525-1536.

NSSMC. Nippon Steel and Sumitomo Metal. http://www.nssmc.com/en/news/old_smi/2011/news2011-07-08.html/, Retrieved in September 2013.

Nurberger, U., 1996. Stainless Steel in Concrete. State of the Art Report. Publication number 18, European Federation of Corrosion.

Ohashi, Y., 1992. An experimental study on axial and flexural behavior of concrete filled L-shaped steel tubes. Architecture Institute of Japan; 8: 1813–1814 [in Japanese].

Orito, Y., Sato, T., Tanaka, N. & Watanabe, Y., 1987. Study on the unbonded steel tube concrete structures. Engineering Foundation Conference on Composite Constructions, Henniker, New Hampshire, USA.

Oshima, M. & Hashimoto, C. 1984. Mechanical properties of concrete confined by steel rings. In: Summaries of the 39th annual convention, volume V. Japan Society of Civil Engineers.

Outokumpu, 2013. http://www.outokumpu.com/en/stainless-steel/grades/duplex, Retrieved in September 2013.

Porco, G., Spadea, G. & Zinno, R., 1994. Finite element analysis and parametric study of steel-concrete composite beams. Cement and Concrete Composites; 16: 261-272.

Ramberg, W. & Osgood, W.R., 1943. Description of stress-strain curves by three parameters. NACA Technical Note No. 902.

Rasmussen, K.J.R., 2000a. Recent research on stainless steel tubular structures; 54: 75-88.

Rasmussen, K. J. R., 2000b. The Development of an Australian Standard for Stainless Steel Structures. Proceedings of the Fifteenth International Speciality Conference on Cold-formed Steel Structures. St. Louis, Missouri, USA. 659-671.

Rasmussen, K.J.R., 2003. Full-range stress-strain curves for stainless steel alloys. Journal of Constructional Steel Research; 59: 47-61.

Rasmussen, K.J.R. & Rondal, J., 1997. Explicit approach to design of stainless steel columns. Journal of Structural Engineering, ASCE; 123: 7, 857-863.

Ren, Q., Lv, Y., Jia, L. & Liu, D., 2011. Preliminary analysis on inclined concrete-filled steel tubular stub columns with circular section under axial compression. Applied Mechanics and Materials; (88-89): 46-49.

Richart, F.E., Brandzaeg, A., & Brown, R.L., 1928. A study of the failure of concrete under combined compressive stresses. Bull. 185. Champaign, University of Illinois Eng Exp Station. USA.

Riks, E., 1972. The application of Newton's method to the problem of elastic stability. Journal of Applied mechanics; 39: 1060-1065.

Riks, E., 1979. An incremental approach to the solution of snapping problems. International Journal of Solids and Structures; 15: 529-551.

SABS, 1997. Structural use of steel – part 4: The design of cold-formed stainless steel structural members. SABS 0162-4:1997.

Saenz, L.P., 1964. Discussion of 'Equation for the stress-strain curve of concrete' by Desayi P. and Krishnan S.J. American Concrete Institute; 61: 1229-1235.

Saliba, N. & Gardner, L., 2013a. Cross-section stability of lean duplex stainless steel welded I-sections. Journal of Constructional Steel Research; 80: 1-14.

Saliba, N. & Gardner, L., 2013b. Experimental study of the shear response of lean duplex stainless steel plate girders. Engineering Structures; 46: 375-391.

Schneider, S. P., 1998. Axially loaded concrete-filled steel tubes. Journal of Structural Engineering; 124 (10): 1125-1138.

Shams, M. & Saadeghvaziri, M. A., 1997. State of the art of concrete-filled steel tubular columns. ACI Structural Journal; 94(5): 558–571.

Sheikh, S.A. & Uzmeri, S.M., 1988. Strength and ductility of tied concrete columns, ASCE, Journal of Structural Division, No. 5; 106 (198): 1079-1102.

Sieurin, H., Sandström, R. & Westin, E.M., 2007. Fracture toughness of the lean duplex stainless steel LDX 2101. Metallurgical and Materials Transactions A; 37(10): 2975-2981.

SMC. Shanghai Metal Corporation, http://www.shanghaimetal.comFracture, Retrieved in January 2013.

SSBJA, 1995. The design and construction specifications for stainless steel structures. Stainless Steel Building Association of Japan [in Japanese].

SSEF. Fun is in the Details: Innovation in Steel Connections. http://tboake.com/SSEF1/shapes.shtml, Retrieved in September 2013.

Sun, J. & Butterworth, J.W., 1998. Behaviour of steel single angle compression members axially loaded through one leg.Proceedings of the Australian Structural Engineering Conference. Auckland: 859-866.

Talja, A. & Salmi, P., 1995. Design of stainless steel RHS beams, columns and beam-columns. VTT Research notes 1619. Espoo: Technical Research Centre of Finland.

Tao, Z., Uy, B., Han, L.H. & Wang, Z.B., 2009. Analysis and design of concrete-filled stiffened thin-walled steel tubular columns under axial compression. Thin-Walled Structures; 47(12):1544-1556.

Tao Z., Uy B, Liao, F.Y. & Han, L.H., 2011. Nonlinear analysis of concrete-filled square stainless steel stub columns under compression. Journal of Constructional Steel Research; 67: 1719-1732.

Theofanous, M., Chan, T.M. & Gardner, L., 2009a. Flexural behavior of stainless steel oval hollow sections. Thin-Walled Structures; 47: 776-787.

Theofanous, M., Chan, T.M. & Gardner, L., 2009b. Structural response of stainless steel oval hollow section compression members. Engineering Structures; 31: 922-934.

Theofanous, M. & Gardner, L., 2010. Experimental and numerical studies of lean duplex stainless steel beams. Journal of Constructional Steel Research; 66: 816- 825.

Theofanous, M. & Gardner, L., 2009. Testing and numerical modelling of lean duplex stainless steel hollow section columns. Engineering Structures; 31: 3047-3058.

Tomii, M., 1991. Ductile and strong columns composed of steel tube, infilled concrete and longitudinal steel bars. Special volume. In: Proceedings of the third international conference on steel–concrete composite structures. Fukuoka, Japan: Association of Steel-Concrete Structures: 39–66.

Tomii, M. Y., Yoshimura, K. & Morishita, Y., 1977. Experimental Studies on Concrete filled steel tubular columns under concentric loading. Proeedings International Colloquium on Stability of Structures under Static and Dynamic Loads; 718-741.

Truman, J., 1985. The initiation and growth of high alloy (stainless) steel production. Journal of Historical Metallurgy Society. 19(1): 116-125.

Umbarkar, K.R., Patton, M.L. & Singh, K.D., 2012. Effect of single circular perforation in lean duplex stainless steel (LDSS) hollow circular stub columns under pure axial compression. Thin-Walled Structures; 54: 72-81.

Uy, B., 1998. Local and post-local buckling of concrete filled steel welded box columns. Journal of Constructional Steel Research; 47(1–2): 47–72.

Uy, B. & Patil, S.B., 2006. Concrete filled high strength steel box columns for tall buildings: behaviour and design. Structural Design of Tall Buildings; 5(2):75–94.

Uy, B., Tao, Z. & Han, L.H., 2011. Behaviour of short and slender concrete-filled stainless steel tubular columns. Journal of Constructional Steel Research; 67: 360-378.

Virdi, K.S., 1981. Design of circular and rectangular hollow section columns. Journal of Constructional Steel Research; 1(4): 35-45.

Vrcelj, Z. & Uy, B., 2002. Strength of slender concrete-filled steel box columns incorporating local buckling. Journal of Constructional Steel Research; 58: 275-300.

Wahalathantri, B.L., Thambiratnam, D.P., Chan, T.H.T. & Fawzia, S., 2011. A material model for flexural crack simulation in reinforced concrete elements using Abaqus. In proceedings of the first international conference on Engineering, Designing and Developing the Built Environment for Suistainable Wellbeing, Queensland Universit of Technology, Brisbane; 260-264.

Wang, T.C., Li, X.H., Wang, T.Z. & Kang, G.Y., 2007. Hysteretic behavior of frame with specially shaped columns subjected to cyclic loading; Journal of Jilin University, Engineering and Technology Edition; 37(1): 224-228 [in Chinese].

Wang, D. & Lu, X., 2005. Experimental study on the seismic behavior of concrete filled steel tubular columns with TL section. Journal of Building Structures; 26: 39-44.

Wempner, G.A., 1971. Discrete approximation related to nonlinear theories of solids. International Journal of Structural Division; 7: 1581-1599.

Wikimedia. The Celtic Gateway Footbridge, UK. http://commons.wikimedia.org/wiki/File:Top_section_of_the_Celtic_Gateway_footbridge_-_geograph.org.uk_-_743313.jpg, Retrieved in September 2013.

Wikipedia. SEG Plaza. http://en.wikipedia.org/wiki/SEG_Plaza, Retrieved in September 2013.

Wu, M.H., 2000. Numerical analysis of concrete filled steel tubes subjected to axial force. MS thesis, Dept. of Civil Engineering, National Cheng Kung Univ., Tainan, Taiwan, R.O.C.

Xu, Y. & Wu, B., 2009. Fire resistance of reinforced concrete columns with L-, T-, and +-shaped cross-sections. Fire safety Journal; 44: 869-880.

Yang, Y.F. & Han, L.H., 2012. Concrete filled steel tube (CFST) columns subjected to concentrically partial compression. Thin-Walled Structures; 50: 147-156.

Yang, H., lam, H., & Gardner, L., 2008. Testing and analysis of concrete-filled elliptical hollow sections. Engineering Structures; 30: 3771 – 3781.

Yang, Y., Yang, H. & Zhang, S., 2010. Compressive behavior of T-shaped concrete-filled steel tubular columns. International Journal of Steel Structures; 10-04: 419-430.

Yau, C.Y., Chan, S.L. & So, A.K.W., 1993. Biaxial bending design of arbitrarily shaped reinforced concrete column. ACI Structural Journal; 90(3): 269-279.

Young, B. & Ellobody, E., 2006. Experimental investigation of concrete-filled cold-formed high strength stainless steel tube columns. Journal of Constructional Steel Research; 62(5): 484–92.

Young, B. & Hartono, W., 2002. Compression tests of stainless steel tubular members. Journal of Structural Engineering, ASCE; 128(6): 754–761.

Young, B. & Lui, W.M., 2005. Behavior of Cold-Formed High Strength Stainless Steel Sections. Journal of Structural Engineering, ASCE; 1738-1745.

Yu, T., Teng, J.G., Wong, Y.L. & Dong, S.L., 2010. Finite element modeling of confined concrete-I: Drucker-Prager type plasticity model. Engineering Structures; 32: 665-679.

Zhang, W. & Shahrooz, B. M., 1999. Comparison between ACI and AISC for concrete-filled tubular columns. Journal of Structural Engineering; 125(11): 1213–1223.

Zhang, J. & Yang, J., 2012. Study on mechanism of L-shaped concrete-filled steel tubular columns subjected to axial compression. Advanced Materials Research; 476-478: 2463-2468.

Zhang, D. & Ye, X.G., 2003. Non-linear analysis of special-shaped reinforced concrete columns. Journal of Hefei University of Technology; 26(4): 490-494 [in Chinese].

Zhao, X.L., Han, L.H., & Lu, H., 2010. Concrete-filled tubular members and connections. London: Spon Press.

Zhao, X.L., Lu, H. & Galteri, S., 2007. Tests of elliptical sections filled with SCC (self-compacting concrete). In: Proceedings of the fifth international conference on advances in steel structures. Singapore: 950–955.

Zhao, X.L. & Packer, J.A., 2009. Tests and design of concrete-filled elliptical hollow section stub columns. Thin-Walled Structures; 47(6–7): 617–628.

Zhou, F. & Young, B., 2005. Tests of cold-formed stainless steel tubular flexural members. Thin-Walled Structures; 43: 1325-1337.

Zuo, Z.L., Cai J., Yang, C., Chen, Q.J. & Sun, S., 2012. Axial load behavior of L-shaped CFT stub columns with binding bars. Engineering Structures; 37: 88-98.

APPENDIX A

SQUARE HOLLOW TUBULAR STUB COLUMN DESIGN SAMPLE

Cross-section resistance calculation for SHC with thickness of 10 mm (Class 4 section) and 40 mm (Class 3 section) as per European specification (EN 1993-1-4, 2006) and American specification (ASCE 8-02, 2002) presented in Chapter 3 are given below. SHC with cross-sectional dimension (600 x 600 mm) and thickness of 10 mm and 40 mm are shown in Figure A.1.

Figure A.1: (a) SHC – 600x600x10 mm and (b) SHC – 600x600x40 mm.

SHC material and geometric properties:

E_s = 197200 MPa; $f_y/\sigma_{0.2}$ = 657 MPa

A_g = (600*600)-(580*580) = 23600 mm^2 for SHC – 600x600x10 mm

A_g = (600*600)-(520*520) = 89600 mm^2 for SHC – 600x600x40 mm

Class classification:

As per EN 1993-1-4(2006);

$c/t\varepsilon \leq 30.70$ => Class 3 sections and $c/t\varepsilon > 30.70$ => Class 4 sections.

where, $\varepsilon = \left(\frac{235}{f_y}\frac{E_s}{210000}\right)^{0.5} = \left(\frac{235}{657}\frac{197200}{210000}\right)^{0.5} = 0.58$

For SHC – 600x600x10 mm; c = 600-2*10 = 580 mm

$c/t\varepsilon$ = 580/(10*0.58) = **100** > 30.70; Hence, **Class 4 section** (slender section).

For SHC – 600x600x40 mm; c = 600-2*40 = 520 mm

$c/t\varepsilon$ = 520/(40*0.58) = **22.41** ≤ 30.70; Hence, **Class 3 section** (stocky section).

Effective area determination for Class 4 section (600x600x10 mm):

$A_e = A_g - n_s t(c - B_e)$

As per EN 1993-1-4 (2006);

$$\overline{\lambda}_p = \frac{\left(\frac{c}{t}\right)}{28.4\varepsilon\sqrt{k}} = \frac{\left(\frac{580}{10}\right)}{28.4*0.58*\sqrt{4.0}} = 1.761$$

$$\rho = \frac{0.772}{\overline{\lambda}_p} - \frac{0.125}{\overline{\lambda}_p^{\,2}} \text{ but} \le 1.0 \quad = 0.398$$

$B_e = \rho c$ = 0.398*580 = 230.84mm

B_{ineff} =c - B_e = 580-230.84 = 349.16 mm

Hence, A_e = 23600 – (4*10*349.16) = **9637.50 mm^2**

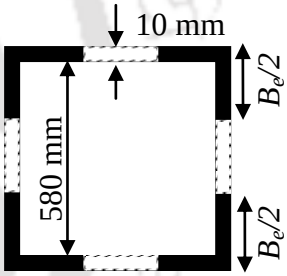

As per ASCE 8-02 (2002);

$$\lambda = \left(\frac{1.052}{\sqrt{k}}\right)\left(\frac{c}{t}\right)\left(\sqrt{\frac{f}{E_s}}\right) = \left(\frac{1.052}{\sqrt{4.0}}\right)\left(\frac{580}{10}\right)\left(\sqrt{\frac{657}{197200}}\right) = 1.761$$

$$\rho = \frac{1}{\lambda} - \frac{0.22}{\lambda^2} \text{ but} \le 1.0 = 0.497$$

Conditions; For λ ≤ 0.673 $B_e = c$

For λ > 0.673 $B_e = \rho c$

$B_e = \rho c$ = 0.497*580 = 288.221mm (as λ > 0.673)

B_{ineff} =c - B_e = 580-288.221 = 291.78 mm

Hence, A_e = 89600 – (4*10*291.78) = **11928.85 mm^2**

Unfactored Cross-sectional resistance:

For Class 3 section (stocky section) of SHC – 600x600x40 mm;

$P_{EN1993\text{-}1\text{-}4} = f_y A_g$ = 657*89600 = **58867.20 kN**

$P_{ASCE\ 8\text{-}02} = f_y A_g$ = 657*89600 = **58867.20 kN**

For Class 4 section (slender section) of SHC – 600x600x10 mm;

$P_{EN1993\text{-}1\text{-}4} = f_y A_e$ = 657* 9637.50 = **6331.84 kN**

$P_{ASCE\ 8\text{-}02} = f_y A_e$ = 657* 11928.85 = **7837.25 kN**

APPENDIX B

FIXED-ENDED SQUARE HOLLOW TUBULAR SLENDER COLUMN DESIGN SAMPLE

Design strength calculation for SHC with thickness of 5.25 mm (Class 3 section) as per European specification (EN 1993-1-4, 2006) and American specification (ASCE 8-02, 2002) presented in Chapter 4 are given below. SHC with cross-sectional dimension (600 x 600 mm) and thickness of 5.25 mm and L = 4000 mm is shown in Figure B.1.

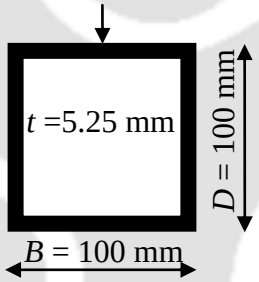

Figure B.1: SHC – 600x600x40 mm - L = 4000 mm.

SHC material and geometric properties:

E_s= 197200 MPa; $f_y/\sigma_{0.2}$ = 657 MPa; n = 4.7

$Le = (L/2) = 4000/2 = 2000$ mm

$I = ((100*100^3) - (89.5*89.5^3))/12 = 2986324.58$ mm^4

$A_g = (100*100)-(89.5*89.5) = 1989.75$ mm^2

$$r = \sqrt{\left(\frac{I}{A}\right)} = \sqrt{\left(\frac{2986324.58}{1989.75}\right)} = 38.74 \text{ mm}$$

$$\bar{\lambda} = \frac{L_e}{r}\frac{1}{\pi}\sqrt{\frac{\sigma_y \beta_A}{E_s}} = \frac{2000}{38.74}\frac{1}{3.143}\sqrt{\frac{657*1}{197200}} = 0.95$$

Class classification:

As per EN 1993-1-4(2006);

$c/t\varepsilon \leq 30.70$ => Class 3 sections and $c/t\varepsilon > 30.70$ => Class 4 sections.

Where, $\varepsilon = \left(\frac{235}{f_y}\frac{E_s}{210000}\right)^{0.5} = \left(\frac{235}{657}\frac{197200}{210000}\right)^{0.5} = 0.58$

For SHC – 100x100x5.25 mm; c = 100-2*5.25 = 89.5 mm

$c/t\varepsilon$ = 89.5/(5.25*0.58) = **29.39** ≤ 30.70; Hence, **Class 3 section** (stocky section).

Unfactored Design strength:

As per EN 1993-1-4 (2006);

$$\varphi = 0.5(1+\alpha(\overline{\lambda}-\overline{\lambda_0})+\overline{\lambda^2}) = 0.5(1+0.49(0.95-0.40)+0.95^2) = 1.086$$

$$\chi = \frac{1}{\varphi+(\varphi^2-\overline{\lambda^2})^{0.5}} \leq 1.0 = \frac{1}{1.086+(1.086^2-0.95^2)^{0.5}} = 0.62$$

$P_{EN1993\text{-}1\text{-}4} = \chi f_y A_g$ = 0.62*657*1989.75 = **810.5 kN**

As per ASCE 8-02 (2002);

Check 1: f = 657 MPa

$$E_t = \frac{f_y E_s}{f_y + 0.002nE_s\left(\frac{f}{f_y}\right)^{n-1}} = \frac{657*197200}{657+0.002*4*197200*\left(\frac{657}{657}\right)^{4-1}} = 51603.71 \text{ MPa}$$

$$f_n = \frac{\pi^2 E_t}{\left(\frac{L_e}{r}\right)^2} \leq f_y = = \frac{3.143^2*51603.71}{\left(\frac{2000}{38.74}\right)^2} = 191.27 \neq 657 \text{ (assumed value)}$$

Check 2: f = 500 MPa

$$E_t = \frac{f_y E_s}{f_y + 0.002nE_s\left(\frac{f}{f_y}\right)^{n-1}} = \frac{500*197200}{500+0.002*4*197200*\left(\frac{500}{657}\right)^{4-1}} = 97275.72 \text{ MPa}$$

$$f_n = \frac{\pi^2 E_t}{\left(\frac{L_e}{r}\right)^2} \le f_y = = \frac{3.143^2 * 97275.723}{\left(\frac{2000}{38.74}\right)^2} = 360.56 \neq 500 \text{ (assumed value)}$$

Check 3: f = 442.3MPa

$$E_t = \frac{f_y E_s}{f_y + 0.002 n E_s \left(\frac{f}{f_y}\right)^{n-1}} = \frac{442.3 * 197200}{442.3 + 0.002 * 4 * 197200 * \left(\frac{442.3}{657}\right)^{4-1}} = 119329 \text{ MPa}$$

$$f_n = \frac{\pi^2 E_t}{\left(\frac{L_e}{r}\right)^2} \le f_y = = \frac{3.143^2 * 119329}{\left(\frac{2000}{38.74}\right)^2} = 442.3 = 442.3 \text{ (assumed value)}$$

Hence, f_n = 442.3MPa

$P_{\text{ASCE 8-02}} = A_g f_n$ = 1989.75 *442.3 = **880.07 kN**

APPENDIX C

FE MODELLING OF THE CONCRETE CORE: D-P PLASTICITY MODEL

The modeling of the inadequately confined concrete core of the CFDSST stub columns in Chapter 5 through D-P yield criterion provided in FE software package Abaqus (2006) is explained as follows. Figure C.1 presents the equivalent uniaxial stress-strain curve for the confined concrete core in concrete-filled tubular stub columns.

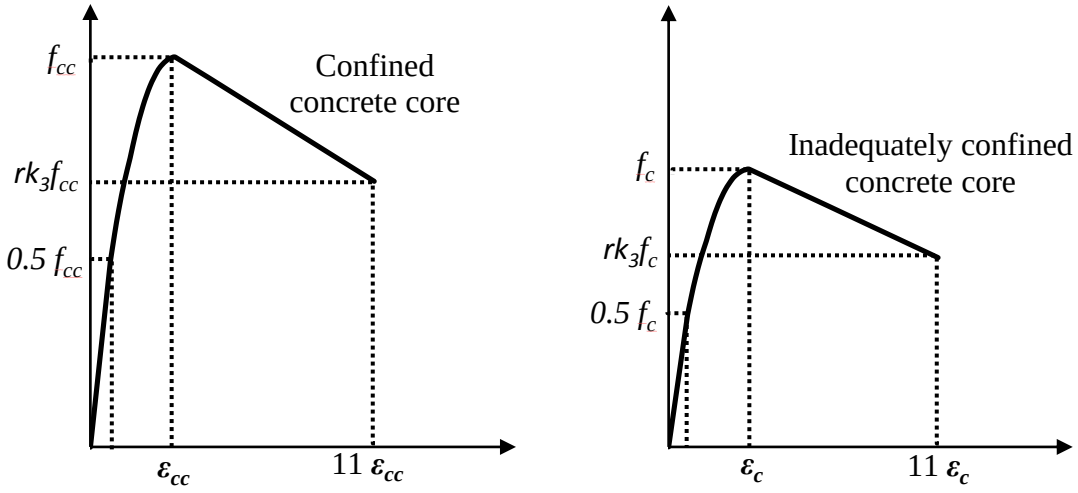

(a) Confined concrete core (Saenz, 1964) (b) Adopted in the FE studies

Figure C.1: Equivalent uniaxial stress-strain curve for the concrete core in concrete-filled tubular columns.

The development of the stress–strain relationship of the confined concrete core as proposed by Saenz (1964) is shown in Figure C.1a and is detailed in Section 2.2. However, in the present study, the concrete core in the CFDSST stub column FE models were considered as inadequately confined (as detailed in Section 5.4.2). Hence, the f_{cc} in Equation 2.7 and the corresponding ε_{cc} in Equation 2.8 becomes f_c and ε_{cc}, respectively.

Figure C.1b shows the adopted inadequately confined concrete core model in the concrete-filled tubular stub column FE models.

The linear elasticity model was used in conjunction with the plasticity models. Classical linear isotropic elastic constants of the confined concrete core such as E_c and v_c (the elastic part upto the proportional limit is taken as ($0.5f_c$) as detailed in Section 2.7.2) are taken care of by the *Elastic material option available in the Abaqus material library as (e.g. for f_{ck} = 25 MPa):

*Elastic
E_c → 21019., 0.2 ← v_c

The yielding part of the confined stress-strain curve for concrete core, which is part after the proportional limit, is treated by the D-P yield criterion model available in the Abaqus material library. This D-P model is intended to simulate material response under essentially monotonic loading, such as the behavior of the concrete core in concrete-filled tubular stub columns under pure axial compression, and also followed by many researchers (e.g. Dai and Lam, 2010, Ellobody and Young, 2006, Hassanein, 2010, Hassanein *et al.*, 2013). Because the concrete in the concrete-filled tubular columns is usually subjected to triaxial compressive stresses, the failure of concrete is dominated by the compressive failure surface expanding with increasing hydrostatic pressure. Figure C.2 shows a plot of second deviatoric stress invariant (J) with the first stress invariant (I_1) to model the yield surface of the confined concrete core.

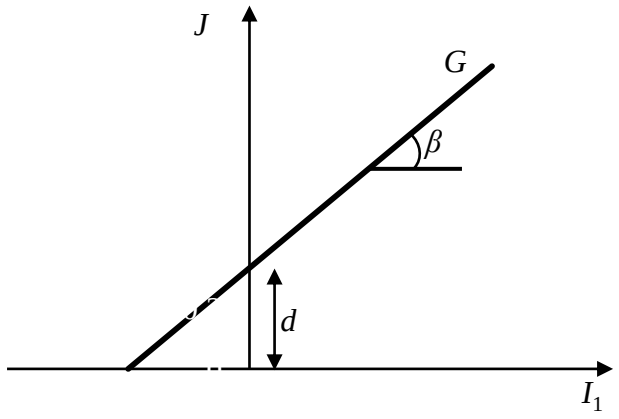

Figure C.2: Linear D-P yield criterion for confined concrete core (Hu *et al.*, 2003).

Linear D-P yield criterion (G) is expressed in Equation C.1 as:

$$G = t - I_1 \tan\beta - d = 0 \tag{C.1}$$

where

$$I_1 = -\frac{(\sigma_1 + \sigma_2 + \sigma_3)}{3} \tag{C.2}$$

$$d = \left(1 - \frac{\tan\beta}{3}\right) f_{cc} \tag{C.3}$$

$$J = \frac{\sqrt{3J_2}}{2}\left[1 + \frac{1}{K} - \left(1 - \frac{1}{K}\right)\left(\frac{r}{\sqrt{3J_2}}\right)^3\right] \tag{C.4}$$

$$r = \left[\frac{9}{2}(S_1^3 + S_2^3 + S_3^3)\right]^{\frac{1}{3}} \tag{C.5}$$

where σ_1, σ_2, σ_3 are the principal stresses, J_2 is second stress invariant of the stress deviator tensor, S_1, S_2, S_3 are the principal stress deviators.

The D-P plasticity model parameters in Abaqus are invoked with the *Drucker Prager option, which is given below as:

*Drucker Prager

20., 0.8, 0.

β K ψ

where ψ is the dilation angle. The constants β and K are material parameters determined from experimental data. K = 0.8, β = 20°, and ψ = 0 are used in the present study based on similar studies for concrete-filled tubular stub columns (e.g. Hu *et al*., 2003, Wu, 2000, Dai and Lam, 2010, Ellobody and Young, 2006, Hassanein, 2010, Hassanein *et al*., 2013).

The response of the concrete is modeled by an elastic-plastic theory with associated flow and isotropic hardening rule. On plastic deformation of the concrete core, there should be a certain parameter to guide the expansion of the yield surface. A commonly used approach is to relate the multidimensional stress and strain conditions to a pair of

quantities, namely, f_c and ε_c, such that results obtained following different loading paths can all be correlated by means of the equivalent uniaxial stress-strain relationship proposed by Saenez (1964), and is detailed in Chapter 2. The developed uniaxial stress-strain curve (see Figure C.1) is then feeded in the Abaqus through the *Drucker Prager Hardening option available in the Abaqus library.

APPENDIX D

CONCRETE-FILLED SQUARE TUBULAR STUB COLUMN DESIGN SAMPLE

Cross-section resistance calculation for S3C25 as per European specification (EN 1994-1-1, 2006) and American specification (ASCE 8-02, 2002) presented in Chapter 5 are given below. S3C25 with cross-sectional dimension (600 x 600 x 10 mm) and f_{ck} = 25 MPa are shown in Figure D.1.

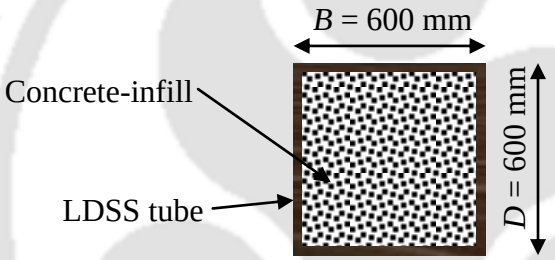

Figure D.1: S3C25 – 600x600x10 mm

S3C25 material and geometric properties:

E_s = 197200 MPa; $E_{cc} = 4700\sqrt{f_{cc}} = 4700\sqrt{20}$ = 21019.04 MPa;

$f_y/\sigma_{0.2}$ = 657 MPa; f_{ck} = 25 MPa;

$f_c = 0.8\ f_{ck}$ = 20 Mpa; t = 10 mm

A_s = (600*600)-(580*580) = 23600 mm^2

A_c = (580*580) = = 336400 mm^2

Class classification:
As per EN 1993-1-1(2006);

$c/t\varepsilon \leq 30.70$ => Class 3 sections and $c/t\varepsilon > 30.70$ => Class 4 sections.

Where, $\varepsilon = \left(\frac{235}{f_y}\frac{E_s}{210000}\right)^{0.5} = \left(\frac{235}{657}\frac{197200}{210000}\right)^{0.5} = 0.58$

For SHC – 600x600x10 mm; c = 600-2*10 = 580 mm

$c/t\varepsilon$ = 580/(10*0.58) = **100** > 30.70; Hence, **Class 4 section** (slender section).

Effective area determination for S3C25:

$A_e = A_g - n_s t(c - B_e)$

As per EN 1993-1-4 (2006);

$$\bar{\lambda}_p = \frac{\left(\frac{c}{t}\right)}{28.4\varepsilon\sqrt{k}} = \frac{\left(\frac{580}{10}\right)}{28.4*0.58*\sqrt{4.0}} = 1.761$$

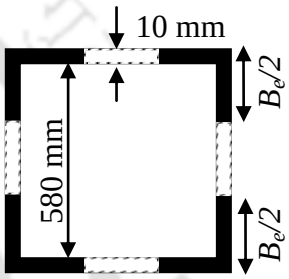

$$\rho = \frac{0.772}{\bar{\lambda}_p} - \frac{0.125}{\bar{\lambda}_p^{\,2}} \text{ but} \le 1.0 \quad = 0.398$$

$B_e = \rho c$ = 0.398*580 = 230.84mm

B_{ineff} =c - B_e = 580-230.84 = 349.16 mm

Hence, A_e = 23600 – (4*10*349.16) = **9637.50 mm^2**

As per ASCE 8-02 (2002);

$$\lambda = \left(\frac{1.052}{\sqrt{k}}\right)\left(\frac{c}{t}\right)\left(\sqrt{\frac{f}{E_s}}\right) = \left(\frac{1.052}{\sqrt{4.0}}\right)\left(\frac{580}{10}\right)\left(\sqrt{\frac{657}{197200}}\right) = 1.761$$

$$\rho = \frac{1}{\lambda} - \frac{0.22}{\lambda^2} \text{ but} \le 1.0 = 0.497$$

Conditions; For $\lambda \le 0.673$ $B_e = c$

For $\lambda > 0.673$ $B_e = \rho c$

$B_e = \rho c$ = 0.497*580 = 288.221mm (as $\lambda > 0.673$)

B_{ineff} =c - B_e = 580-288.221 = 291.78 mm

Hence, A_e = 89600 – (4*10*291.78) = **11928.85 mm^2**

Unfactored cross-sectional resistance:

$P_{EN1994\text{-}1\text{-}1}$ = $(f_y A_e + f_c A_c)$

= (657*9637.5+20*336400)

= **13059.84 kN**

$P_{ASCE\ 8\text{-}02}$ = $(f_y A_e + f_c A_c)$

= (657*11928.85+20*336400)

= **14565.25 kN**

APPENDIX E

FE MODELLING OF THE CONCRETE CORE: CDP MODEL

The CDP model provided in the material library of Abaqus (2006) was used for modeling the concrete core in the CFDSST slender column FE models described in Chapter 6. The CDP model is used to represent complete inelastic behavior of the concrete core both in tension and compression including damage characteristics, as also recommended by other researchers (e.g. Wahalathantri *et al*., 2011, An *et al*., 2012, Tao *et al*., 2011). Strength enhancement of the concrete core at the state of triaxial loading can be achieved by the definition of the yielding surface and the description of the plastic behavior coming from the equivalent stress-strain relationship of the confined concrete core, and discussed below. The linear elasticity model was used in conjunction with the CDP model as discussed in Appendix C.

The determining parameters of the yielding surface can be easily governed through two variables, such as K_c (describes the shape of the deviatoric plane) and σ_{b0}/σ_{c0} (ratio of maximum biaxial compressive strength and the maximum uniaxial strength), along with three other variables, such as dilation angle, the eccentricity and the viscosity parameter. These parameters are introduced in the Abaqus through *Concrete Damage Plasticity option available.

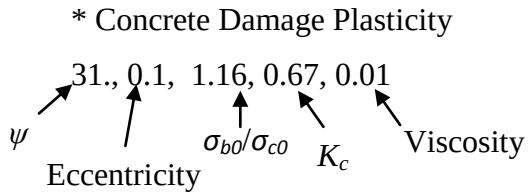

The value of ψ, σ_{b0}/σ_{c0}, and K_c were taken as 30^0 (Lee and Fenves, 1998), 1.16 (Kupfer and Gerstle, 1973), and 0.67 (Lubliner *et al*., 1989), respectively. A value of 0.1 has been

taken for eccentricity and even lower values for viscosity, inorder to maximize the convergence.

To determine the two stress-strain curves of plastic hardening, under the assumption of pure tension and pure compression; besides, two evolutionary damage laws have to be also defined under both states. The development of the compressive stress–strain relationship proposed by Saenz (1964) (as detailed in Chapter 2) along with the corresponding damage parameter (*dc*) for the confined concrete core is given in Figure E.1a.

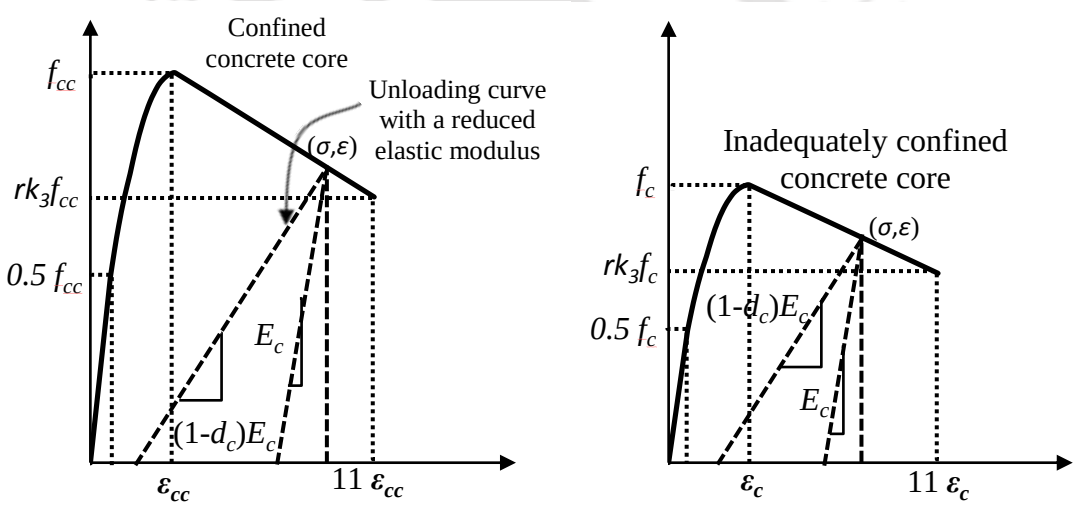

(a) Confined concrete core (Saenz, 1964) (b) Adopted in the FE studies

Figure E.1: Equivalent uniaxial stress-strain curve for the concrete core in concrete-filled tubular columns.

In the present study, the concrete core in the CFDSST stub column FE models were considered as inadequately confined (as detailed in Section 6.4.2). Hence, the f_{cc} in Equation 2.7 and the corresponding ε_{cc} in Equation 2.8 becomes f_c and ε_{cc}, respectively. Figure E.1b shows the adopted inadequately confined concrete core model in the concrete-filled tubular stub column FE models.

Damage is generally characterized by the reduction of elastic constants. Both the reduction of unloading stiffness and unrecoverable deformation have been clearly observed in concrete compression tests (Maekawa et al., 2003, Oshima and Hashimoto, 1984) as illustrated in Figure E.1, which suggests that the concept of plasticity should be combined with the concept of damage to correctly represent the nonlinear behavior of concrete. The scalar damage elasticity equation for concrete subjected to uniaxial monotonic loading compression is given by Equation E.1.

$$\sigma = (1 - d_c) E_c (\varepsilon - \varepsilon^p) \tag{E.1}$$

where σ and ε are the corresponding compressive stress and strain of concrete in the loading direction, respectively, ε^p is the plastic strain in the loading direction.

Figures E.2 and E.3 show different forms of tension stiffening models for concrete in uniaxial tension as proposed by Nayal and Rasheed (2006) and Wahalathantri *et al*. (2011).

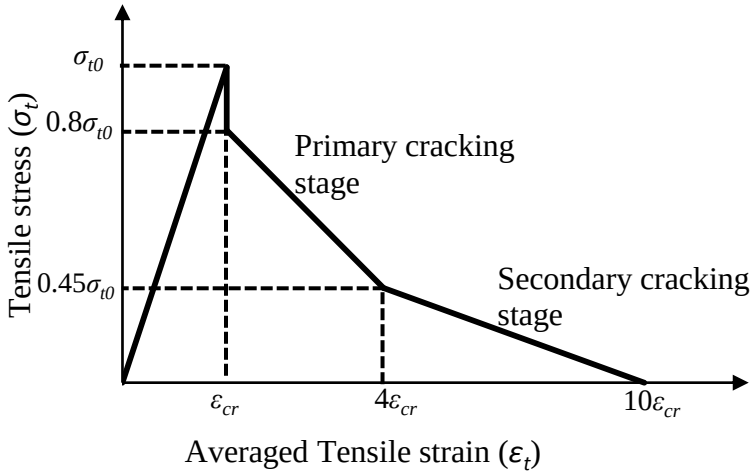

Figure E.2: Nayal and Rasheed (2006) tension stiffening model

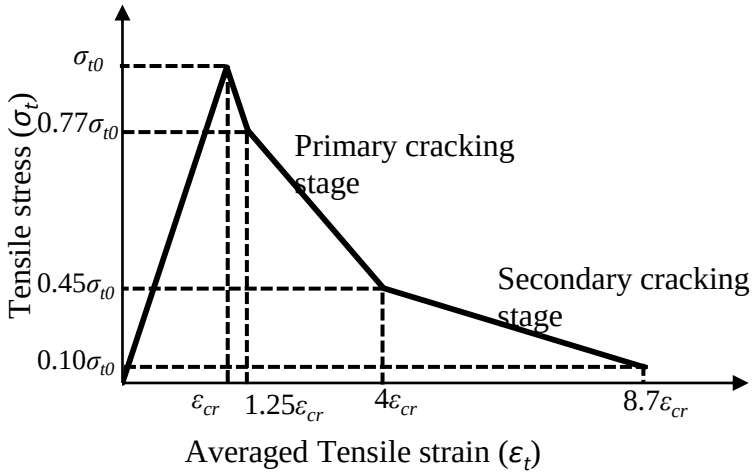

Figure E.3: Modified tension stiffening model for Abaqus (Wahalathantri *et al*. (2011).

The current study adopted the modified version of Nayal and Rasheed (2006) model (i.e Wahalathantri *et al*. (2011) model) in view of avoiding Abaqus run time errors issues in the former model as discussed further. The sudden drop at critical tensile strain (ε_{cr}) from maximum tensile stress (σ_{t0}) as used by Nayal and Rasheed (2006) is slanted from (ε_{cr}, σ_{t0}) to (1.25 ε_{cr}, 0.77 σ_{t0}) and secondary cracking stage stops at (8.7 ε_{cr}, 0.10 σ_{t0}) to avoid Abaqus run time errors. The value of σ_{t0} is approximately taken as 0.1*fck*. Similar process, as followed in the calculation of d_c, was also followed for the calculation of damage parameter in tension (d_t).

APPENDIX F

FIXED-ENDED CONCRETE-FILLED SQUARE TUBULAR SLENDER COLUMN DESIGN SAMPLE

Design strength calculation for SC25L30000 as per European (EN 1994-1-1, 2004) and American (ANSI/AISC 360-05, 2005) specificationS presented in Chapter 6 are given below. SC25L30000 with cross-sectional dimension (600 x 600 x 10 mm) and f_{ck} = 25 MPa are shown in Figure F.1.

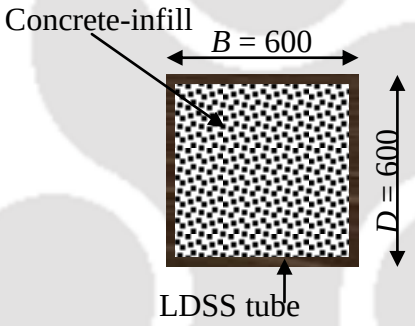

Figure F.1: SC25L30000 – 600x600x10 mm - L = 30000 mm.

SC25L30000 material and geometric properties:

E_s= 197200 MPa; $E_{cc} = 4700\sqrt{f_{cc}} = 4700\sqrt{20}$ = 21019.04 MPa;

$f_y/\sigma_{0.2}$ = 657 MPa; $f_c = 0.8\, f_{ck}$ = 20 Mpa;

n = 4.7; $Le = (L/2)$ = 30000/2 = 15000 mm

$I_s = ((600*600^3) - (580*580^3))/12$ = 1369586666.67 mm^4

$I_c = (580*580^3)/12$ = 9430413333.33 mm^4

A_s = (600*600)-(580*580) = 23600 mm^2; A_c = (580*580) = = 336400 mm^2

$$r = \sqrt{\left(\frac{I_s}{A_s}\right)} = \sqrt{\left(\frac{1369586666.67}{23600}\right)} = 240.90 \text{ mm}$$

Class classification:

As per EN 1993-1-4(2006);

$c/t\varepsilon \leq 30.70$ => Class 3 sections and $c/t\varepsilon > 30.70$ => Class 4 sections.

Where, $\varepsilon = \left(\frac{235}{f_y}\frac{E_s}{210000}\right)^{0.5} = \left(\frac{235}{657}\frac{197200}{210000}\right)^{0.5} = 0.58$

For SHC – 600x600x10 mm; c = 600-2*10 = 580 mm

$c/t\varepsilon$ = 580/(10*0.58) = **100** > 30.70; Hence, **Class 4 section** (slender section).

Effective area determination for SC25L30000:

$A_e = A_g - n_s t(c - B_e)$

As per EN 1993-1-4 (2006);

$$\bar{\lambda}_p = \frac{\left(\frac{c}{t}\right)}{28.4\varepsilon\sqrt{k}} = \frac{\left(\frac{580}{10}\right)}{28.4*0.58*\sqrt{4.0}} = 1.761$$

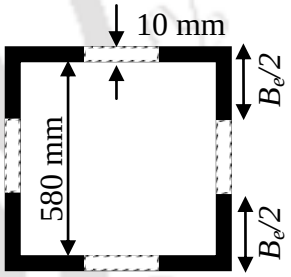

$$\rho = \frac{0.772}{\bar{\lambda}_p} - \frac{0.125}{\bar{\lambda}_p^{\,2}} \text{ but} \leq 1.0 \quad = 0.398$$

$B_e = \rho c$ = 0.398*580 = 230.84mm

B_{ineff} =c - B_e = 580-230.84 = 349.16 mm

Hence, A_e = 23600 – (4*10*349.16) = **9637.50 mm^2**

As per ASCE 8-02 (2002);

$$\lambda = \left(\frac{1.052}{\sqrt{k}}\right)\left(\frac{c}{t}\right)\left(\sqrt{\frac{f}{E_s}}\right) = \left(\frac{1.052}{\sqrt{4.0}}\right)\left(\frac{580}{10}\right)\left(\sqrt{\frac{657}{197200}}\right) = 1.761$$

$$\rho = \frac{1}{\lambda} - \frac{0.22}{\lambda^2} \text{ but} \leq 1.0 = 0.497$$

Conditions; For $\lambda \leq 0.673$ $B_e = c$

For $\lambda > 0.673$ $B_e = \rho c$

$B_e = \rho c$ = 0.497*580 = 288.221mm (as $\lambda > 0.673$)

B_{ineff} =c - B_e = 580-288.221 = 291.78 mm

Hence, A_e = 89600 – (4*10*291.78) = **11928.85 mm^2**

Unfactored Design strength:

As per EN 1993-1-4 (2006);

$$N_{cr} = \frac{\pi^2 (E_s I_s + 0.6 E_{cc} I_c)}{L_e^2}$$

$$= \frac{3.143^2 * (197200 * 1369586666.67 + 0.6 * 21019.04 * 9430413333.33)}{15000^2}$$

= **17079.33 kN**

$N_o/N_{pl,Rd} = A_e f_y + A_c f_c$

= (9637.50*657) + (336400*20)

= 13059.838 kN

$$\bar{\lambda} = \sqrt{\frac{N_0}{N_{cr}}} = \sqrt{\frac{13059.84}{17079.33}} = 0.874$$

$$\varphi = 0.5(1 + \alpha(\bar{\lambda} - \bar{\lambda_0}) + \bar{\lambda^2}) = 0.5 * (1 + 0.21 * (0.874 - 0.40) + 0.874^2) = 1.0$$

$$\chi = \frac{1}{\varphi + (\varphi^2 - \bar{\lambda^2})^{0.5}} \leq 1.0 = \frac{1}{1.0 + (1.0^2 - 0.874^2)^{0.5}} = 0.751$$

$P_{EN1994\text{-}1\text{-}1} = \chi N_o$

= 0.751*13059.838

= 9808 kN

As per ANSI/AISC 360-05 (2005);

$$N_{cr} = \frac{\pi^2 \left(E_s I_s + \left(0.6 + 2 * \left(\frac{A_s}{A_c} \right) \right) E_{cc} I_c \right)}{L_e^2}$$

$$= \frac{3.143^2 * \left(197200 * 1369586666.7 + \left(0.6 + 2 * \left(\frac{23600}{336400} \right) \right) * 21019.04 * 9430413333.3 \right)}{15000^2}$$

= **18971.34 kN**

Check 1: Assume f = 657 MPa

$$E_t = \frac{f_y E_s}{f_y + 0.002 n E_s \left(\frac{f}{f_y}\right)^{n-1}} = \frac{657 * 197200}{657 + 0.002 * 4.7 * 197200 * \left(\frac{657}{657}\right)^{4.7-1}} = 51604 \text{ MPa}$$

$$f_n = \frac{\pi^2 E_t}{\left(\frac{L_e}{r}\right)^2} \le f_y = = \frac{3.143^2 * 51604}{\left(\frac{15000}{240.90}\right)^2} = 131.48 \neq 657 \text{ (assumed value)}$$

Check 2: Assume f = 500 MPa

$$E_t = \frac{f_y E_s}{f_y + 0.002 n E_s \left(\frac{f}{f_y}\right)^{n-1}} = \frac{500 * 197200}{500 + 0.002 * 4.7 * 197200 * \left(\frac{500}{657}\right)^{4.7-1}}$$

= 97275.72 MPa

$$f_n = \frac{\pi^2 E_t}{\left(\frac{L_e}{r}\right)^2} \le f_y = = \frac{3.143^2 * 97275.72}{\left(\frac{15000}{240.90}\right)^2} = 247.85 \neq 500 \text{ (assumed value)}$$

Check 3: Assume f = 373 MPa

$$E_t = \frac{f_y E_s}{f_y + 0.002 n E_s \left(\frac{f}{f_y}\right)^{n-1}} = \frac{373 * 197200}{373 + 0.002 * 4.1 * 197200 * \left(\frac{373}{657}\right)^{4.7-1}}$$

= 146358.51 MPa

$$f_n = \frac{\pi^2 E_t}{\left(\frac{L_e}{r}\right)^2} \le f_y = = \frac{3.143^2 * 146358.51}{\left(\frac{15000}{240.90}\right)^2} = 373 = 373 \text{ (assumed value)}$$

Hence, f_n = 373MPa

$N_o/N_{pl,Rd} = A_e f_n + A_c f_c$

= (11928.85*373) + (336400*20)

= 11297.105 kN

$$\bar{\lambda} = \sqrt{\frac{N_0}{N_{cr}}} = \sqrt{\frac{11297.105}{18971.34}} = 0.772$$

$$P_{ANSI/AISC\ 360\text{-}05} = 0.658^{\left(\frac{N_o}{N_{cr}}\right)} N_o \qquad \text{for } N_{cr} \geq 0.44\ N_o$$

$$P_{ANSI/AISC\ 360\text{-}05} = 0.877 N_{cr} \qquad \text{for } N_{cr} < 0.44\ N_o$$

Here;

$$0.44\ N_o = 0.44 * 11297.105 = 4970.73\ \text{kN} \leq N_{cr}$$

Hence;

$$P_{ANSI/AISC\ 360\text{-}05} = 0.658^{\left(\frac{N_o}{N_{cr}}\right)} N_o$$

$$= 0.658^{\left(\frac{11297.105}{18971.34}\right)} 11297.105$$

= 8804.89 kN

LIST OF PUBLICATIONS

JOURNALS

Patton, M.L. & Singh, K.D., 2012. "Numerical modelling of lean duplex stainless steel hollow columns of Square, L-, T-, and +-shaped cross sections under pure axial compression". Thin-walled structures; 53: 1-8.

Patton, M.L. & Singh, K.D., 2013. "Buckling of fixed-ended lean duplex stainless steel hollow columns of Square, L-, T-, and +-shaped sections under pure axial compression - a finite element study". Thin-walled structures; 63: 106-116.

Patton, M.L. & Singh, K.D., 2012. "Finite element modelling of concrete-filled lean duplex stainless steel tubular stub columns". International journal of steel structures. **(under communication)**

Patton, M.L. & Singh, K.D., 2012. "Effect of cross-sectional shape on the behaviour of concrete-filled lean duplex slender stainless steel stub columns: FE study". Engineering structures. **(manuscript prepared)**

Patton, M.L. & Singh, K.D., 2012. "Buckling of fixed-ended concrete-filled lean duplex slender stainless steel columns under axial compression". Journal of structural engineering. **(manuscript prepared)**

CONFERENCES

Patton, M.L. & Singh, K.D., 2012. "Lean duplex stainless steel hollow stub columns of Square, L-, T-, and +-shaped cross sections under pure axial compression – a finite element study." 14th International Symposium on Tubular Structures. London.